

Université du Québec
Institut National de la Recherche Scientifique
Centre Énergie Matériaux Télécommunications

Nanoscale phenomena influencing phage-displayed enzymes and emerging technologies to analyze activity towards complex substrates

By
Sharifun Nahar

A thesis submitted for the achievement of the
degree of Philosophy doctor (Ph.D.) in Energy and Materials Science

Jury Members

President of the jury and
Internal Examiner

Prof. Fiorenzo Vetrone
INRS-EMT

External Examiner

Prof. Sarah Hedtrich
University of British Columbia

External Examiner

Prof. Ryan Wylie
McMaster University

Director of Research

Prof. Marc A. Gauthier
INRS-EMT

AKNOWLEDGEMENTS

I would like to thank Prof. Marc A. Gauthier for giving me the opportunity to pursue my PhD study. I learned to become more critical in decision-making steps. I am very grateful to him for all his support and help, especially for being very patient and kind during the entire period.

I would like to thank Prof. Tsuneyuki Ozaki for all his support and for letting me perform the experiments in his lab.

I gratefully acknowledge Prof. Toshihiko Kiwa, Okayama University, Japan who accepted me as summer intern in his lab and facilitated to perform experiment with the THz emission. I am grateful to him for his kind help and continuous support for the entire period of my Japan stay. Special thanks to his group who trained me on performing the experiments and data analysis, specially Takuya Kuwana for his technical assistance with the THz emission technology. I appreciate their help not only in training, but also for fruitful discussions on scientific aspects of the work

I want to thank Dr. Esen Sokullu who guided me for phage display work. I appreciate all her help not only in training, but also for fruitful discussions on scientific aspects of the work.

Special thanks to Ahlem Meziadi who helped me for translating the thesis summary in French.

I would like to thank Dr. Andrea Greschner for not only discussions on scientific aspects, but also her lovey support when I felt down.

I want to thank Dr. Xavier Ropagnol who trained me on performing the experiments by using THz emission system. I also thank to Mohammed Ahmed for performing those lengthy experiments. I appreciate all their help not only in training, but also for fruitful discussions on scientific aspects of the work.

It was an immense pleasure to work with wonderful colleagues who accompanied me at INRS, namely, Fatemeh Zare, Dr. Ahlem Zaghmi, Sabrine Messoudi, Dr. Hu Lei, Dr. Amir Hassanpour, Dr. Anees Palapuravan, Xu Geng, Kevin Coutu. I am very thankful for their support and help. I was very lucky to have nice people around me who always provided their endless support.

Special thanks to Cybelle Soares, Hasna Hena Zamal, Maria João Paolo, Denis Ferachou. They have been more than colleagues for me.

I would like to thank to the administrative and technical staff at INRS-EMT. They were very kind and helpful, particularly H  l  ne Tanguay, Louise Hudon, Nathalie M  tras, H  l  ne Sabourin, and Georges Lamoureux.

I would like to acknowledge my lovely husband Dr. Nazmul Alam for holding me up all the time. Special thanks to my two LOVELY daughters Sadia and Nabeeha for their sacrifice throughout my entire PhD period.

Finally, I would like to thank to my family in Bangladesh, my mother, my sisters and brothers and my in-laws for their support, love and encouragement during this study.

ABSTRACT

The use of enzymes, in some cases, face challenges due to less stability towards extreme condition, purification of intermediate products from each step of a multistep reaction or even finding the appropriate technology to follow the reaction predominantly when the sample is complex or raw material. To overcome this need, in addition of doing enzyme engineering, enzyme immobilization on solid support has become standard though the recent trends are more focused towards enzyme's microenvironment engineering. In the second chapter of this thesis, we explored the templated effect of phage on enzyme activity. We evaluated the effect of solution parameters on the catalytic activity of phage displayed *Bacillus subtilis* Lipase A (BSLA). While the pH and temperature-activity profiles of BSLA were not intrinsically affected by phage display, the nanoscale distribution of BSLA within the micellar assay buffer was. This causes a pronounced increase of activity of phage–BSLA relative to the free enzyme, due to the accumulation of phage–BSLA at the substrate-rich micelles. Considering this result, attention should be taken and similar effects should be considered when selecting other enzymes/proteins by phage display, as the activity of the displayed protein may differ from that of the free protein.

Then, we explored the potential of nanoscale distribution of multi-enzyme templated phage. We immobilized glucose oxidase and horseradish peroxidase onto the p8 major coat protein on the M13 phage that already displayed BSLA on its p3 coat protein. These three enzymes together perform a cascade reaction. We explored whether this model three-enzyme cascade system, yields an advantageous acceleration of the overall reaction relative to the free enzymes in solution. Phages were crosslinked by biotin–streptavidin interactions, which appeared to create a more favorable microenvironment. Our result indicated that the three-enzyme cascade, BSLA→GOx→HRP, can indeed be enhanced compared to the free enzymes in solution by templating on a phage. Ultimately, this proof-of-concept study suggests that phage-templated enzyme cascade systems may be promising platforms for green manufacturing, though predicting the effect of microenvironmental effects on all the enzymes remains a challenge.

Later, we investigated terahertz (THz) emission technology for label-free monitoring of chemical changes. Enzymatic reactions are typically monitored using surrogate substrates that produce quantifiable optical signals. In this study, THz emission technology is used as a non-invasive and label-free technique to monitor the kinetics of lipase-induced hydrolysis of several substrate molecules (including the complex substrate whole cow's milk) and horseradish peroxidase-catalyzed oxidation of o-phenylenediamine in the presence of hydrogen peroxide. This technique was found to be quantitative, and kinetic parameters are compared to those obtained by proton NMR spectroscopy or UV/Vis spectroscopy. This study sets the stage for investigating THz emission technology as a tool for research and development involving enzymes, and for monitoring industrial processes in the food, cosmetic, detergent, pharmaceutical, and biodiesel sectors.

Keywords: Phage display; Enzyme; *Bacillus subtilis* lipase A (BSLA); Substrate micelles; Enzyme cascade; crosslinking; Microenvironment; Glucose oxidase; Horseradish peroxidase; *Candida Antarctica* lipase B (CALB); Terahertz emission; Milk.

RÉSUMÉ

Dans certains cas, l'utilisation d'enzymes est confrontée à des défis tels que l'instabilité dans des conditions extrêmes, la purification des produits intermédiaires de chaque étape d'une réaction à plusieurs étapes, ou même la recherche de la technologie appropriée pour suivre la réaction de manière prédominante lorsque l'échantillon ou la matière première sont complexes. Pour répondre à ce besoin, en plus de l'ingénierie des enzymes, l'immobilisation sur un support solide est devenue un standard, bien que les tendances récentes soient plus axées sur l'ingénierie du microenvironnement. Dans cette thèse, nous avons exploré l'effet modélisé du phage sur l'activité enzymatique. Nous avons évalué l'effet des paramètres de la solution sur l'activité catalytique de la lipase A de *Bacillus subtilis* (BSLA) affichée par le phage. Alors que les profils d'activité en fonction du pH et de température de la BSLA n'étaient pas affectés par l'affichage du phage, la distribution à l'échelle nanométrique de la BSLA dans le tampon d'essai micellaire l'était. Cela a causé une augmentation prononcée de l'activité du phage-BSLA par rapport à l'enzyme libre, en raison de l'accumulation du phage-BSLA dans les micelles riches en substrat. Compte tenu de ce résultat, il convient de faire attention lors de la sélection d'autres enzymes/protéines par affichage phagique, car l'activité de la protéine affichée peut différer de celle de la protéine libre.

Ensuite, la glucose oxydase et la peroxydase de raifort ont été immobilisées sur la protéine d'enveloppe majeure P8 du phage-BSLA, ces trois enzymes effectuant ensemble une réaction en cascade. Puis, les phages ont été réticulés par des interactions biotine-streptavidine, ce qui semble créer un microenvironnement différent autour des enzymes. Nos résultats indiquent que la cascade de trois enzymes, BSLA→GOx→HRP, peut en effet être améliorée par rapport aux enzymes libres en solution par la fixation d'un modèle sur un phage. En fin de compte, cette étude de preuve de concept suggère que les systèmes de cascade d'enzymes modélisés par des phages peuvent être des plateformes prometteuses pour la fabrication écologique, bien que la prédiction de l'effet du microenvironnement sur toutes les enzymes reste un défi.

Enfin, nous avons étudié la technologie d'émission terahertz (THz) pour le suivi sans étiquette des changements chimiques. Les réactions enzymatiques sont généralement surveillées à l'aide de substrats de substitution qui produisent des signaux optiques quantifiables. Dans cette étude, la technologie d'émission THz est utilisée comme une technique non invasive et sans marqueur pour surveiller la cinétique de l'hydrolyse induite par la lipase de plusieurs molécules de substrat (y compris le substrat complexe qu'est le lait de vache entier) et l'oxydation catalysée par la peroxydase de raifort de l'o-phénylènediamine en présence de peroxyde d'hydrogène. Cette technique s'est avérée quantitative, et les paramètres cinétiques sont comparés à ceux obtenus par spectroscopie RMN des protons ou par spectroscopie UV/Vis. Cette étude ouvre la voie à l'étude de la technologie d'émission THz en tant qu'outil de recherche et de développement impliquant des enzymes.

Mots clés : Affichage de phages ; Enzyme ; lipase A de *Bacillus subtilis* (BSLA) ; micelles de substrat ; cascade d'enzymes ; réticulation ; microenvironnement ; glucose oxydase ; peroxydase de raifort ; lipase B de *Candida antarctica* (CALB) ; émission térahertz ; lait.

SYNOPSIS

Titre : Phénomènes à l'échelle nanométrique influençant les enzymes révélées par les phages et technologies émergentes pour analyser l'activité vers des substrats complexes

1. INTRODUCTION

Les enzymes catalysent les réactions chimiques avec une grande spécificité et efficacité. Leur utilisation industrielle fait donc l'objet d'une demande croissante, en particulier dans le domaine des soins de santé et de la fabrication "verte".¹⁻⁴ Les enzymes sont couramment utilisées pour la production de produits de la vie quotidienne, tels que le papier, le textile, l'alimentation, les aliments pour animaux, les produits de nettoyage, les produits chimiques et pharmaceutiques, etc. Certaines des enzymes les plus utilisées industriellement sont les lipases,⁵ α -amylase,⁶ protéase,⁷ lactase,⁸ estérase,⁹ phospholipases,¹⁰ pectinases,¹¹ etc. La combinaison de plusieurs enzymes ensemble réalise également des réactions utilisées dans notre vie quotidienne. Par exemple, les détergents sont complétés par des protéases, des lipases, des amylases, des oxydases, des peroxydases et des cellulases afin de rompre différents types de liaisons chimiques dans l'eau. Il est essentiel qu'ils conservent leur activité à des températures élevées (60 °C) et à des valeurs de pH élevées (pH 9-11), particulièrement lorsqu'ils sont mélangés à d'autres composants de la poudre à laver. En outre, la combinaison de réactions enzymatiques dans un processus bio-catalytique en plusieurs étapes et en un seul pot apporte des avantages supplémentaires, notamment le fait qu'il n'est pas nécessaire d'isoler les intermédiaires de réaction car ils sont directement transférés à l'étape suivante de la séquence réactionnelle.¹²⁻
¹⁴Ainsi, en raison de la forte demande d'enzymes, les chercheurs se concentrent sur l'identification et la production de biocatalyseurs robustes, stables et adaptés à une application dans une gamme plus large de processus industriels.

Tout d'abord, le développement de la technologie moderne de l'ADN recombinant permet aux chercheurs de produire des enzymes à partir de micro-organismes recombinants, et de modifier la fonction d'une enzyme en termes de stabilité, de spécificité et de stéréosélectivité. Le réglage des enzymes par l'ingénierie des protéines permet de créer des enzymes qui fonctionnent mieux dans des conditions non naturelles, comme dans des solvants organiques ou à des pH ou températures extrêmes, ou avec des substrats non naturels.¹⁵ Par exemple, en changeant un seul acide aminé (Asn336Ser) de l'amine oxydase, on obtient une large spécificité de substrat et

une haute énantiosélectivité vis-à-vis d'une large gamme d'amines chirales par rapport à l'enzyme de type sauvage. ¹⁶

Ensuite, l'immobilisation de l'enzyme sur un support solide ou une modification chimique augmente également la stabilité et la réutilisabilité des enzymes. Alors que les approches génétiques permettent la découverte,^{17,18} la mutation¹⁷ et la conception de nouveau design¹⁹ d'enzymes ayant l'activité désirée, l'immobilisation est tout aussi importante pour doter les catalyseurs enzymatiques de caractéristiques importantes pour les applications pratiques, notamment la résistance mécanique, la réutilisabilité, la stabilité et même une meilleure performance catalytique.²⁰⁻²⁴ Le comportement des enzymes immobilisées diffère de celui des enzymes dissoutes en raison des effets du matériau de support, ou matrice, ainsi que des changements de conformation de l'enzyme qui résultent des interactions avec le support et de la modification covalente des résidus d'acides aminés.

Enfin, la tendance plus récente de l'ingénierie enzymatique est une approche qui se concentre sur le contrôle de l'environnement à l'échelle nanométrique et microscopique d'une enzyme dans le but de promouvoir des conditions optimales à proximité de l'enzyme malgré des conditions défavorables dans l'environnement global. Un microenvironnement favorable peut améliorer les performances de l'enzyme en contrôlant le pH et la température locaux, en concentrant les réactifs et les cofacteurs, en améliorant l'efficacité des réactions par compartimentation (en particulier pour les réactions en cascade), etc. Ces effets peuvent être utiles pour réguler la performance de l'enzyme sans nécessiter d'ingénierie de l'enzyme. ²⁵ Par exemple, les interactions électrostatiques entre un substrat chargé et des résidus de charge opposée à la surface de l'enzyme peuvent augmenter la concentration locale du substrat à proximité du site actif de l'enzyme. Par conséquent, l'ADN est lié à l'enzyme pour créer des structures enzyme-ADN qui renforcent les interactions de liaison substrat-enzyme loin du site actif, ce qui entraîne une augmentation des concentrations locales de substrat, réduisant efficacement la constante de Michaelis apparente ($K_{M,app}$) et entraînant des taux catalytiques plus élevés à de faibles concentrations globales de substrat. ^{26,27} Il est donc très intéressant de trouver des moyens d'optimiser la performance des enzymes, de nouvelles stratégies d'ingénierie du microenvironnement et de comprendre les mécanismes sous-jacents. La plupart du temps, l'ingénierie du microenvironnement est la combinaison de l'ingénierie des protéines et de l'immobilisation car ces deux événements créent une distribution modifiée à l'échelle nanométrique autour de l'enzyme (**Figure 1**).

En outre, la plupart des processus biologiques sont en fait accomplis par des voies de synthèse multi-enzymes. Par exemple, le métabolisme du glucose par la glycolyse implique la participation de dix enzymes qui travaillent de manière séquentielle et efficace. Sur le plan industriel, la combinaison de réactions enzymatiques dans un processus bio-catalytique à plusieurs étapes et à un seul pot apporte des avantages supplémentaires, notamment l'absence de nécessité d'isoler les intermédiaires réactionnels, car ils sont directement transférés à l'étape suivante de la séquence réactionnelle. Globalement, cela peut réduire les coûts, le temps, les efforts et augmenter le rendement final du produit.

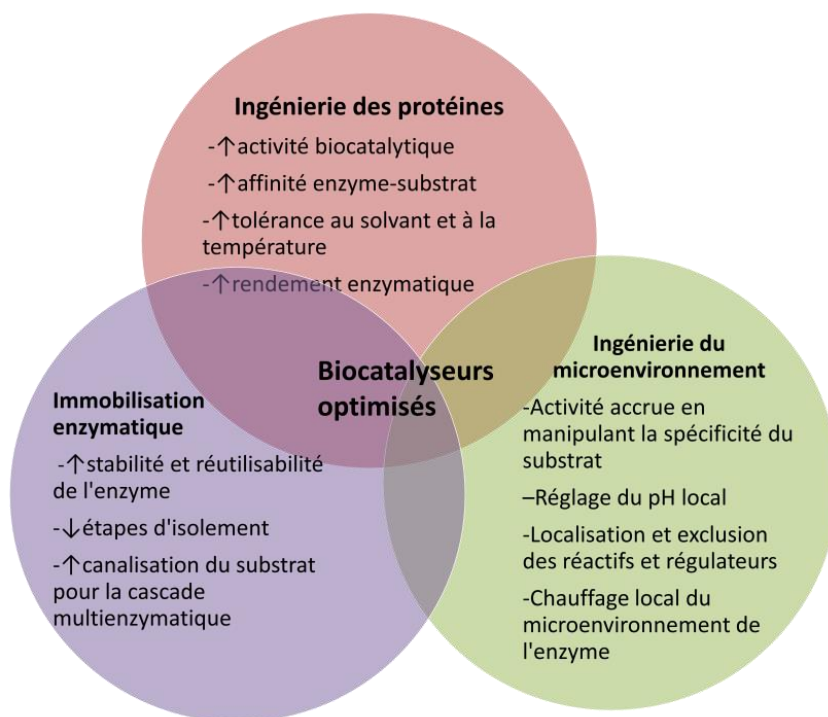


Figure 1: Représentation schématique d'une approche multidisciplinaire visant à créer des biocatalyseurs optimaux. La mise en œuvre des biocatalyseurs dans les technologies industrielles devra non seulement tenir compte de l'optimisation de la fonctionnalité de l'enzyme, mais aussi de l'augmentation de la stabilité opérationnelle de l'enzyme à l'interface avec les supports utilisés pour l'immobilisation.

En outre, l'utilisation d'enzymes dans divers domaines est parfois confrontée à des difficultés liées à la difficulté de trouver les bons outils et la bonne technologie analytique pour surveiller la réaction enzymatique. Cela est particulièrement vrai lorsque le produit de départ est complexe (c'est-à-dire des mélanges de substrats), hétérogène et absorbe/diffuse la lumière, ou même lorsque la cinétique de la réaction est trop rapide pour être suivie par des techniques conventionnelles (par exemple, la chromatographie). La plupart des réactions enzymatiques sont

contrôlées à l'aide de substrats de substitution qui produisent des signaux commodément quantifiables (par exemple, optiques) dans des conditions de réaction modèles qui simplifient l'analyse. Pour répondre à ces besoins non satisfaisant, dans cette thèse, nous avons essayé de comprendre :

1) **L'effet du modelage sur un modèle à l'échelle nanométrique, et l'influence de ce modèle sur la distribution à l'échelle nanométrique en solution.** Pour explorer cette possibilité, le bactériophage M13 a été utilisé comme modèle à l'échelle nanométrique où la lipase A de *Bacillus subtilis* (BSLA) a été exprimée sur sa protéine d'enveloppe mineure p3 comme protéine de fusion. L'activité de la BSLA fixée par le phage a été comparée à celle de la BSLA libre en modifiant les environnements de réaction, c'est-à-dire le pH, la force ionique du tampon, la température et l'ajout de PEG non réactif.

2) Ayant constaté que la distribution à l'échelle nanométrique a un effet important sur l'activité, nous avons **exploré le potentiel de la distribution à l'échelle nanométrique, par l'oligomérisation contrôlée d'enzymes placées sur un modèle à l'échelle nanométrique. De plus, nous avons exploré l'influence de la distribution à l'échelle nanométrique sur la communication entre les enzymes.** Pour atteindre cet objectif, deux autres enzymes, la glucose oxydase (GOx) et la peroxydase de raifort (HRP), ont été fixées à la protéine d'enveloppe majeure p8 sur la matrice du phage portant la BSLA. Ces trois enzymes participent ensemble à une réaction en cascade. Ce phage M13 porteur d'enzymes (c'est-à-dire un modèle nanométrique) a été oligomérisé par réticulation et l'effet de l'oligomérisation sur la réaction en cascade des enzymes a été étudié.

3) Par la suite, nous avons **mis au point une technique analytique adaptée à l'analyse de substrats complexes, et pouvant être utilisée avec les enzymes complexes immobilisées à l'échelle nanométrique mentionnées ci-dessus.** En se basant sur ces résultats, nous avons examiné si la technologie d'émission THz peut être utilisée pour l'enzymologie quantitative en temps réel et sans marquage d'une lipase vis-à-vis de quatre substrats " optiquement inactifs ", notamment le butyrate de méthyle (BuOMe), l'acétate d'éthyle (AcOEt), l'octanoate de méthyle (OcOMe) et l'acétate de benzyle (AcOBn), ainsi que pour l'analyse qualitative d'un substrat " complexe " modèle, le lait de vache entier.

2. MÉTHODES EXPÉRIMENTALES

2.1 L'effet du modelage sur un modèle à l'échelle nanométrique, et l'influence de ce modèle sur la distribution des nanoparticules en solution

2.1.1 Affichage du phage M13 de la lipase A de *Bacillus subtilis* (BSLA)

Conception des amorces, construction des plasmides et affichage des phages de BSLA

BSLA a été exprimé sur la protéine d'enveloppe mineure p3 du phage M13 par une méthode d'affichage basée sur le « phagemid ». La séquence d'ADN de *LipA* a été acquise à partir de l'ADN génomique de *B. subtilis* (ATCC® Number: 23857D-5™, Cedarlane, Canada) en utilisant l'amorce directe et inverse comme suit : LIPF-5' ATAT **GGCC CAGC C GGCCATG** GCG ATG AAA TTT GTA AAA AGA 3', LIPR-5' ATAT **GGCC TCCCG GGCC** TTA ATT CGT ATT CTG GCC 3'. Les sites de restriction sont mentionnés en gras italique. La séquence *lipA* a été amplifiée à partir de l'ADN génomique de *B. subtilis* 168 en utilisant les amorces LIPF et LIPR. La PCR a été réalisée en utilisant l'ADN polymérase Phusion HF avec le protocole PCR : 30 s 98 °C, 35 cycles de 10 s 98 °C, et 15 s 72 °C. À la fin, la production d'ADN a été terminée pendant 10 min à 72 °C. Le fragment de gène amplifié a été purifié à l'aide du kit de purification QIAquick PCR (QIAGEN) digéré avec SfiI. Le gène codant 639-bp pour BSLA a été cloné dans le phagemid pADL-20c (Antibody Design Laboratories) pour construire le plasmide recombinant selon le protocole du fabricant. L'ADN d'insertion purifié et digéré et le phagemid ont été ligaturés à l'aide de la ligase T4 et transformés en cellules ultracompétentes XL10-Gold selon le protocole du fabricant. Avant l'affichage du phage, la cellule transformée a été séquencée pour vérifier la séquence correcte des paires de bases (Plate-forme d'Analyses Génomiques, Université Laval, Québec). Le stock a été conservé à -80 °C avec 50% de glycérol jusqu'à son utilisation.

Les bactéries contenant des phagémides ont été inoculées dans une plaque d'agar LB et incubées pendant la nuit à 37°C. Une seule colonie a été cultivée dans 3 mL de 2x YT à 37°C dans un incubateur à agitateur pendant la nuit, puis on a procédé à une PCR avec les amorces LIPF et LIPR. Seuls les tubes positifs à la PCR ont poursuivi leur croissance jusqu'à ce qu'une DO de 0,5 à 600 nm soit atteinte. Dans cette phase de croissance exponentielle, 1 µL de phage auxiliaire (provenant d'un stock de $2,0 \times 10^{12}$ pfu/mL) a été ajouté à chaque 1 mL de culture bactérienne (à une concentration finale de 2×10^9 phages/mL). Après 16 h de croissance à 30 °C (incubateur à agitation), la culture a été centrifugée et le surnageant contenant les phages a été transféré dans un autre tube, laissant les bactéries dans le culot, et les phages ont été précipités par l'addition de PEG/NaCl contenant 20 % p/v de polyéthylène glycol (8 kDa)/2,5 M NaCl. Les phages précipités ont été remis en suspension dans 0,5 ml de tampon Tris-HCl 10 mM (pH 7,4). Le nombre de particules de phage en suspension a été déterminé par

spectrophotométrie. La relation entre le nombre de virions et l'absorption a été calculée à l'aide de l'équation suivante : $\text{Virions/mL} = (\text{Ab}_{269} - \text{Ab}_{320}) \times (6 \times 10^{16}) \div 4569$

2.1.2 Activité enzymatique des phages-BSLA

Le tampon d'essai pour mesurer l'activité catalytique était composé de 50 mM de phosphate de sodium, pH 8, 0,36% de Triton X-100 (v/v) et 0,1% (p/v) de gomme arabique. Ce tampon a été utilisé pour tous les essais enzymatiques et modifié si nécessaire pour étudier l'effet des additifs. L'activité enzymatique a été déterminée par spectrophotométrie via l'hydrolyse de l'octanoate de 4-nitrophényle (4-NPO). Le K_M , la vitesse maximale (V_{\max}) et le nombre de tours (k_{cat}) de la lipase native et de celle liée aux phages ont été déterminés en utilisant des concentrations de substrat allant de 0,05 mM à 2 mM dans 0,1 mL de tampon de test en présence de 1,9 $\mu\text{g/mL}$ de lipase ou de 5×10^{12} particules de phage/mL. L'absorbance a été mesurée à 410 nm pour la production de 4-nitrophénol. Dans tous les cas, l'hydrolyse de fond du substrat dans les témoins sans enzyme (blancs) a été soustraite des données de l'échantillon. Les réactions ont été répétées en trois exemplaires.

2.1.3 Effet des additifs sur l'activité enzymatique

Pour évaluer l'effet des additifs sur l'activité enzymatique, on a utilisé dans tous les cas la BSLA native (1,2 $\mu\text{g/mL}$) et la BSLA phagique (1×10^{12} particule de phage) avec 0,2 mM de 4-NPO. Par la suite l'activité a été mesurée en présence de tous les additifs. L'effet du pH sur l'activité de la lipase a été mesuré dans le tampon d'essai ayant différents pH (pH 4-12). L'activité enzymatique a également été mesurée dans des solutions équivalentes contenant 0,5 mM de NaCl. Pour mesurer l'activité enzymatique en présence de sel, des cristaux solides de NaCl ont été ajoutés au tampon d'essai pour atteindre des concentrations finales de 0 à 2000 mM, et l'activité enzymatique a été mesurée. L'effet du PEG ou du phage M13 de type sauvage en tant qu'agents d'encombrement sur l'activité catalytique de la BSLA native et phagique a été évalué à différentes concentrations (en pourcentage) de PEG (8 kDa ; 0-20 % en poids) ajoutées au tampon d'essai. Pour observer l'effet du M13 de type sauvage, une solution mère de M13 (3×10^{15} phages/mL) a été préparée dans un tampon TBE 1x (tampon Tris-HCl 10 mM, pH 7,4, contenant 1 mM d'EDTA) et 0,12 μL ou 1,2 μL de cette solution a été ajouté à 100 μL de tampon d'essai pour obtenir 0,069 ou 0,697 mg/mL de phage. La concentration de phage en solution a été calculée en utilisant le poids moléculaire de M13 ($1,2 \times 10^7$ Da). L'effet de la température sur l'activité de la lipase a été mesuré dans une plage de 24 à 70 °C. Alternativement, la BSLA native

et la BSLA avec phage ont été incubées à des températures de 24 - 80 °C pendant 20 minutes, puis l'activité a été mesurée à température ambiante avec le phage-BSLA traité thermiquement. De plus, les BSLA natifs et les phages ont été incubés à 65 °C pendant 2 à 20 min, puis l'activité a été mesurée à r.t. Les réactions ont été répétées en trois exemplaires.

2.2 Exploration du potentiel de la distribution à l'échelle nanométrique par l'oligomérisation d'enzymes placées sur un modèle à l'échelle nanométrique

2.2.1 Conception et concept des oligomères

Le phage-BSLA a été choisi comme modèle à l'échelle nanométrique, tandis que les deux autres enzymes, la glucose oxydase (GOx) et la peroxydase de raifort (HRP), ont été attachées au phage scaffold en utilisant des interactions non covalentes de haute affinité. Plus précisément, la HRP a été immobilisée sur protéine majeure de l'enveloppe de la P8 sous la forme d'un conjugué anticorps anti-P8-HRP. En revanche, la GOx-biotine a été immobilisée par l'intermédiaire d'un conjugué anti-P8-biotine et d'un lieur de streptavidine. Un tampon phosphate 10 mM pH 7,4 a été utilisé pour la préparation des échantillons et les tests enzymatiques. Le ratio BSLA-phage : GOx : HRP a été maintenu constant à 1 :1 :1 et la quantité d'anti-P8-biotine et de streptavidine a été modulée pour contrôler la densité de réticulation (**Figure 7a**). En bref, la GOx-biotine et l'anti-P8-biotine ont été ajoutées au tampon phosphate (10 mM, pH 7,4), puis la streptavidine a été ajoutée. La solution a été incubée pendant 2 heures à température ambiante sur un rotateur. Ensuite, l'anti-P8-HRP a été ajouté, mélangé, et enfin le BSLA-phage a été ajouté. Puis la solution a été incubée pendant 2 heures à température ambiante sur un agitateur rotatif, puis conservée à 4 °C jusqu'à une analyse ultérieure. Un échantillon témoin a également été préparé en remplaçant le BSLA-phage par du BSLA libre en l'absence de lieurs. La première enzyme de la cascade, BSLA, hydrolyse le 6-O-acétyl glucose pour produire du D-glucose, qui est ensuite oxydé par GOx pour produire du peroxyde d'hydrogène. La HRP utilise ensuite ce peroxyde d'hydrogène pour convertir l'o-phényl diamine (oPD) en 2,3-diaminophénazine (DAP), qui peut être mesurée par spectroscopie.

2.1.2 Cinétique de Michaelis-Menten des enzymes avant et après immobilisation

Une analyse cinétique de la HRP a été réalisée par spectrophotométrie. Des solutions mères de HRP (5 nM) et d'anti-P8-HRP (5 nM) avec le phage-BSLA (8,3 nM) ont été préparées dans un tampon phosphate 10 mM à pH 7,4. La concentration de l'oPD a varié dans la gamme de 0,03 à

2 mM tandis que la concentration de H₂O₂ était fixée à 1 mM dans les réactions. L'analyse cinétique de la GOx a été réalisée sous forme de réaction couplée avec la HRP en présence d'un excès d'anti-p8-HRP, de sorte que l'activité de la GOx soit l'étape limitant la vitesse de la réaction. Dans les conditions examinées ci-dessous, un excès de 3 fois l'anti-P8-HRP a été utilisé afin que la vitesse de réaction devienne indépendante de la concentration de HRP. Un échantillon en cascade a été préparé dans un tampon phosphate 10 mM pH 7,4 contenant 6,7 nM d'anti-P8-biotine, 2 nM de streptavidine, 6,7 nM de GOx-biotine, 25 nM d'anti-P8-HRP sur 8,3 nM de phage-BSLA. Des concentrations similaires de GOx-biotine et d'anti-P8-HRP ont été utilisées pour préparer une solution où l'anti-P8-biotine, la streptavidine et le phage-BSLA étaient absents. Pour mesurer la cinétique de la réaction, le D-glucose a été utilisé dans une gamme de 10-70 mM tandis que la concentration de l'oPD était fixe (30 mM). Dans tous les cas, la production de DAP a été mesurée à 415 nm ($\epsilon_{415} = 16,700 \text{ M}^{-1}\text{-cm}^{-1}$) en fonction du temps. L'analyse cinétique de la BSLA a été déterminée par l'hydrolyse de la 4-NPO. Une solution mère de 10 mM de 4-NPO dans du méthanol a été préparée. Des réactions avec différentes concentrations de la solution de 4-NPO (0,05-4 mM) ont été préparées dans 0,1 mL de tampon d'essai (tampon phosphate 50 mM contenant 0,1% de gomme arabique et 0,36% de Triton X-100). La réaction a été initiée par des enzymes à une concentration finale de 343 nM de BSLA ou 64 nM de phage-BSLA et l'absorbance a été mesurée à 410 nm pour la production de 4-nitrophénol (coefficient d'extinction molaire 18 000 M⁻¹-cm⁻¹). Dans tous les cas, les échantillons témoins ne contenant pas d'enzyme ont été soustraits des données des échantillons correspondants pour tenir compte de la dégradation du substrat. Les réactions ont été répétées en trois exemplaires.

2.2.3 Activité catalytique de l'enzyme simple et de l'enzyme en cascade en utilisant des oligomères

Pour l'activité HRP de **1-5**, des solutions de réaction ont été préparées avec 5 µL d'oPD (à partir d'un stock de 0.1 M dans PBS), 1 µL de H₂O₂ (à partir d'un stock de 0.1 M) dans 84 µL de PBS, et finalement 10 µL des solutions de stock de **1-5** (les échantillons de cascade assemblés) ont été ajoutés pour commencer la réaction. Pour l'activité GOx → HRP de **1 à 7**, des solutions de réaction ont été préparées avec 5 µL d'oPD (à partir d'un stock de 0,1 M dans du PBS), 10 µL de D-glucose (à partir d'un stock de 0,1 M), dans 75 µL de PBS, et finalement 10 µL des solutions mères de **1 à 7** ont été ajoutés pour commencer la réaction. Pour le HRP BSLA → GOx → des échantillons en cascade **1-7**, des solutions contenant 25 µL d'oPD (à partir d'un stock de 0,1 M dans du PBS) et 25 µL de 6-O-acétyl-D-glucose (à partir d'un stock de 0,2 M dans du PBS) ont été préparées. La catalyse a été initiée par l'addition de 50 µL des solutions mères de **1-7**. Dans

tous les cas, la production de DAP a été mesurée à 415 nm ($\epsilon_{415} = 16,700 \text{ M}^{-1}\text{-cm}^{-1}$) en fonction du temps. De plus, les échantillons témoins ne contenant pas d'enzyme ont été soustraits des données des échantillons correspondants pour tenir compte de la dégradation du substrat. Les réactions ont été répétées en triplicata.

2.3 Mise au point d'une technique analytique pour l'analyse de substrats complexes : Suivi quantitatif et sans étiquette de la cinétique enzymatique par émission de térahertz

2.3.1 Configuration optique Téraherertz

Le composant clé du montage optique térahertz est la plaque de détection, composée d'une couche de Si (600 nm d'épaisseur) déposée sur un substrat de saphir de 500 μm d'épaisseur. La couche supérieure s'oxyde naturellement en SiO_2 (épaisseur de $\sim 3 \text{ nm}$; **figure 2**). Le faisceau de la pompe optique frappe la plaque de détection à un angle d'incidence de 45° dans l'air, depuis le côté saphir, ce qui permet à la plaque de détection d'être parallèle à la table optique. Un porte-échantillon en plastique a été fabriqué par impression 3D et fixé à la plaque de détection avec un adhésif résistant à l'eau. Le rayonnement THz est généré à travers la couche de Si par l'accélération des porteurs libres par le champ de déplétion.

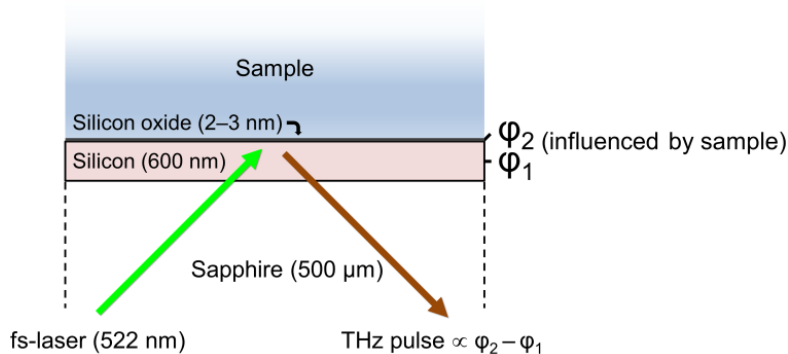


Figure 2 : L'émission THz émane d'une " plaque de détection " composée d'un film SiO_2/Si déposé sur un saphir de qualité laser. Une couche d'appauvrissement est formée près de la limite SiO_2/Si en raison de la flexion de la bande et donne lieu à un champ électrique local ($\phi_2 - \phi_1$). Lorsqu'un laser femtoseconde frappe la plaque de détection, des porteurs sont générés dans le film de Si, qui sont ensuite accélérés par ce champ. Cela génère une impulsion THz dans la direction spéculaire de la réflexion. L'amplitude du signal THz est influencée par l'échantillon, car la finesse de la couche de SiO_2 rend ϕ_2 sensible à la composition chimique de l'échantillon.

2.3.2 Surveillance de l'activité enzymatique à l'aide du dispositif optique THz

L'activité de l'enzyme *Candida antarctica* lipase B (CALB) avec quatre substrats " optiquement inactifs ", dont le butyrate de méthyle (BuOMe), l'acétate d'éthyle (AcOEt), l'octanoate de méthyle (OcOMe) et l'acétate de benzyle (AcOBn), a été comparée aux données obtenues par spectroscopie de résonance magnétique nucléaire (RMN ¹H). Les réactions pour CALB ont été réalisées dans un tampon phosphate 50mM, pH 8, contenant 0,1 vol% de Triton X-100 et 0,36% en poids de gomme arabique. À titre d'exemple représentatif, 168 µL de tampon de dosage ont d'abord été placés sur la plaque de détection. L'amplitude du signal THz a été enregistrée à intervalles de 9 secondes. Une fois que le signal THz est devenu stable (~2 minutes), 2,1 µL de BuOMe (pour atteindre une concentration finale de 100 mM) ont été ajoutés au puits d'échantillon et mélangés avec l'embout de la pipette pendant que l'amplitude THz était enregistrée en continu. Après environ 1 à 2 minutes, le signal THz est devenu stable, mais a été surveillé pendant 5 minutes pour visualiser un signal clairement stable. À ce stade, la réaction enzymatique a été initiée en ajoutant 5 µL de CALB (à partir du stock de 0,35 mM dans le tampon d'essai) pour atteindre une concentration finale de 9,7 µM. L'amplitude du THz a été surveillée jusqu'à ce que la réaction soit terminée (environ 10 minutes). Ce processus a été adapté pour obtenir différentes concentrations de substrat, et répété pour tous les autres substrats.

3. RÉSULTAT ET DISCUSSION

3.1 L'effet du modelage sur un modèle à l'échelle nanométrique, et l'influence de ce modèle sur la distribution des nanoparticules en solution

Nous avons affiché la BSLA sur le bactériophage M13, le phage filamenteux le plus couramment utilisé pour la technologie d'affichage des phages. De plus, les lipases sont largement utilisées dans l'industrie et les réactions typiques des lipases se produisent dans des émulsions organiques-aqueuses. BSLA était donc un excellent modèle pour étudier l'influence du phage scaffold sur l'activité enzymatique dans des solutions colloïdales complexes. Le système phagemid permet non seulement d'élargir la taille limite de la protéine affichée, mais aussi de maintenir un niveau d'affichage faible, de sorte que les protéines d'enveloppe de type sauvage conservent leur fonction naturelle. Dans notre cas, de zéro à une copie de BSLA a été affichée pour cinq copies de pIII, de sorte que le phage a encore restauré son ineffectivité ; cependant, en raison du niveau d'affichage variable, il était difficile d'estimer la concentration exacte de BSLA. Comme nous avons observé que le phage-BSLA et le BSLA libre donnaient une valeur KM

similaire pour l'hydrolyse de la 4-NPO à l'état d'équilibre ($0,42 \pm 0,06$ et $0,4 \pm 0,1$ mM pour le BSLA natif et le phage-BSLA respectivement) (**Figure 3a**).

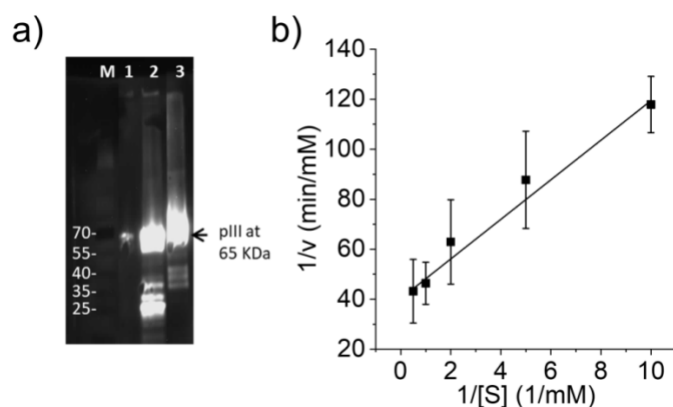


Figure 3 : Caractérisation du phage affiché BSLA. (a) Analyse Western Blot avec anticorps monoclonal anti-M13 p3 de souris (M : échelle de poids moléculaire, voie 1 : phage affiché BSLA, voie 2 : M13 de type sauvage, voie 3 : phage auxiliaire M13KO7). (b) Tracé de Lineweaver-Burke pour déterminer le k_M du phage affiché BSLA. Les données sont présentées sous forme de moyenne \pm SD (n = 3).

Ces résultats sont similaires aux données publiées par d'autres,²⁸ et suggèrent que la fusion de BSLA sur la capsid du phage n'a pas influencé l'affinité du substrat et que BSLA est correctement repliée. Cependant, comme la concentration de BSLA dans les échantillons de phage était difficile à estimer (en raison du niveau d'affichage variable), la concentration de BSLA native et de BSLA fixée sur le phage a été ajustée de façon empirique pour obtenir des taux de réaction similaires qui convenaient à l'analyse. Ensuite, les valeurs de V_{max} déterminées à partir de cette analyse ont été converties en nombres de rotation k_{cat} (mole de produit formé par mole de BSLA par seconde), pour comparer l'activité enzymatique sur une base molaire. Pour le phage-BSLA, le k_{cat} est rapporté au nombre de phages en solution, ce qui surestime la concentration en enzyme. La k_{cat} a été trouvée à $1,28 \text{ s}^{-1}$ et $5,6 \text{ s}^{-1}$ pour BSLA et phage-BSLA, respectivement. Une augmentation similaire de la k_{cat} a été observée par Dröge et al. (18 s^{-1} et 84 s^{-1} , respectivement, pour la lipase libre et la lipase affichée par le phage).²⁸ Ainsi, en conjonction avec l'analyse Western Blot (**Figure 3a**), l'augmentation de k_{cat} dans ces échantillons de phage, lorsqu'elle est normalisée à la concentration molaire de BSLA ou de phage, suggère que la BSLA affichée par le phage est substantiellement plus active que sa forme libre en solution. Pour mieux comprendre ces différences, des expériences ont été réalisées pour évaluer l'effet de l'affichage du phage sur les profils d'activité de l'enzyme en fonction du pH et de la température, ainsi que sur sa distribution à l'échelle nanométrique dans le tampon d'essai colloïdal. L'activité

optimale de la lipase de la souche 168 de *Bacillus subtilis* est de pH 10, alors qu'un pH optimal de 8-9 a été signalé pour les lipases de certaines espèces de *Bacillus* (Ma et al., 2006 ; Nawani, Khurana, & Kaur, 2006). Comme l'illustre la **figure 4a**, l'activité de la BSLA, qu'elle soit libre ou attachée à un phage, est optimale dans cette gamme de pH. L'ajout de NaCl 0,5 M à ces solutions a donné des conclusions similaires, bien que les valeurs absolues de l'activité aient augmenté d'un facteur de 2 à 4 pour le phage-BSLA (**Figure 4b**).

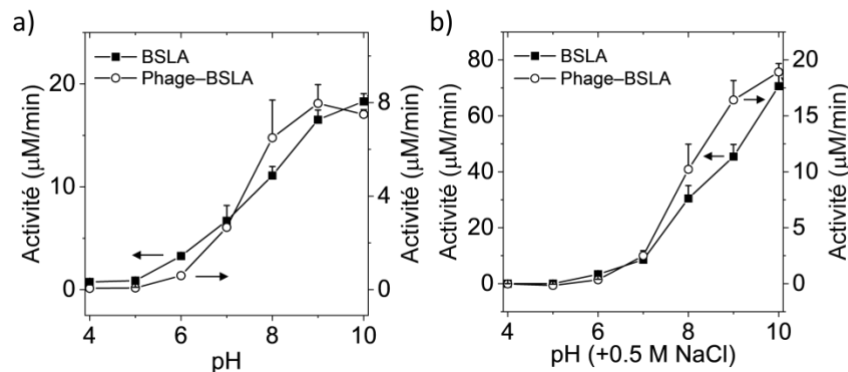


Figure 4 : Profils pH-activité pour BSLA et phage-BSLA. L'activité a été mesurée soit dans le tampon d'essai (a), soit dans le tampon d'essai complété par 0,5 M NaCl (b). Les données sont présentées en tant que moyenne + SD (n = 3).

Afin de déterminer si l'affichage phagique modifiait la stabilité de l'enzyme, l'activité catalytique a été mesurée à différentes températures, ainsi qu'à température ambiante après une pré incubation à une température donnée pendant 20 min. Dans la **figure 5a**, l'activité a augmenté en fonction de la température pour les deux formes de BSLA, et une augmentation de 2 à 3 fois de l'activité a été observée entre la température ambiante et 65°C pour les deux échantillons. Aucun effet important du phage display sur l'activité dépendant de la température n'a été observé. Ensuite, les enzymes ont été incubées pendant 20 minutes à différentes températures, puis l'activité a été mesurée (**Figure 5b**). Les résultats montrent que les deux formes de BSLA commencent à perdre leur activité à 30°C, et que l'activité diminue progressivement avec la température. Aucune différence évidente n'a été observée entre BSLA et phage-BSLA. En ce qui concerne la stabilité à haute température, la BSLA et le phage-BSLA ont été incubés à 65°C pendant différents temps, puis l'activité a été évaluée à t.r. (**Figure 5c**). Les résultats montrent que la BSLA native perd ~33% d'activité en 2 min, mais reste stable par la suite. En revanche, le phage-BSLA a perdu la plupart de son activité en 10 minutes, ce qui suggère qu'un autre mécanisme de perte d'activité pourrait être en jeu.

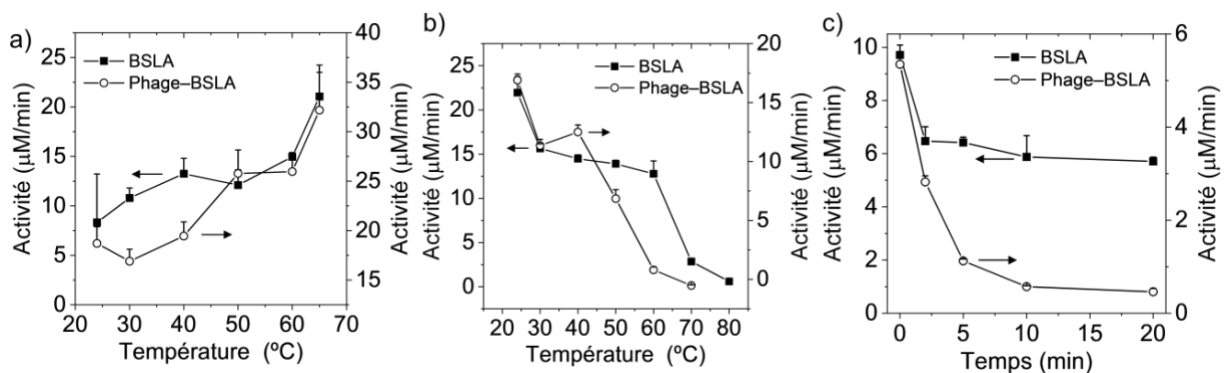


Figure 5 : **Stabilité thermique de BSLA et de phage-BSLA. (a) Activité catalytique mesurée en fonction de la température. (b) Activité catalytique mesurée au r.t., après une pré-incubation à température variable pendant 30 minutes. (c) Activité catalytique mesurée au r.t. après une pré-incubation à 65°C pendant différents temps. Les données sont présentées sous forme de moyenne + écart-type (n = 3). BSLA, *Bacillus subtilis* Lipase A ; r.t., température ambiante.**

Étant donné que l'affichage du phage ne semble pas affecter l'environnement local ou la stabilité de la BSLA, l'activité accrue de la BSLA-phage par rapport à la BSLA libre pourrait résulter d'une distribution différente à l'échelle nanométrique dans le tampon d'essai hétérogène. Par exemple, l'accumulation près des micelles riches en substrat pourrait entraîner une activité accrue.

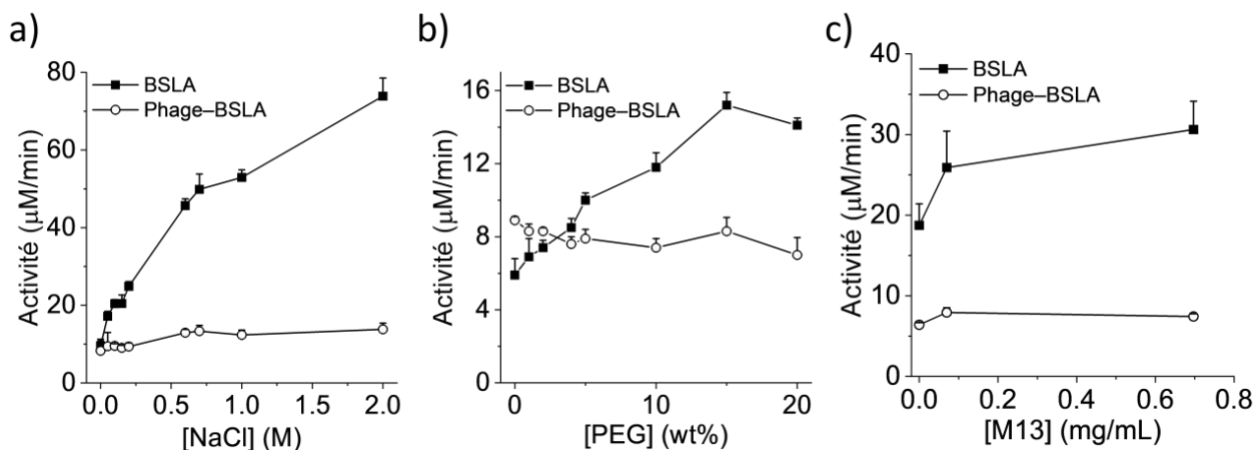


Figure 6: **Effet du sel, du PEG et du phage de type sauvage sur l'activité catalytique. Influence du NaCl (a), du PEG 8 kDa (b), et du M13 de type sauvage (c) sur l'activité catalytique de BSLA et du phage-BSLA. Les données sont présentées en tant que moyenne + SD (n = 3). BSLA, *Bacillus subtilis* Lipase A ; PEG, poly (éthylène glycol).**

Pour caractériser cette possibilité, l'effet de la concentration en sel sur l'activité enzymatique a été évalué tout en maintenant un pH constant de 8. L'activité de la BSLA a augmenté d'un facteur de ~16 sur la gamme de concentration en sel examinée, alors que l'activité moyenne de la phage-BSLA est restée constante sur cette même gamme (**Figure 6a**). Ce résultat suggère que la BSLA et la phage-BSLA se trouvent dans des environnements nanométriques qui répondent très différemment au sel, ce qui pourrait être à l'origine de l'activité apparente plus élevée de la phage-BSLA par rapport à la BSLA native. En effet, une explication possible de cette observation est que le phage-BSLA peut être partiellement associé aux micelles de gomme arabique/ Triton-X (qui contiennent le substrat hydrophobe 4-NPO) et que la présence du BSLA est plutôt prédominante dans la phase aqueuse où la concentration du substrat est beaucoup plus faible. Ainsi, une augmentation de la concentration en sel pousserait la BSLA de la phase aqueuse vers les micelles, ce qui s'apparente à un effet de relargage. Pour valider cette hypothèse, du poly (éthylène glycol) (PEG, 8 kDa) a été ajouté au tampon d'essai, en raison de sa capacité connue à exercer un effet de volume exclu sur les protéines en solution. L'ajout de PEG 8 kDa à la solution devrait chasser les protéines et les phages de la phase aqueuse (c'est la prémisse de la précipitation des protéines et des phages induits par le PEG), et potentiellement vers l'interface des micelles. Comme l'illustre la **figure 6b**, l'activité de la BSLA a progressivement augmenté pour atteindre le triple de sa valeur initiale après l'ajout de PEG, ce qui suggère une redistribution de la BSLA vers les micelles riches en substrat. En revanche, l'activité de la phage-BSLA n'a pas été affectée par la présence de PEG. Ces résultats combinés suggèrent que la différence d'activité entre BSLA et phage-BSLA réside principalement dans l'association préférentielle du phage-BSLA avec les micelles de substrat. Enfin, pour valider que les phages eux-mêmes n'affectent pas d'une manière ou d'une autre l'activité, par exemple en modifiant la structure des micelles contenant le substrat, le phage M13 de type sauvage a été ajouté au tampon de test. En effet, alors qu'une augmentation rapide de l'activité de la BSLA libre a été observée après l'ajout d'une petite quantité de phage, l'augmentation globale de l'activité était faible (< ~1,5 fois) et s'est rapidement stabilisée à une concentration plus élevée de phage (**Figure 6c**). Dans l'ensemble, ce travail illustre que le microenvironnement et la stabilité de BSLA ne semblent pas être intrinsèquement affectés par l'affichage du phage, bien que le phage ait modifié la distribution à l'échelle nanométrique de BSLA dans le tampon d'essai micellaire.

3.2 Exploration du potentiel de la distribution à l'échelle nanométrique par l'oligomérisation d'enzymes placées sur un modèle à l'échelle nanométrique

Conception et concept des oligomères

Après avoir considéré que ni le microenvironnement ni la stabilité de BSLA n'étaient affectés par la présence du phage, nous avons présenté dans le deuxième chapitre un modèle de cascade de trois enzymes, où les trois enzymes étaient immobilisées sur le même phage. GOx-biotine a été immobilisée sur la protéine d'enveloppe majeure P8 du phage-BSLA via un conjugué anti-P8-biotine et une liaison streptavidine. En raison de l'une des plus fortes interactions non covalentes connues dans la nature rapportée à ce jour (l'affinité de liaison, K_a , est de $\sim 10^{15} \text{ molL}^{-1}$)²⁹⁻³¹, le complexe streptavidine-biotine est largement utilisé dans divers outils biologiques, notamment pour les étiquettes d'affinité, la détection et l'immobilisation des protéines et les applications de détection biochimique, en particulier dans l'identification de nouvelles cibles médicamenteuses possibles³². Cette plateforme de conjugaison a été considérée comme idéale pour étudier les possibilités et les limites des réactions en cascade déclenchées par les phages, en raison de la commodité de maintenir constant le ratio des enzymes, tout en contrôlant le degré de réticulation des phages via les quantités relatives de streptavidine et d'anti-P8-biotine (**figure 7**).

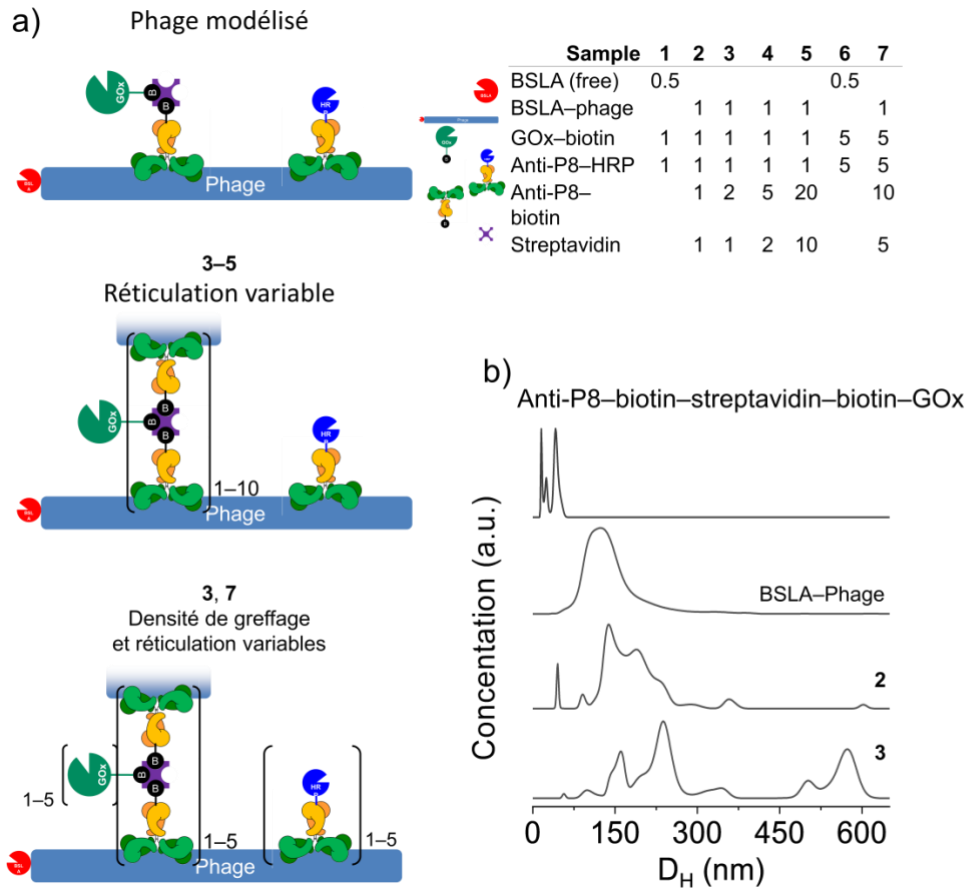


Figure 7 : Illustration de la cascade de phages étudiée dans cette étude. (a) Stœchiométrie des composants utilisés pour assembler les cascades. (b) Analyse NTA de BSLA-phage et 2.

La caractérisation de l'immobilisation de l'enzyme a été suivie par une analyse de suivi des nanoparticules (NTA). L'analyse de BSLA-phage par NTA révèle une population d'espèces monomères en solution, avec une taille de ~125 nm. L'analyse de l'échantillon 2 (non réticulé) a montré plusieurs populations d'espèces en solution, avec des populations majeures à ~140 nm 190nm, 235 nm. Considérant que le diamètre hydrodynamique (D_H) approximatif d'un anticorps de la famille des immunoglobulines G est de ~12 nm, l'augmentation de 125 à 140-235 nm reflète approximativement l'addition des composants au phage (anti-P8-HRP, anti-P8-biotine, streptavidine, GOx-biotine).

Effet direct de l'immobilisation des phages

Pour évaluer l'effet de l'immobilisation des enzymes sur la matrice phagique, une analyse de Michaelis-Menten a été réalisée (**Figure 8**). En général, l'immobilisation des enzymes sur la matrice phagique a eu un effet intrinsèque sur l'activité de toutes les enzymes, comme l'indique une faible augmentation du K_M . Ceci pourrait éventuellement suggérer une petite perturbation structurale de la protéine conduisant à une distorsion du site catalytique. Les valeurs obtenues sont similaires à celles trouvées dans la littérature pour ces enzymes/substrats.^{28,33,34} De plus, une augmentation d'environ 3 fois de la k_{cat} a été observée pour la HRP, alors que la k_{cat} de GOx n'a pas été modifiée par l'immobilisation sur le phage. Une augmentation d'environ 6 fois de la k_{cat} a été observée pour BSLA, ce qui est cohérent avec des observations antérieures lors de l'utilisation de solutions micellaires d'octanoate de 4-nitrophényle (4-NPO) comme substrat.³⁴ Augmentation de k_{cat} a été rationalisée par une interaction préférentielle du phage BSLA avec les micelles du substrat, par rapport au BSLA seul.

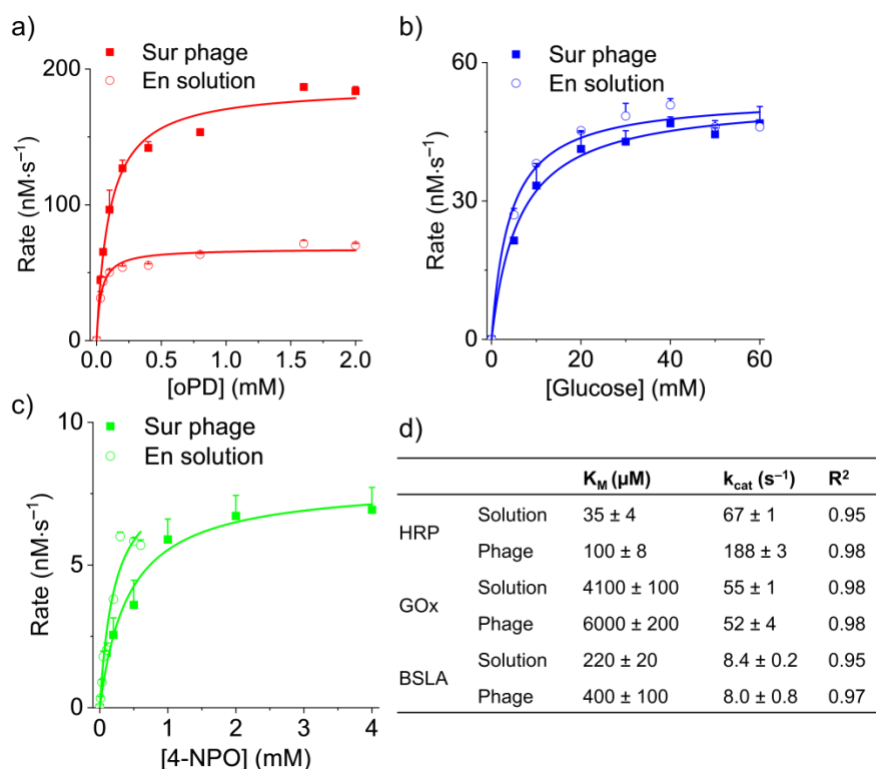


Figure 8 : Caractérisation individuelle des propriétés des trois enzymes immobilisées sur la matrice phagique. Graphiques de Michaelis-Menten pour (a) HRP, (b) GOx, et (c) BSLA. (d) Paramètres de Michaelis-Menten. Notez que les graphiques a-c sont normalisés à une concentration d'enzyme de 1 nM, pour faciliter la comparaison. Données présentées en tant que moyenne + ou \pm SD (n = 3).

Effet de la réticulation du phage et de la densité de greffage

Pour mieux comprendre l'influence de la modélisation phagique sur les enzymes pour les sept différents systèmes de cascade de la **Figure 7**, les propriétés catalytiques de la HRP ont été évaluées par l'ajout d'oPD et de H_2O_2 , tandis que le couple $GOx \rightarrow HRP$ a été évalué par l'ajout de glucose et d'oPD. Enfin, la cascade entière a été analysée par l'ajout de 6-O-acétyl glucose et d'oPD. Comme l'illustre la **figure 9a**, l'augmentation du degré de réticulation (échantillons **2 à 5**) a produit une augmentation de 1,2 à 1,6 fois de l'activité du HRP par rapport à l'échantillon **1** (solution). Compte tenu du grand nombre de copies et de la charge négative de la principale protéine d'enveloppe de la P8, ces résultats pourraient suggérer que l'amélioration reste un effet intrinsèque de l'immobilisation sur l'activité de la HRP,³⁵ peut-être due à une acidification locale, comme on le soupçonne de se produire sur d'autres modèles à charge négative.³⁶ Analyse de la paire de $HRP \rightarrow GOx$ en utilisant le D-Glucose comme substrat pour initier la cascade a conduit à l'observation que le taux de production de DAP a diminuée par rapport à l'utilisation de la HRP seule. Cela suggère que la GOx est l'enzyme la plus lente des deux et qu'elle limite donc la vitesse de la cascade. Les échantillons non réticulés (**2**) et réticulés à l'intérieur des phages (**3**) n'ont montré qu'une augmentation d'un facteur 1,5 du taux de catalyse, tandis que la réticulation entre les phages a conduit à une augmentation d'un facteur 3 du taux de catalyse (échantillon **5**) par rapport aux enzymes libres en solution (**Figure 9b**). Les taux de catalyse plus élevés observés lors de la réticulation inter-phages (**4** et **5**) suggèrent que le microenvironnement dans lequel évolue GOx est plus acide, en raison de la plus grande proximité de l'enzyme avec la matrice phagique chargée négativement (due à la réticulation). L'augmentation du degré de greffage de la GOx et de la HRP sur la matrice phagique (échantillon **7**) a conduit à une augmentation du taux absolu de catalyse (**Figure b**) et à la disparition de la phase transitoire avant d'atteindre la cinétique de l'état stable. Dans ces conditions de greffage plus élevées, une augmentation d'environ 1,3 fois de l'activité est maintenue par rapport au contrôle en solution (**6**). L'analyse de la cascade $BSLA \rightarrow GOx \rightarrow HRP$ en utilisant le 6-O-acétyl glucose pour initier l'ensemble de la cascade (**Figure 9c**), pour les échantillons **2-4**, une augmentation de l'activité catalytique de ~1,4-1,9 fois a été observée qui était indépendante de la densité de réticulation. Cependant, l'échantillon **5 a** présenté une augmentation de l'activité de 4,6 fois, ce qui indique que la réticulation interphagique a un effet bénéfique sur la cascade. Les résultats combinés de cette étude indiquent que la cascade de trois enzymes, $BSLA \rightarrow GOx \rightarrow HRP$, peut en effet être améliorée par rapport aux enzymes libres en solution par le modelage sur un phage. Cette étude de preuve de concept suggère que les systèmes de cascade d'enzymes modélisés par des phages peuvent être des plateformes prometteuses pour la fabrication écologique, bien que la

prédiction de l'effet des effets micro-environnementaux sur toutes les enzymes puisse être un défi.

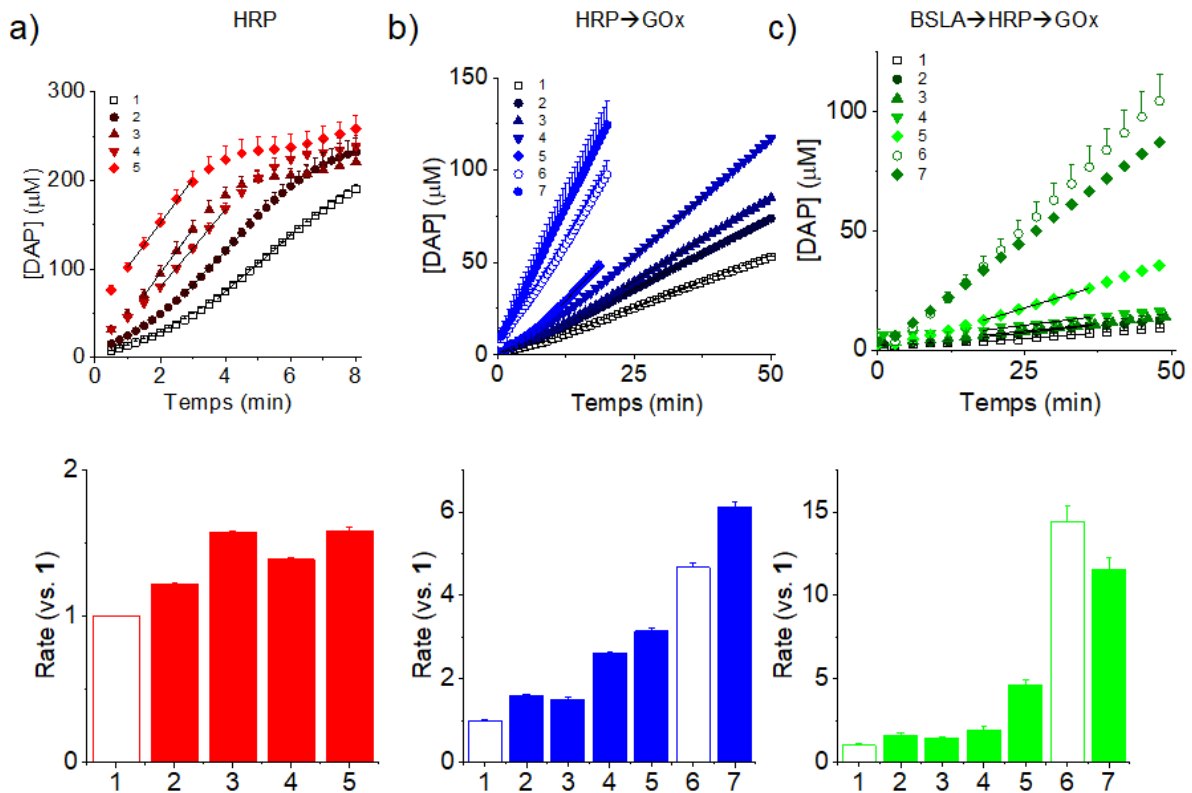


Figure 9 : Réactions en cascade. a) Schéma de l'ensemble de la réaction en cascade. b) Graphique de la formation du produit en fonction du temps par tous les échantillons assemblés pour b) HRP, c) GOx-HRP, d) BSLA-GOx-HRP. Comparaison de l'activité enzymatique parmi les échantillons assemblés e) HRP f) GOx-HRP g) comparaison de l'activité BSLA-GOx-HRP.

3.3 Suivi quantitatif et sans marqueur de la cinétique enzymatique à l'aide de l'émission de térahertz

La cinétique de la lipase vers les substrats non optiques, BuOMe et AcOEt) a été suivie par la technologie d'émission THz. Une expérience illustrative utilisée pour mesurer l'activité catalytique de la lipase vers le substrat, BuOMe, est présentée dans la **Figure 10**. Le signal initial (impulsion THz) correspondant au tampon d'essai stable dans le temps et normalisé à zéro. Lors de l'ajout du substrat, une forte augmentation a été observée en raison de l'équilibre entre le BuOMe en solution et celui adsorbé sur le film de SiO₂ ("Eq." dans la **Figure 10a, b** ; régi par l'équilibre 1).

Par la suite, un plateau a été atteint, la composition chimique dans la région affectant l'amplitude THz ("région de détection") reflétant celle de la solution brute. L'ajout de lipase produit un deuxième changement brusque de l'amplitude THz causé par l'adsorption de la lipase (équilibre 2) sur le film de SiO_2 , la réaction enzymatique se produisant à cet endroit, et l'équilibre du produit résultant entre la plaque de détection et la solution (équilibre 3). Dans la "région d'analyse" suivante, la réaction enzymatique devient l'étape limitant la vitesse du système et peut être utilisée pour la quantification, jusqu'à ce qu'un plateau final soit observé lorsqu'il ne reste plus de substrat. Pour la quantification du produit, l'amplitude THz (μV) est nécessaire pour convertir en unités de concentration, les courbes d'étalonnage pour le substrat et le produit ont été établies à partir des plateaux 'Substrat' et 'Produit', respectivement, en faisant varier la concentration initiale des substrats (**Figure 10c** pour BuOMe et **10d** pour AcOEt).

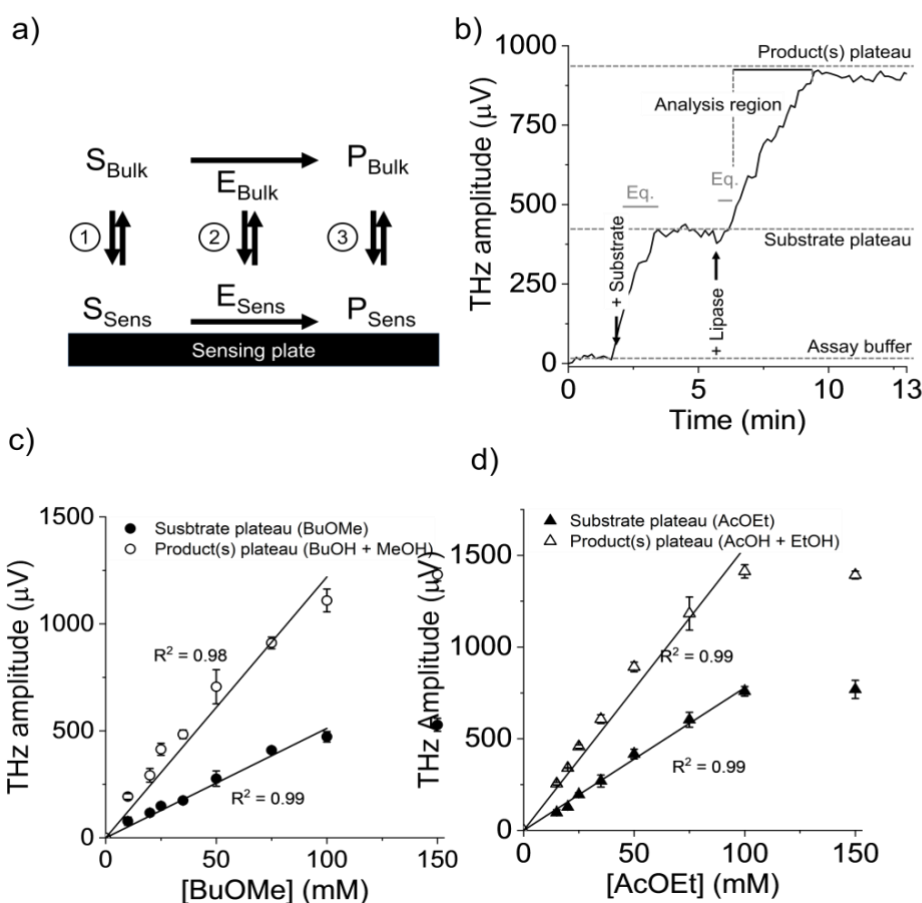


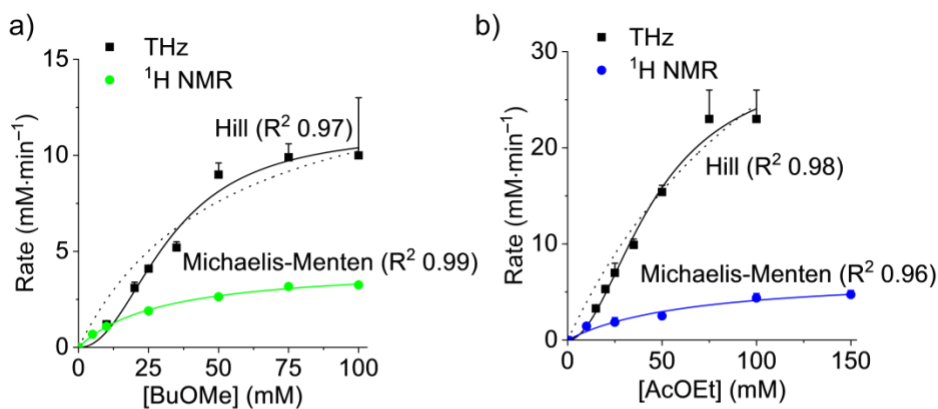
Figure 10 : (a) Influence des équilibres de l'échantillon et des réactions chimiques sur l'amplitude de l'émission THz. (a) Équilibres impliquant le substrat (S), l'enzyme (E) et les produits (P) ainsi que les réactions ayant un effet sur l'émission THz. (b) Déroulement typique d'une expérience utilisée pour mesurer l'activité de la lipase vers le BuOMe. Courbes de l'amplitude THz mesurée au "plateau du substrat" et au "plateau du produit" en fonction de la concentration

de BuOMe (c) et d'AcOEt (d). Ces courbes linéaires sont utilisées pour convertir l'amplitude THz en unités de concentration de produit. Données présentées sous forme de moyenne + écart-type, n = 3.

La concentration molaire du produit à un moment donné peut être extraite de l'amplitude THz brute selon l'équation suivante, de sorte que la cinétique de la réaction peut être comparée à d'autres techniques analytiques.

$$[P]_t = \frac{THz_t - \alpha[S]_0}{\beta - \alpha}$$

où $[P]_t$ est la concentration du produit au temps t (en mM), THz_t est l'amplitude THz au temps t (en μV), $[S]_0$ est la concentration du substrat au temps zéro (en mM), α est la pente de la courbe d'étalonnage du substrat ($\mu V/mM$), et β est la pente de la courbe d'étalonnage du produit ($\mu V/mM$). Pour la comparaison, la cinétique de la réaction a été également suivie par spectroscopie RMN 1H , via l'intégration des pics correspondant aux molécules de produit en fonction du temps. De façon remarquable, les valeurs mesurées de K_M étaient très similaires pour les deux techniques, tandis que k_{cat} était ~ 2 - 6 fois plus élevé lorsqu'il était mesuré par émission THz.



	BuOMe		AcOEt	
	THz	1H NMR	THz	1H NMR
V_{max} (mM·min $^{-1}$)	11 \pm 3	4.3 \pm 0.1	30 \pm 4	7 \pm 1
$K_M / K_{0.5}$ (mM)	32 \pm 4	30 \pm 3	46 \pm 8	70 \pm 20
k_{cat} (s $^{-1}$)	19 \pm 5	7.4 \pm 0.2	26 \pm 3	6 \pm 1
n	2.2 \pm 0.5	–	2.0 \pm 0.3	–
R 2	0.97	0.99	0.98	0.96

Figure 11 : Plots de Michaelis-Menten des données obtenues par émission THz et spectroscopie RMN ^1H BuOMe (a) ou AcOEt (b) utilisés pour déterminer les paramètres enzymatiques k_{cat} et K_M . Le tableau montre les paramètres cinétiques obtenus par émission THz et comparés à ceux obtenus par RMN. Les données sont présentées sous forme de moyenne + écart-type, $n = 3$.

La reproductibilité des données THz et la grande linéarité des courbes d'étalonnage suggèrent que l'émission THz peut être utilisée comme un outil quantitatif. En ce qui concerne la différence avec le résultat de la RMN ^1H , l'hyperactivation des lipases a été signalée dans certaines publications lorsque l'enzyme est adsorbée sur une surface hydrophobe, entraînant une augmentation de l'activité d'environ 3 fois pour certains substrats ^{37,38} Les lipases ont en effet une grande affinité pour les surfaces hydrophobes (comme la plaque de détection recouverte de molécules de substrat ester hydrophobe), ce qui les place dans un environnement localement hydrophobe. L'analyse de la technologie d'émission THz de la **figure 11** à l'aide d'un modèle de Hill (plutôt que Michaelis-Menten) a produit des ajustements fiables aux données ($R^2 > 0,98$) et a indiqué une déviation de la cinétique de Michaelis-Menten. Le "coefficient de coopérativité", n , était supérieur à un, ce qui a été interprété comme une altération potentielle de la structure moléculaire de l'enzyme lors de son immobilisation sur la plaque de détection ³⁹ Notez que lorsque $n = 1$, l'équation de Hill se réduit à l'équation de Michaelis-Menten. Cela expliquerait donc les taux de réaction plus élevés observés par l'émission THz, sans effet sur $K_M/K_{0,5}$. Dans l'ensemble, ces résultats confirment que la technologie d'émission THz est sensible aux changements chimiques et peut être utilisée pour le suivi quantitatif des réactions chimiques.

Pour illustrer le potentiel de l'émission THz pour surveiller qualitativement les processus catalytiques dans des échantillons complexes, de la lipase a été ajoutée à un échantillon de lait de vache entier, qui est un substrat complexe composé de variétés de graisses, de protéines, de sucres et de sels, difficile à analyser par les techniques analytiques habituelles.

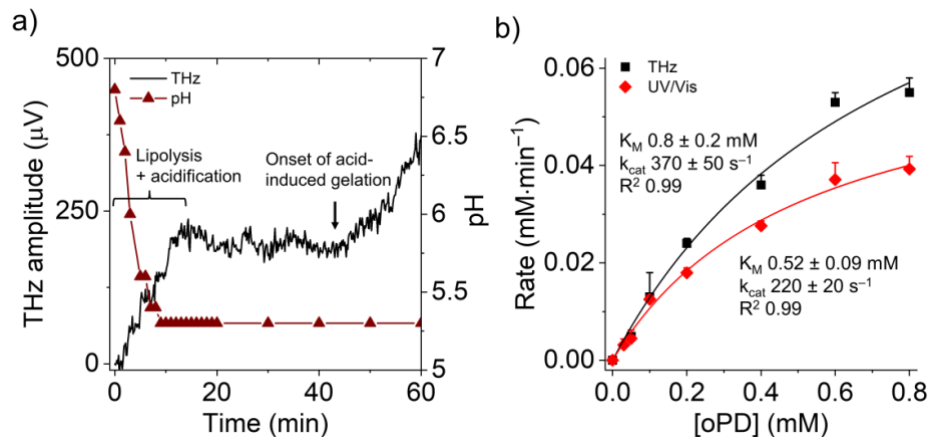


Figure 12 : **Activité de la lipase dans le lait entier et activité de la peroxydase de raifort par la technologie d'émission THz. (a) Changements du pH et de l'amplitude THz du lait de vache entier exposé à la CALB (n = 1). (b) Vitesses de réaction en fonction de la concentration utilisées pour déterminer les paramètres cinétiques enzymatiques de la peroxydase du raifort par analyse de Michaelis-Menten par émission THz et absorption optique (UV/Vis). Données présentées sous forme de moyenne + écart-type, n = 3-4.**

L'ajout de CALB au lait entier (**figure 12a**) a entraîné une augmentation de l'amplitude THz due à l'hydrolyse des molécules de graisse. Cela a coïncidé avec une diminution du pH de 6,8 à 5. Ensuite, un plateau de l'amplitude THz a été observé en raison de la consommation complète de la graisse dans l'échantillon, et aucune autre évolution du pH n'a été observée. Remarquablement, à 40 minutes, une seconde augmentation de l'amplitude THz a été observée en raison de la gélification du lait causée par la déstabilisation des micelles de caséine induite par l'acide. La gélification produit un changement important dans la micro/nanostructure de la solution, influençant ainsi les interactions chimiques avec la plaque de détection. Ainsi, en plus de détecter les changements chimiques dans cet échantillon complexe, l'amplitude de l'émission THz était sensible aux changements physiques qui peuvent être importants pour certains processus industriels. Enfin, pour illustrer que cette technique d'émission THz est applicable à d'autres systèmes enzymatiques, l'oxydation de l'oPD par la peroxydase de raifort et le H_2O_2 a été mesurée, et comparée aux données obtenues par absorbance optique. Comme l'illustre la **figure 12b**, les paramètres cinétiques obtenus par l'analyse de Michaelis-Menten étaient hautement comparables par les deux techniques, et les effets induits par l'immobilisation, tels que ceux observés pour la lipase, n'étaient pas présents. Ces données prouvent que la technologie d'émission THz peut être appliquée à d'autres systèmes enzymatiques.

4. CONCLUSION

Dans l'ensemble, cette thèse illustre que le microenvironnement et la stabilité de BSLA ne semblent pas être intrinsèquement affectés par l'affichage du phage, bien que le phage ait modifié la distribution à l'échelle nanométrique de BSLA dans le tampon d'essai micellaire. Compte tenu de la diversité des applications et des propriétés attendues des protéines d'intérêt, l'effet observé ici pour la BSLA peut être observé pour d'autres protéines, en particulier lorsque l'application prévue implique des solutions complexes (par exemple, colloïdales ou autres). Trois enzymes en cascade portant des oligomères de phage ont montré une activité accrue de 4,6 fois par rapport à la quantité équivalente d'enzymes libres en solution et de 2,3 fois par rapport à un mélange d'enzymes individuelles immobilisées sur des monomères de phage. Ce résultat suggère que l'oligomérisation du modèle nanométrique a un effet sur la distribution nanométrique des enzymes ce qui favorise la canalisation du substrat pour la réaction en cascade multi-enzyme. Enfin, l'émission THz a été utilisée avec succès pour le suivi quantitatif de la cinétique des transformations chimiques, sans marquage et de manière non invasive, ce qui en fait un outil idéal pour le criblage des bibliothèques de substrats (par exemple, l'analyse de la promiscuité des enzymes). La sensibilité de l'émission THz aux changements chimiques et physiques des échantillons est utile pour analyser des réactions complexes, bien que les futures conceptions de plaques de détection doivent viser à réduire le temps nécessaire aux molécules pour s'équilibrer à sa surface. Elle peut être un outil idéal pour la recherche et le développement impliquant des enzymes, et pour la surveillance des processus industriels dans les secteurs de l'alimentation, des cosmétiques, des détergents, des produits pharmaceutiques et du biodiesel.

AUTHOR CONTRIBUTIONS

This thesis is written as article-based version, based on the INRS Guide-2019, in order to fulfill the requirement of the PhD program. Chapter 1 consists of inspiration of the work and general introduction based on literature review. Chapters 2-4 present our work and Chapter 5 includes general discussion. Following is my contribution to Chapters 2-4:

Chapter 2: Published as Sharifun Nahar, Esen Sokullu, & Marc A. Gauthier, The phage display of *Bacillus subtilis* Lipase A significantly enhances catalytic activity due to altered nanoscale distribution in colloidal solution; *Biotechnology and bioengineering* (2019). I was responsible for experiments and data analysis as well as the manuscript composition and revision. Esen Sokullu guided me phage work mostly for primer design and cloning. Marc A. Gauthier was the supervisory author and was involved with concept formation, manuscript composition and revision.

Chapter 3: Prepared for the submission for publication as “Enhancement of enzyme cascade reactions on M13 bacteriophage and oligomers thereof”, I was responsible for data collection and analysis as well as the manuscript composition and revision. Marc A. Gauthier is the supervisor and was involved with concept formation, manuscript composition and revision.

Chapter 4: Submitted as Non-invasive, label-free, and quantitative monitoring of lipase kinetics using Terahertz emission technology; Sharifun Nahar, Ahmed Mohamed, Xavier Ropagnol, Amir Hassanpour, Toshihiko Kiwa, Tsuneyuki Ozaki, and Marc A Gauthier. *Biotechnology and bioengineering*. I participated in the design of the study, carried out NMR and UV-vis spectroscopy experiments, data analysis, wrote and revised the manuscript. Ahmed Mohamed collected the THz emission data and wrote THz emission part of the manuscript. Xavier Ropagnol guided for THz setup. Amir Hassanpour contributed to manuscript revision. Toshihiko Kiwa was the inventor of THz emission system and contributed to the scientific discussion. Tsuneyuki Ozaki contributed to the scientific discussion and endorsed us to use THz emission system in his laboratory. Marc A. Gauthier was the supervisory author and was involved with concept formation and manuscript composition and revision.

TABLE OF CONTENTS

ACKNOWLEDGEMENTS	iii
ABSTRACT	v
RÉSUMÉ	vi
SYNOPSIS	vii
AUTHOR CONTRIBUTIONS	xxxii
TABLE OF CONTENTS	xxxii
LIST OF FIGURES	xxxv
LIST OF TABLES	xxxix
LIST OF ABBREVIATIONS	xi
1. CHAPTER 1: INTRODUCTION	1
1.1. Inspiration	1
1.2. Modifying the activity of an enzyme by protein engineering	4
1.2.1. Strategies of enzyme engineering.....	4
1.2.2. Methods for high throughput screening	6
1.3. Phage display	9
1.3.1. Structure and properties Bacteriophage M13	9
1.3.2. Phage display method	10
1.3.3. Phage display Selection	12
1.4. Enzyme immobilization	14
1.4.1. Choice of support for immobilization	14
1.4.2. Strategies of enzyme immobilization for industrial use	18
1.5. Influencing enzyme activity by nano/micro-environment engineering	21
1.5.1. Concentrating and eliminating of reactants and regulators	23
1.5.2. Regulating microenvironmental pH	26
1.5.3. Tuning the micro environmental temperature	28
1.6. Enzyme cascade	29
1.7. Michaelis-Menten (steady-state) Kinetics	33
1.8. Conclusion	36
1.9. Objectives of the thesis	37
1.10. Overview of this thesis	38

2. CHAPTER 2: THE PHAGE DISPLAY OF BACILLUS SUBTILIS LIPASE A SIGNIFICANTLY ENHANCES CATALYTIC ACTIVITY DUE TO ALTERED NANOSCALE DISTRIBUTION IN COLLOIDAL SOLUTION	41
2.1. Introduction	43
2.2. Materials and methods	44
2.2.1. Plasmid, bacterial strain, helper phage and culture media.....	44
2.2.2. Genomic DNA and enzymes	45
2.2.3. Primer Design and PeIB Leader Sequence (Oligonucleotides)	45
2.2.4. Construction of the plasmids	47
2.2.5. Phage display of BSLA	48
2.2.6. Electrophoresis	48
2.2.7. Counting phage lipase	48
2.2.8. Nanoparticle Tracking Analysis	49
2.2.9. Concentration of native BSLA	49
2.2.10. Composition of assay buffer	50
2.2.11. Lineweaver-Burke analysis	50
2.2.12. Effect of additives effect on enzyme activity.	50
2.2.13. Statistical analysis	52
2.3. Result and discussion	52
3. CHAPTER 3: ENHANCEMENT OF ENZYME CASCADE REACTIONS ON M13 BACTERIOPHAGE AND OLIGOMERS THEREOF	61
3.1. Introduction	62
3.2. Materials and Methods	64
3.2.1. Materials	64
3.2.2. SDS-PAGE	64
3.2.3. Nanoparticle Tracking Analysis (NTA)	64
3.2.4. Assembly of cascade samples	65
3.2.5. Catalytic activity of BSLA	66
3.2.6. Catalytic activity of GOx	68
3.2.7. Catalytic activity of HRP	69
3.3. Results.....	70

3.3.1. Design and concept	70
3.3.2. Cascade assembly and characterization	73
3.3.3. Direct effect of phage immobilization	76
3.3.4. Effect of phage crosslinking and grafting density	76
3.4. Discussion	81
3.5. Conclusions	82
4. CHAPTER 4: NON-INVASIVE, LABEL-FREE, AND QUANTITATIVE MONITORING OF LIPASE KINETICS USING TERAHERTZ EMISSION TECHNOLOGY	85
4.1 Introduction	87
4.2 Materials and methods	90
4.2.1 Materials	90
4.2.2 Terahertz optical setup	91
4.2.3 Monitoring enzyme activity using the THz optical setup	92
4.2.4 Monitoring enzyme activity by ¹ H NMR spectroscopy	92
4.2.5 Monitoring lipase activity in whole milk	93
4.2.6 Monitoring horseradish peroxidase activity.....	93
4.2.7 Conversion to THz signal to units of concentration (Lipase)	94
4.2.8 Conversion to THz signal to units of concentration (HRP)	94
4.3 Results and Discussion	95
4.4 Conclusions	106
4.5 Acknowledgments	107
5. CHAPTER 5: GENERAL DISCUSSION, CONCLUSION, AND FUTURE DIRECTION.....	108
6. BIBLIOGRAPHY	112
7. APPENDIX	125
7.1 Letters of copyright permission.....	125

LIST OF FIGURES

Figure 1.1	A comparison of the steps involved in rational protein engineering and directed protein evolution4
Figure 1.2	Overview of screening technologies. (A) Experimental steps from obtaining the gene library as PCR product to the actual screen. Note that cloning and transformation efficiency are often limiting library size, (B) explanation of symbols, (C) cell growth/survival selection and agar plate screening, (D) microtiter plate screening, (E) cell as micro-reactor, (F) cell surface display, (G) cell-in-droplet, and (H) <i>in vitro</i> compartmentalization7
Figure 1.3	Schematic of the structure of M13 bacteriophage9
Figure 1.4	The three types of phage display. (A) Phage systems: The phage genome contains only one copy of p3 (black), and the displayed sequence (white) is fused to that copy. Consequently, every p3 displays the same fusion protein (triangle). (B) Hybrid systems: The phage genome contains two copies of p3, one with a fusion partner and one without. The promoters for these two genes are generally designed such that the wild-type p3 is expressed at higher levels in the cell. The more common wild-type protein thus appears more frequently in the virion. (C) Phagemid systems: Instead of a phage genome, the virion contains the phagemid, which is generally smaller. Infection with helper phage drives the expression of phage proteins, and the phagemid expresses the p3 fusion library11
Figure 1.5	Schematic of step-by-step phagemid-based phage display method13
Figure 1.6	Design and assembly of DNA origami. (A) Targeted shape for DNA origami. (B) The AFM image of a representative assembled DNA origami structure16
Figure 1.7	Schematic of different enzyme immobilization techniques. Physical and covalent immobilization techniques are shown on flat graphene sheet and carbon nanotube respectively. Schematic of encapsulation is shown to a porous geometry, while cross-linking is illustrated to show the distance between two individual GOx20
Figure 1.8	Schematic representation of a multidisciplinary approach aimed to create optimal biocatalysts. Implementation of biocatalysts in industrial technologies will have to not only consider optimization of the enzyme functionality but further, lead to increase in enzyme operational stability at the interface with supports used for immobilization.23
Figure 1.9	Schematic of stimulating interactions between enzyme and substrates. (A) Substrate–DNA interactions attract the substrates around an enzyme and hence increase the local concentration of substrates. The gray circles represent substrate molecules and the red ones represent products. (B) A supercharged nano-reactor regulates the substrate specificity through electrostatic interactions24

Figure 1.10	Microenvironmental pH effect on single enzymes and multiple enzymes. (A) Schematic representation of the proton distribution between a polyanionic matrix and the bulk solution (upper left panel), and an illustration of the shifts in the pH-activity profile of chymotrypsin bound on a polyanionic or polycationic matrices (upper right panel). (B). Activity enhancement in the DAAO -Cyt c cascade by creating a more acidic pH microenvironment for Cyt c27
Figure 1.11	Two proposed strategies to increase the local temperature around enzymes. (A) Immobilization of enzymes on gold nanorods followed by encapsulation in Calcium alginate beads. (B) Incorporation of platinum nanoparticles inside enzymes29
Figure 1.12	A Schematically Represented Cascade Reaction comprising four enzymes. S represents the initial substrate added to the reaction, while P represents the final product of the cascade process. P1, P2, and P3 are the intermediate products released by each enzyme, which are then used as substrates for the following enzyme. The cascade reaction proceeds until the final desired product is formed.....33
Figure 1.13	Schematic illustration of the substrate (S1 and S2) channeling effect between (a) two free-floating enzymes (E1 and E2) and (b) two proximate enzymes (E1/E2).....35
Figure 1.14	Michaelis–Menten saturation curve for an enzyme reaction showing the relation between the substrate concentration and reaction rate33
Figure 2.1	A) The phagemid pADL-20c map and B) schematic representation of the molecular structure of the vector used for the cloning of <i>lipA</i> gene. After Sfi I and Bgl I digestion, the <i>lipA</i> gene was cloned in <i>E. coli</i> into the Sfi I and Bgl I sites of the phagemid pADL-20c. C) Agarose gel electrophoresis of Lipase A DNA. Lane 1: 1 kb DNA ladder; 2: negative control of PCR (no DNA); 3: <i>lipA</i> DNA PCR product using LIPF & LIPR primers; 4: uncut phagemid; 5: cut phagemid after digestion with SfiI; 6–9: colony PCR after transforming to <i>E.coli</i> with LIPF and LIPR primers.....46
Figure 2.2	Characterization of phage displayed BSLA. (a) Western Blot analysis immune-stained with mouse anti-M13 p3 monoclonal antibody (M: molecular weight ladder, Lane 1: phage displayed BSLA, Lane 2: wild-type M13, Lane 3: M13KO7 helper phage). (b) Lineweaver-Burke plot to determine K_M of phage displayed BSLA. Data presented as Mean \pm SD (n = 3).....53
Figure 2.3	Nanoparticle tracking analysis of phage– BSLA in water (a), phage–BSLA in enzyme assay buffer (b), and the assay buffer alone (c)54
Figure 2.4	pH–activity profiles for BSLA and phage–BSLA. Activity was measured either in assay buffer (a) or in assay buffer supplemented with 0.5M NaCl (b). Data presented as mean+SD (n=3). BSLA, <i>Bacillus subtilis</i> Lipase A55
Figure 2.5	Thermal stability of BSLA and phage–BSLA (a) Catalytic activity measured as a function of temperature. (b) Catalytic activity measured at r.t., following pre-

incubation at variable temperature for 30min. (c) Nanoparticle analysis of phage–BSLA samples following 30min incubation at different temperatures. (d) Catalytic activity measured at r.t. following pre-incubation at 65°C for different times. For panels a, b, and d, data are presented as mean+SD (n=3). BSLA, Bacillus subtilis Lipase A; r.t., room temperature57

Figure 2.6 Effect of salt, PEG, and wild-type phage on catalytic activity. Influence of NaCl (a), PEG 8kDa (b), and wild-type M13 (c) on the catalytic activity of BSLA and phage–BSLA. Data presented as mean+SD (n=3). BSLA, Bacillus subtilis Lipase A; PEG, poly(ethylene glycol)59

Figure 3.1 Design and assembly of phage-templated enzyme cascade. (a) The relative stoichiometry of the components enables independent control of the degree of crosslinking as well as the density of enzymes grafted onto the phage. (b) Representative characterization of the self-assembly of selected components by nanoparticle tracking analysis.....71

Figure 3.2 Schematic of three-enzyme cascade reaction. To monitor HRP reaction o-PD and H₂O₂ are used as substrates. For GOx→HRP reaction, D-Glucose and o-PD were added as substrates. For BSLA→GOx→HRP reaction, 6-O-acetyl glucose and o-PD were added as substrates. In all cases DAP was measured as end product.....72

Figure 3.3 individual characterizations of the properties of the three enzymes immobilized on the phage template. Michaelis-Menten plots for (a) HRP (0.5 nM anti-P8–HRP (solution or immobilized), 1 mM H₂O₂, variable oPD), (b) GOx (0.7 nM GOx–biotin (solution or immobilized), 2.5 nM anti-P8–HRP (solution or immobilized), 30 mM oPD, variable glucose), and (c) BSLA in solution and immobilized on phage (343 nM BSLA (solution), 64 nM BSLA–phage (immobilized), variable 4-NPO). (d) Michaelis-Menten parameters. Note that plots a–c are normalized to an enzyme concentration of 1 nM, for ease of comparison. Data presented as Mean + or ± SD (n = 3). The composition of all solutions tested is provided in Table 3.575

Figure 3.4 Influence of cascade parameters on the rate of (a) HRP, (b) GOx→HRP, and (c) BSLA→GOx→HRP. Data presented as Mean + SD (n = 3).77

Figure 3.5 Influence of cascade parameters on the rate of (a) HRP, (b) GOx→HRP, and (c) BSLA→GOx→HRP. Data presented as Mean + SD (n = 3). Absolute values for the rate of DAP production can be found in Figure 3.3.80

Figure 4.1 Optical setup used to monitor chemical reactions by THz emission. (a) A 522-nm femtosecond laser pulse is directed towards the sensing plate, resulting in THz emission that is detected by photoconductive sampling (using a 1045-nm probe line). (b) The sensing plate is composed of a SiO₂/Si film deposited on laser-grade sapphire substrate. A depletion layer is formed near the SiO₂/Si boundary due to band bending and gives rise to a local electric field ($\phi_2 - \phi_1$). When the femtosecond laser hits the sensing plate, carriers are generated in the Si film, which are then accelerated by this field. This generates a THz pulse that is detected in the specular direction of reflection. The amplitude of the THz signal is influenced by the sample, because the thinness of the SiO₂ layer makes ϕ_2 sensitive to the chemical composition of the sample.89

Figure 4.2	<p>Influence of sample equilibria and chemical reactions on THz emission amplitude. (a) Equilibria involving substrate (S), enzyme (E), and products (P) as well as reactions with an effect on THz emission. THz amplitude is only sensitive to changes immediately above the sensing plate (“Sens”), corresponding to molecules within the first nanometers above the sensing plate, including those adsorbed to the latter. (b) Typical time-course of an experiment used to measure lipase activity towards BuOMe (description in text).96</p>
Figure 4.3	<p>Analysis of lipase activity by THz emission technology. (a,b) Plots of THz amplitude measured at the “Substrate plateau” and “Product plateau” as a function of BuOMe (a) and AcOEt (b) concentration. These linear curves are used to convert THz amplitude into units of product concentration. Evolution of product concentration upon addition of lipase to the sample solution containing BuOMe (c) or AcOEt (d), calculated from raw THz amplitude. Time “zero” corresponds to the moment lipase was added. Data presented as Mean + SD, n = 3. Fit parameters in Table 4.198</p>
Figure 4.4	<p>Analysis of lipase activity by ¹H NMR spectroscopy. (a) Representative spectra used to monitor the progress of CALB-catalyzed substrate (from top to bottom: BuOMe, AcOEt, OcOMe, or AcOBn) hydrolysis by ¹H NMR spectroscopy in deuterated phosphate buffer. Selected peaks associated with substrate and product peaks that were used for integration are assigned. DMSO is used as internal integration reference. (b,c) Evolution of product concentration upon addition of lipase to the sample solution containing BuOMe (b) or AcOEt (c). Time “zero” corresponds to the moment lipase was added. An approximate delay of 2 min was required to lock and shim the sample before spectra could be recorded. Data presented as Mean + SD, n = 3.100</p>
Figure 4.5	<p>Comparison of lipase kinetics analyzed by THz emission technology and ¹H NMR spectroscopy. (a,b) Concentration-dependant reaction rates used to determine enzyme kinetic parameters either using the Hill equation (THz emission) or the Michaelis-Menten equation. The dotted line corresponds to the Michaelis-Menten equation fitted to the THz emission data ($R^2 < 0.92$) to illustrate the poor fit. (c) Fit parameters obtained by non-linear regression of data in (a,b). (d) Comparison of the rate of hydrolysis of four substrates (50 mM) by CALB obtained by ¹H NMR spectroscopy and THz emission technology. The rates measured by THz emission are systematically higher due to adsorption of CALB onto the sensing plate. Data in panes a, b, and d are presented as Mean + SD, n = 3.101</p>
Figure 4.6	<p>Evolution of product concentration upon addition of lipase to the sample solution containing OcOMe or AcOBn, calculated by THz emission technology or ¹H NMR spectroscopy. Time “zero” corresponds to the moment lipase was added. An approximate delay of 2 min was required to lock and shim the sample before ¹H NMR spectra could be recorded. Data presented as Mean + SD, n = 3.103</p>
Figure 4.7	<p>Effect of DMSO concentration on the rate of hydrolysis of MeOBu as measured using the THz optical setup. Data presented as Mean ± SD, n = 3.104</p>
Figure 4.8	<p>Lipase activity in whole milk and activity of horseradish peroxidase by THz emission technology. (a) Changes of pH and THz amplitude of whole cow’s milk exposed to CALB (n = 1). Time “zero” corresponds to the moment lipase was added. (b) Production of DAP with time upon action of horseradish peroxidase and H₂O₂ on</p>

oPD, as measured by THz emission technology and optical absorption. Time “zero” corresponds to the moment horseradish peroxidase was added. Data presented as Mean + SD, n = 3.106

LIST OF TABLES

Table 3.1	Concentration of all compounds used to prepared cascade samples described in the section 3.2.4 Assembly of cascade samples66
Table 3.2	Concentration of all compounds used to measure catalytic activity of BSLA→GOx→HRP described in the section 3.2.5 and to generate Figure 3.4c.....67
Table 3.3	Concentration of all compounds used to measure catalytic activity of GOx→HRP described in the section 3.2.6 and to generate Figure 3.4b.69
Table 3.4	Concentration of all compounds used to measure catalytic activity of HRP described in the section 3.2.7 and to generate Figure 3.4a70
Table 3.5	Concentration of all compounds used to generate MM data78
Table 4.1	Linear fit parameters for Figure 4.3a,b. Note that alterations to the THz emission setup, such as changing the sensing plate, can result in different values of slope. It is thus suggested to verify the calibration of the instrument when changes are made.97

LIST OF ABBREVIATIONS

<u>Acronym</u>	<u>Description</u>
4-NPO	4-nitrophenyl octanoate
AcOBn	Benzyl acetate
AcOEt	Ethyl acetate
ANOVA	Analysis of variance
BBO	Beta barium borate
BSLA	<i>Bacillus subtilis</i> lipase A
BuOMe	Methyl butyrate
CALB	<i>Candida antarctica</i> lipase B
ChT	Chymotrypsin
CLEA	Cross-linked enzyme aggregate
CLEC	Cross-linked enzyme crystal
Cyt C	Cytochrome C
D ₂ O	Deuterium oxide
DAAO	D-amino acid oxidase
DAP	2,3-diaminophenazine
D _H	Hydro-diameter
DMSO	Dimethyl sulfoxide
DNA	Deoxyribonucleic acid
E. coli	<i>Escherichia coli</i>

EDTA	Ethylene diamine tetra-acetic acid
ELISA	Enzyme-linked immunosorbent assay
epPCR	Error-prone polymerase chain reaction
GOx,	Glucose oxidase
H ₂ O ₂	Hydrogen peroxide
HCL	Hydrochloric acid
HPLC	High Performance Liquid Chromatography
HRP	Horseradish peroxidase
IgG	Immunoglobulin G
K _{cat}	Turn-over number
KCl	Potassium chloride
KH ₂ PO ₄	Potassium dihydrogen phosphate or Monopotassium phosphate
K _M	Michaelis-Menten constant
LB	Luria broth
LCST	Lower critical solution temperature
<i>Lip</i>	Lipase gene
LIPF	Lipase DNA forward (primer)
LIPR	Lipase DNA reverse (primer)
M	Molar (unit)
Na ₂ HPO ₄	Disodium phosphate, or sodium hydrogen phosphate
NaCl	Sodium chloride
nm	nanometer (unit)
NMR	Nuclear magnetic resonance
NTA	Nanoparticle Tracking Analysis
OcOMe	Methyl octanoate

OD	Optical density
o-PD	o-phenylenediamine
PAGE	Polyacrylamide gel electrophoresis
PBS	Phosphate Buffered Saline
PCR	Polymerase chain reaction
PEG	Poly(ethylene) glycol
Poly(NIPAM)	Poly(N-isopropylacrylamide)
Pt-NPs	Platinum nanoparticles
rSAP	Shrimp alkaline phosphatase
SDS	Sodium dodecyl sulfate
Si	Silicon
SiO ₂	Silicon oxide
SOD	Superoxide dismutase
ssDNA	Single stand deoxyribonucleic acid
Sulfo-SIAB	Sulfo-succinimidyl (4-iodoacetyl) aminobenzoate
TBE	Tris/Borate/EDTA
THz	Terahertz (unit)
UCST	Upper critical solution temperature
UV	Ultraviolet
V _{max}	Maximum velocity
VPL	Virus like particle

CHAPTER 1: INTRODUCTION

1.1 Inspiration

Enzymes can simply be defined as proteins that act as catalyst for various kinds of biochemical reactions without themselves undergoing any kind of change. They enhance the rate of chemical reactions with great specificity and efficiency, which otherwise would take place very slowly. Enzyme technology has an impact in almost every area of industrial use, particularly in healthcare and “green” manufacturing.¹⁻⁴ Enzymes are commonly used for the production of daily life products, such as paper, textile, food, feed, cleaning supplies, chemicals and pharmaceuticals, etc. Some of the most industrially used enzymes are lipases,⁵ α -amylases,⁶ proteases,⁷ lactases,⁸ esterases,⁹ phospholipases,¹⁰ pectinases,¹¹ etc. Combinations of multiple enzymes together also perform reactions that are used in our daily life. For example, detergents are supplemented with proteases, lipases, amylases, oxidases, peroxidases, and cellulases in order to breakdown different types of chemical bonds in water. It is essential that they maintain their activity at high temperatures (60 °C) and high pH values (pH 9–11), in particular when mixed with other washing powder components. Another example of multiple enzymes participating in one reaction is the multi-enzymatic cascade reactions, i.e., the combination of several enzymatic transformations in concurrent one-pot processes. In such reactions, the product of the first enzyme is consumed by the second and so on which offers considerable advantages: the demand of time, costs and chemicals for product recovery may be reduced, reversible reactions can be driven to completion and the concentration of harmful or unstable compounds can be kept to a minimum.¹²⁻¹⁴ Thus, due to the high demand of enzymes, researchers are focusing on the identification and production of robust, stable biocatalysts suitable for application in a broader range of industrial processes. Moreover, utilizing enzymes faces challenges due to the limitation of finding the right tools and analytical technology to monitor the enzymatic reaction. This holds particularly true when the starting material is complex (i.e., mixtures of substrates), heterogeneous, and absorbs/scatters light, or even when reaction kinetics are too fast to be monitored by conventional offline techniques (e.g.,

chromatography). Most enzymatic reactions are monitored using surrogate substrates that produce conveniently quantifiable (e.g., optical) signals in model reaction conditions that simplify the analysis.

The latest developments in biotechnology, particularly in the area of protein engineering, provide an important tool for the effective development of new enzymes with improved properties for use in technical and industrial applications. Modern recombinant DNA technology enables researcher to produce enzymes from recombinant microorganisms, permits the modification of an enzyme's function in terms of stability, specificity, and stereoselectivity. Tuning enzymes by protein engineering creates enzymes that perform better under unnatural conditions, such as in organic solvents or in extreme pH, temperature, or with non-natural substrates.¹⁵

The immobilization of an enzyme on a solid support or its chemical modification can also increase its stability and reusability. While genetic approaches enable the discovery,^{17,40} mutation,¹⁷ and *de novo* design⁴¹ of enzymes with desired activity, immobilization is equally important to endow enzymatic catalysts with features important for practical applications, including convenient handling, reusability, stability, and even improved catalytic performance.^{20-23,25} The behavior of immobilized enzymes differs from that of dissolved enzymes because of the effects of the support material, or matrix, as well as conformational changes in the enzyme that result from interactions with the support and covalent modification of amino acid residues.

A more recent trend of enzyme engineering is an approach that focuses on controlling the nano- and microscale environment of an enzyme or multienzyme complex, with the aim to create optimal local conditions in proximity to the enzyme despite unfavorable conditions in the bulk environment. For instance, a favorable microenvironment can enhance enzyme performance by controlling local pH and temperature, concentrating reactants and cofactors, improve the efficiency of the reactions by compartmentalization (specially for cascade reactions), etc. These effects can be useful to regulate the enzyme's performance without requiring engineering of the enzyme.²⁵ The common approaches for altering the microenvironment of enzymes are the immobilization on carriers, conjugation with polymers, encapsulation in nano- or microcompartments,

aggregation into complexes, presence of additives, and so forth. For instance, the electrostatic interactions between a charged substrate and oppositely charged residues on the surface of the enzyme can increase the local concentration of substrate next to the active site of the enzyme. For instance, DNA is linked to enzyme horseradish peroxidase (HRP) to create enzyme–DNA structures that enhance substrate–enzyme binding interactions far from the active site that result in increased local substrate concentrations, effectively reducing the apparent Michaelis-Menten constant ($K_{M,app}$) and driving higher catalytic rates at low bulk substrate concentrations.^{26,27} Encapsulation or microenvironmental partitioning of enzymes plays an important role in multienzyme cascade reactions by partitioning reactions that ensures necessary environments for individual enzyme, creates a safe space for volatile reaction intermediates, and protects them from external harmful agents/ toxic intermediates; thus, enhance enzyme cascade throughput.⁴²⁻⁴⁴ Moreover, most biological processes are in fact accomplished by multienzyme synthetic pathways. For instance, the metabolism of glucose by glycolysis involves the participation of ten enzymes that work sequentially in an efficient way. Inspired by Nature’s ingenuity, considerable progress has been made in recent years to develop multistep reactions that combine the synthetic power of several enzymes in one pot. For instance, an artificial 9-step enzyme cascade system was designed that contributes to cascade reaction for the synthesis of benzylamine from L-phenylalanine.⁴⁵ Industrially, combining enzymatic reactions into a multistep one-pot bio-catalytic process brings additional benefits, including no need to isolate reaction intermediates as they are directly transferred to the next step of the reaction sequence.¹²⁻¹⁴ Globally, this can reduce cost, time, effort and increase final yield of product.

It is therefore of substantial interest to find ways to optimize the performance of single enzymes or multienzyme cascades, new strategies for microenvironment engineering as well as understanding the mechanisms behind.

1.2 Modifying the activity of an enzyme by protein engineering

Protein engineering is a widely used tool to produce enzymes with the desired properties, including increased activity,⁴⁶ modified specificity of substrates,^{16,47} thermal and oxidative stability,⁴⁸ pH range⁴⁹ and tolerance to solvents,⁵⁰ etc. Mostly there are two main strategies for protein engineering: directed evolution and rational design, which can be combined into semi-rational design.

1.2.1 Strategies of enzyme engineering

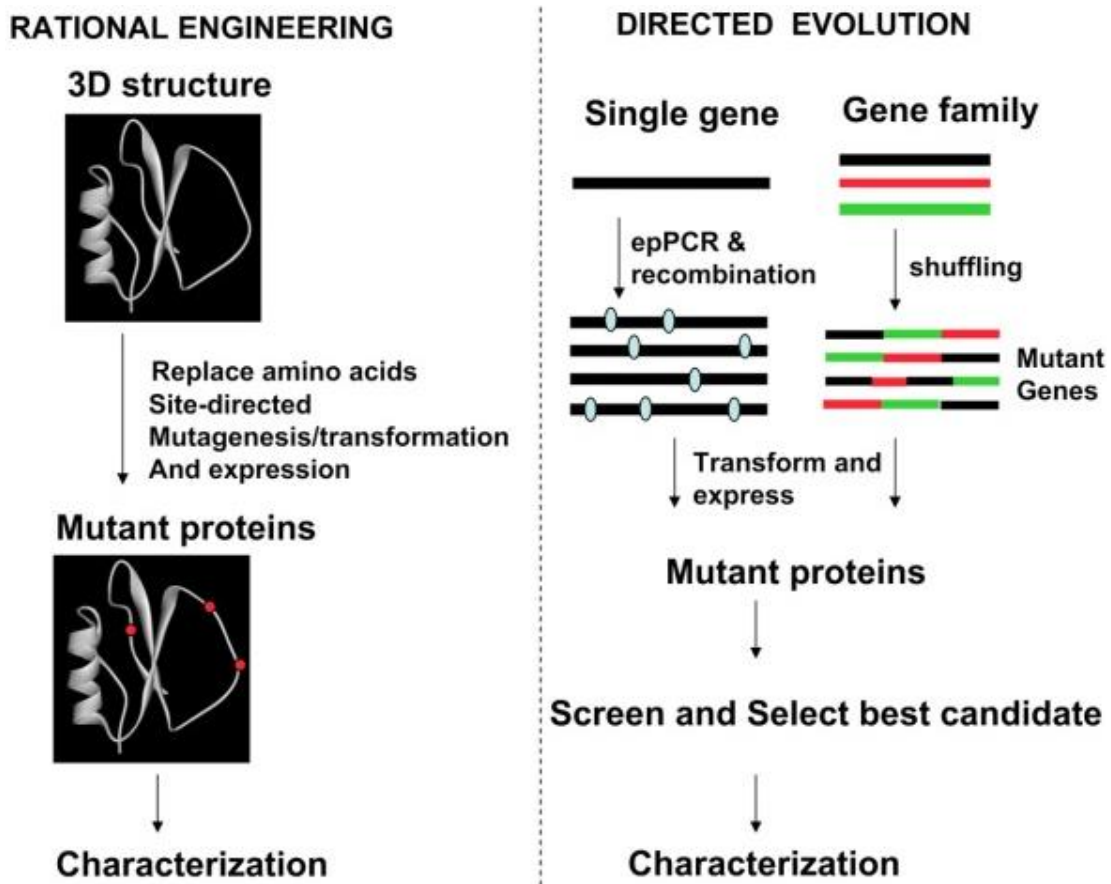


Figure 1.1 A comparison of the steps involved in rational protein engineering (left) and directed protein evolution (right). (Adapted from Ref. 51 with permission from Oxford University Press and Copyright Clearance Center, see appendix on page 125).⁵¹

The advantage of directed evolution is that no structural information is needed and that mutations at unexpected positions distant from the active site can be introduced. However, several rounds of evolution have to be applied and thus a high number of variants have to be screened, which is time and labor consuming and leads to the requirement of high-throughput assays and analytical tools. In rational design, biochemical data such as protein structures and molecular modeling data are evaluated to propose mutations, which are introduced by site-specific mutagenesis. One of the advantages of a rational design approach is an increased probability of beneficial mutations and a significant reduction of the library size and thus less effort and time has to be applied for the screening of the library. Lack of availability of a protein structures, biochemical data, and computational methods make rational design of enzyme engineering challenging.

Multiple approaches have been developed for enzyme engineering in order to alter certain desired abilities such as increased activity, modified specificity, selectivity, or cofactor binding.⁵² The earliest approach was the rational design, which is applicable when there is detailed knowledge of enzyme's structural features of the active site and their contribution to function is available. Biochemical data, protein structures, and molecular modeling data are evaluated to propose mutations, which are introduced by site-specific mutagenesis (**Figure 1.1**). One of the advantages of a rational design approach is an increased probability of beneficial mutations and a significant reduction of the library size and thus less effort and time has to be applied for the screening of the library. The lack of availability of a protein's structure, biochemical data, or computational methods makes rational design of enzyme engineering challenging.⁵³⁻⁵⁵ The complexity of the structure/function relationship in enzymes has proven to be the factor limiting the general application of rational design. Lately, directed evolution has proven to be a powerful tool for the modification of enzyme activity and has become the most widely used approach because it can be accomplished without requiring an in-depth understanding of structure/function relationships, unlike rational design. Briefly, directed evolution enzyme engineering is the combined techniques of generation of a library of enzyme mutants (or variants) and selection of an enzyme with desirable function within that library. The

challenges for enzyme engineering include choosing the appropriate method for library creation and selecting the most active enzyme from the huge library. Libraries are created by random mutagenesis, semi rational design and DNA shuffling. Random mutagenesis introduces mutations throughout the target gene encoding for the enzyme of interest by error-prone polymerase chain reaction (epPCR).⁵⁶ After amplification, the library of mutant coding sequences is cloned into a suitable plasmid. The advantage of directed evolution is that no structural information is needed and that variations at unexpected positions distant from the active site can be introduced. However, several rounds of evolution have to be applied and thus a high number of variants have to be screened, which is time and labor consuming and leads to the requirement of high-throughput assays and analytical tools. Semi-rational design is a combination of random mutagenesis and site-directed mutagenesis. In this case, specific residue positions are determined to play important roles in the enzyme's function, and only the specific position(s) of interest are randomized to all 20 amino acids.⁵⁷ DNA shuffling involves exchanging fragments of genes with one another to create a library of mutant enzyme and is used to rapidly increase DNA library size because it is a recombination between different DNA species with different mutations. A set of genes are fragmented into pieces of 50–100 bp in length and followed by PCR without primers. DNA fragments with overlapping homologous sequence will anneal to each other and are then extended by DNA polymerase. Several rounds of PCR extension create a DNA library with different variants. DNA shuffling recombines natural enzymes with high sequence identity without any need for structural information and can lead to significant improvements in activity.

1.2.2 Methods for high throughput screening

Screening enzymes with the desired function is one of the most challenging steps of the directed evolution process. High throughput screening and selection methods facilitate the rapid identification of desirable variants from a library. Various technologies are available to search for the variants of interest (**Figure 1.2A**). Agar plate screening ⁵⁸ involves the incubation of bacterial colonies with the enzyme substrate.

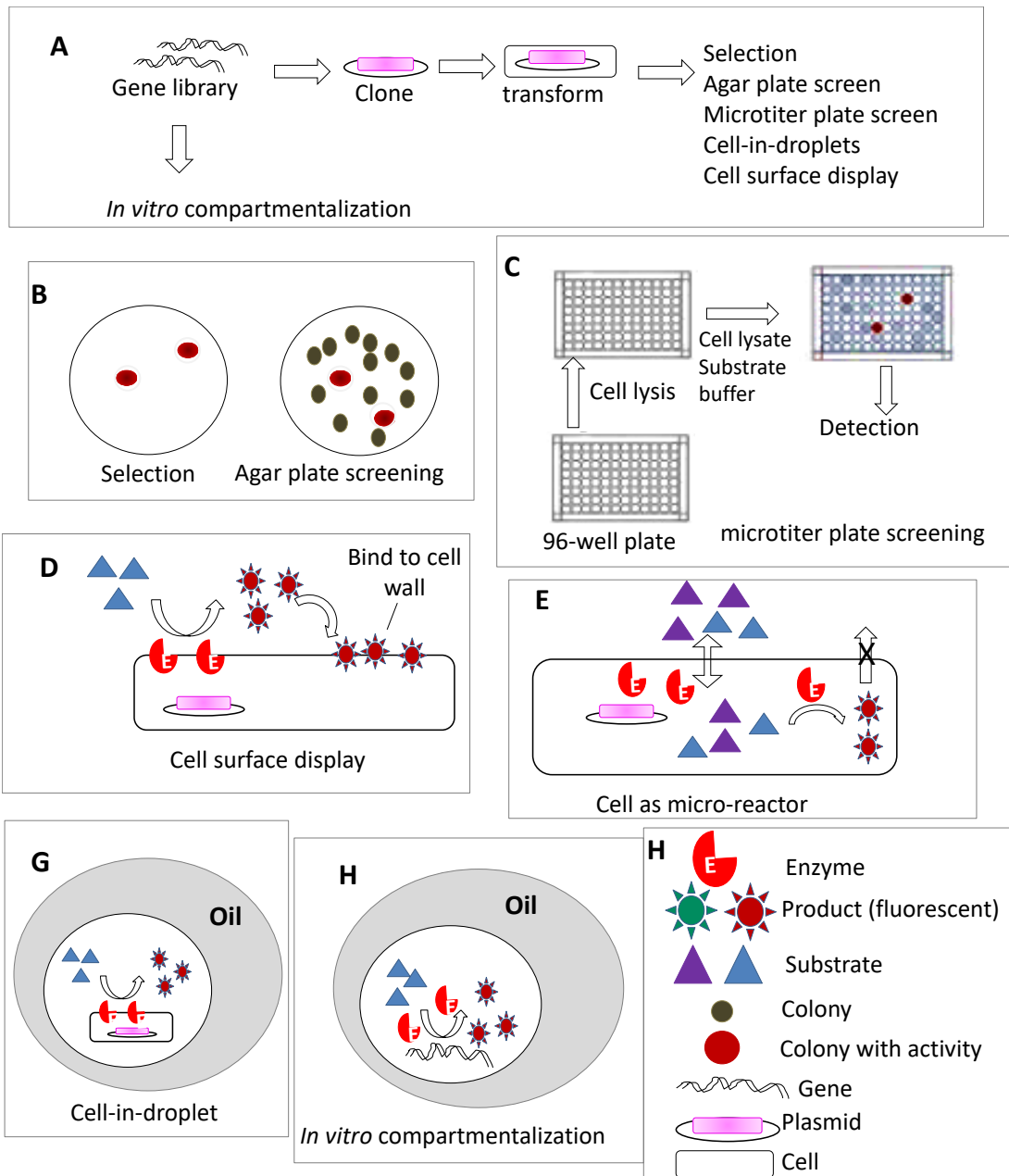


Figure 1.2 Overview of screening technologies. (A) Experimental steps from obtaining the gene library as PCR product to the actual screen. Note that cloning and transformation efficiency are often limiting library size, (B) explanation of symbols, (C) cell growth/survival selection and agar plate screening, (D) microtiter plate screening, (E) cell as micro-reactor, (F) cell surface display, (G) cell-in-droplet, and (H) *in vitro* compartmentalization (Adapted and modified from Ref. 59, it is an open access journal).⁵⁹

The colonies expressing an enzyme with desirable properties will convert the substrate to product, which creates a visual signal, such as fluorescence or color to identify colonies⁵⁹ (**Figure 1.2B**). This is a straightforward and simple method but low throughput (10^2 to 10^4 library size) and laborious.⁶⁰ In microtiter plate-based screenings,^{61,62} single *Escherichia coli* (*E. coli*) transformants are grown in 96- well microtiter plates. After cell lysis, the lysate is transferred to another plate, incubated with substrate, and the reaction is monitored using a colorimetric assay (**Figure 1.2C**). Product formation in microtiter plates-based screenings can also be visualized using antibodies, for example by ELISA (enzyme linked immunosorbent assay). This screening method is also low throughput. In microreactor-based screening methods, a single bacterial cell is used as a “micro-reactors” with volumes of a few femto-liters. Small droplets created by emulsification of water-in-oil are used as compartments that hold together cells, enzymes, substrates, and products.⁶³ The substrates produce fluorescence and product is screened using a fluorescence-activated cell sorting system (**Figure 1.2F**). This method is high throughput but limited to fluorescent products. A cell-free technology has been developed for high-throughput screening for enzyme activities, called in vitro compartmentalization. Gene libraries, along with an appropriate transcription-translation mixture, are trapped in droplets. The genes are transcribed and translated into multiple copies of the encoded protein within the droplet compartments.⁶⁴ Cell surface display is another selection method where both the enzyme variants and the substrates/products are displayed on the surface of cells (**Figure 1.2D**). Display techniques for high-throughput screening, such as plasmid display, phage display, and ribosome display have several advantages: display on the surface allows unhindered accessibility of the substrate and reaction conditions of choice and the bacterium or phage provide the link between the gene and the protein it encodes. Phage display provides a high-throughput platform to screen enzyme libraries based on their binding or catalytic activities (**Figure 1.2E**).⁶⁵⁻⁶⁷

1.3 Phage display

1.3.1 Structure and properties Bacteriophage M13

M13 bacteriophage is a filamentous virus that infects enteric bacteria that is widely used in biotechnological work. It infects and grows only in the male strains (only in the strains that displaying F-pili) such as *E. coli*. This phage has a fixed diameter of ~6 nm and its length is determined by the size of its genome. The 6400 nucleotide base pair of a single stranded DNA genome of M13 phage is encapsulated in 930 nm long phage particles (Day et al. 1988). M13 has five copies of each of its minor coat proteins, with p3 and p6 at one end and p7 and p9 at the other (**Figure 1.3**). Along the length of the phage is the major coat protein, p8, which exists in approximately 2700 copies (Day et al. 1988). The p8 coat protein has three general regions important to its assembly in the M13 coat: The 50 amino acids (a.a.) residue p8 (98% by mass) is composed of three distinct domains, namely, a negatively charged hydrophilic N-terminal domain (1–20), an intermediate hydrophobic domain (21–39), and a positively charged domain (40–50) that interacts electrostatically with phage genomic DNA. Only the N-terminal domain is exposed to the media, allowing it to be targeted for genetic or chemical functionalization.⁶⁸

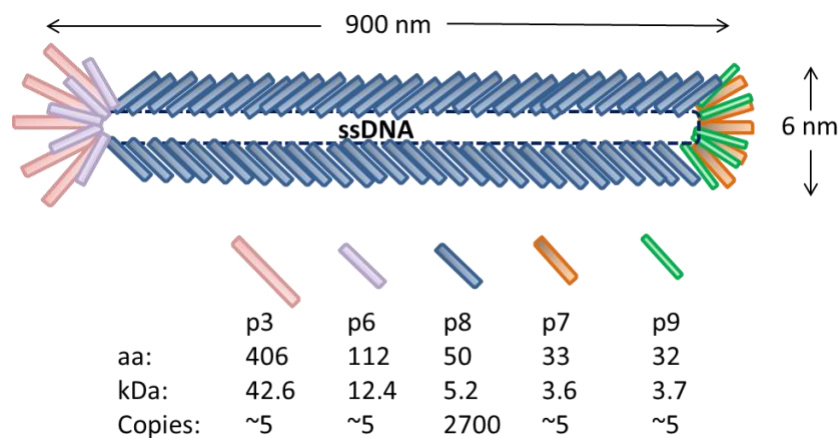


Figure 1.3 Schematic of the structure of M13 bacteriophage

Minor coat protein p3, the most commonly used coat protein for display, is composed of 406 a.a. residues. It is composed of several domains, an N-terminal (composed of N1 and N2) domain, and a C-terminal CT domain. The N-terminal domain is surface exposed and necessary for infectivity whereas the CT domain is likely to be buried within the particle and is necessary for p3 to be incorporated into the phage particle and to mediate termination of assembly and release of phage from the cell.⁶⁹ Though all five capsid proteins in the phage have been utilized for display purposes, p3- or p8-display are mostly common. Display on p7⁷⁰ and p9⁷¹ have been also reported. Usually, the minor coat proteins are used to display larger proteins while p8 is chosen for peptide display

1.3.2 Phage Display

Phage display is a selection technique in which a peptide or protein is fused with a bacteriophage coat protein and displayed on the surface of a virion⁷². Phage display technology is used to study biological interactions such as protein–protein, protein–peptide, and protein–DNA interactions.⁷³ Filamentous phages (M13, f1, or fd) are commonly used to link proteins with the genes that encode them, allowing for selection of antibodies and functional peptides against target antigens.⁷⁴ There are three different types of phage display that have been invented on the basis of the vector to construct genomic sequences: (A) Phage-, (B) Hybrid-, and (C) Phagemid-based systems (**Figure 1.4**).⁷⁵ In phage systems, the phage vectors are used where the DNA of the displayed protein is attached next to the coat protein gene.

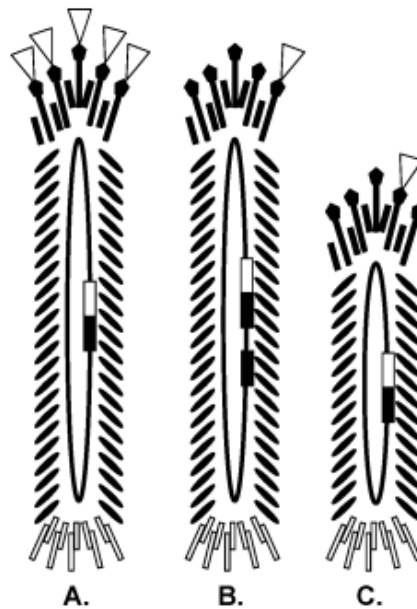


Figure 1.4 The three types of phage display. (A) Phage systems: The phage genome contains only one copy of p3 (black), and the displayed sequence (white) is fused to that copy. Consequently, every p3 displays the same fusion protein (triangle). (B) Hybrid systems: The phage genome contains two copies of p3, one with a fusion partner and one without. The promoters for these two genes are generally designed such that the wild-type p3 is expressed at higher levels in the cell. The more common wild-type protein thus appears more frequently in the virion. (C) Phagemid systems: Instead of a phage genome, the virion contains the phagemid, which is generally smaller. Infection with helper phage drives the expression of phage proteins, and the phagemid expresses the p3 fusion library. (Adapted from Ref. 75 with permission from American Chemical Society, see appendix on page 126).⁷⁵

The phage vectors are directly derived from the genome of filamentous phage and encode all the proteins needed for the replication and assembly of the filamentous phage. If a peptide library is displayed from p8 in a phage system, each virion has a peptide displayed from every copy of p8 – some 2700 copies per virion. Similarly, a peptide library is displayed from p3 in a phage system; each virion has a peptide displayed from each five copies of p3.⁷⁶⁻⁷⁸ After cloning, it produces phages exclusively presenting the fusion coat protein. The second group of phage display systems (Hybrid systems) utilizes phage genome containing two copies of coat protein gene; one with a fusion partner and one without. The promoters for these two genes are generally designed such that the wild-type coat protein is expressed at higher levels in the cell. The more common wild-type

protein thus appears more frequently in the virion.⁷⁹ The third group of phage display systems utilizes phagemid. A phagemid is a plasmid that bears a phage-derived origin of replication in addition (also called intergenic region) to its plasmid origin of replication. The intergenic region (IG) participates in DNA replication and also contains packaging signal that promotes the packaging of the ssDNA in the phage coat.⁸⁰ Since the phagemid vector usually contains only one type of coat protein gene, it needs help from “helper phage” to get other coat protein’s gene. The helper phage provides all other proteins and enzyme’s gene required for phagemid replication and also the structural proteins forming the phage coat. Helper phages are mutated wild-type phages containing the whole genome with a defective origin of replication or packaging signal, therefore are inefficient in self-packaging. Hence, it leads to preferential packaging of the phagemid DNA over the helper phage genome.^{81,82} Therefore, the phagemid bearing phages are generally produced though some phages bear helper phage DNA. Phagemid-based display systems are usually used when the foreign gene is more than 2 kbp DNA; this size is difficult to accommodate in the phage vector. Phagemid-based systems generally yield phages with a hybrid phenotype displaying wild type and fusion coat protein on the same particle.⁸³⁻⁸⁵

1.3.3 Phage display Selection

As defined in **Figure 1.5**, an enzyme is displayed at the phage surface on p3 minor coat protein by using a phagemid vector that contains only the fusion protein gp3 gene. The DNA sequence of the enzyme is first inserted directly into the coding sequence of p3 coat protein of phagemid and then the constructed phagemid is transformed in to *E.coli* (steps 1–2 in **Figure 1.5**).

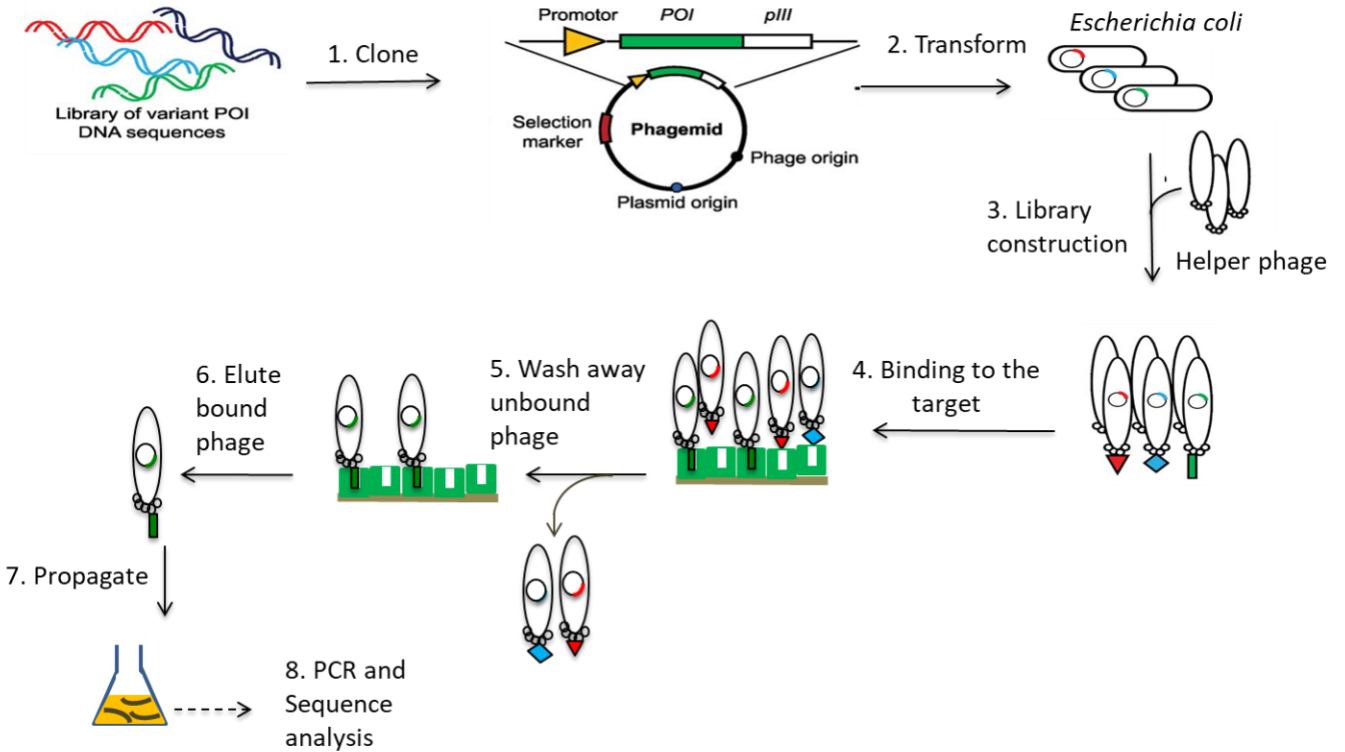


Figure 1.5 Schematic of step-by-step phagemid-based phage display method

Since the phagemid vector usually contains only one type of coat protein gene (here gp3 gene), it takes help from the “helper phage” to get other coat protein’s gene. Upon infecting *E. coli* containing a phagemid by helper phage, the resulting phage virion contains a mixture of wild-type and fusion coat protein, and the genetic information of the fusion protein is encoded by the packaged phagemid (step 3). As helper phages are packaging defected mutated phage, the resulted phage progeny are mainly the phagemid bearing phage.

For the selection, the phage library is incubated with the desired substrate or protein target(s), which has been immobilized to the surface of a microtiter plate well, a process referred to as bio panning. The plates are then washed to remove unbound phages. A

phage that displays a fusion protein that binds to one of those targets on its surface will remain while others are removed by washing. Those that attached with the target are eluted and steps 4–7 (**Figure 1.5**) are repeated several times to enrich the relevant (i.e., binding) phage. Several rounds of bio-panning are performed to get the enzyme with the desired characteristics. Phage eluted in the final step can be used to infect a suitable bacterial host, from which the phagemids can be collected and the relevant DNA sequence excised and sequenced to identify the relevant, interacting proteins or protein fragments.

1.4 Enzyme immobilization

Immobilization is a technical process in which enzymes are fixed to or within distinct support or matrix. The support systems generally stabilize the structure of the enzymes while maintaining their activities, thus, immobilized enzymes are more robust and more resistant to environmental changes in compared to free enzymes in solution.⁸⁶ In addition, immobilization of enzymes allows the easy recovery of both products and enzymes, multiple reuses of enzymes (recycling), continuous operation of enzymatic processes, reduced costs of downstream processing, better stability especially towards organic solvents and higher temperatures. Beside these advantages, some limitations of immobilized enzymes are lower enzyme activity compared to native enzyme and additional costs for carriers and immobilization. For example, the fast kinetics of native enzymes such as amylases or proteases is reduced when immobilized due to diffusion restrictions, making the immobilized enzyme less efficient.⁸⁶ Immobilization strategies vary depending on the choice of support, enzyme structure and the method of attachment.⁸⁷ The selection of support material can be a multifaceted matter since it depends on the type of enzyme, reaction media, safety policy in the field of hydrodynamic conditions and reaction conditions. Different supports offer variability in their physical and chemical properties (e.g. pore size, hydrophilic/hydrophobic balance and surface chemistry) for enzyme attachment. Their differences in morphological and physical characteristics can affect enzyme immobilization and its catalytic properties.

1.4.1 Choice of support for immobilization

The properties of the support, e.g. inertness toward enzymes, hydrophilicity/hydrophobicity and availability at low cost are important for the performance of the immobilized enzyme. Here are examples of supports commonly used to immobilize enzymes:

i) **Polymers-based scaffolds**

Synthetic organic, natural polymers, inorganic polymer, and stimuli-responsive polymers are used as scaffold for enzyme immobilization. For example, Novozyme 435 was coated with a silicone polymer obtained in a hydrosilylation reaction.⁸⁸ A variety of naturally occurring polymers such as cellulose, starch, agarose, and chitosan as well as proteins such as gelatin and albumin have been widely used as supports for the immobilization of enzymes. Inorganic supports are used for the immobilization of enzymes, e.g., silica,⁸⁹ Zeolites⁹⁰ and mesoporous silicas such as MCM-41, and SBA-15.⁹¹ Immobilization of enzymes to stimuli-responsive or 'smart polymers' via covalent attachment has also been tested. Such polymers are macromolecules that are sensitive to specific triggers like light, temperature, electrical or magnetic fields, and chemicals. After exposure to triggers, the activated polymers produce observable or detectable micro- or nanoscale changes, such as morphology, molecular bond rearrangement/cleavage, and molecular motion, which can induce changes in their macroscopic properties such as color, shape, and functionality. Due to the versatile selection of backbone and functional groups, stimuli-responsive polymers can be tailored to have a variety of specific mechanical, chemical, electrical, optical, biological, or other properties. For example, aqueous solutions of thermos-responsive polymer poly-N-isopropylacrylamide (polyNIPAM) exhibit a lower critical solution temperature (LCST) around 32 °C, below which the polymer readily dissolves in water while, above which it becomes insoluble owing to expulsion of water molecules from the polymer network.⁹²

ii) **Nanoparticle-based scaffolds**

Choices of nanoparticles (NPs) for enzyme immobilization are various and include metal nanoparticles, metal oxide nanoparticles, magnetic nanoparticles, porous, polymeric

nanoparticles, etc. Au and Ag nanoparticles have been used to immobilize lysozyme,⁹³ glucose oxidase,⁹⁴ aminopeptidase,⁹⁵ as well as alcohol dehydrogenase.⁹⁶ Cruz et al.⁹⁷ reported the immobilization of *Candida antarctica* lipase B (CALB) on fumed silica nanoparticles for applications in non-aqueous media and they observed that catalytic activities were remarkably high. One of the simplest and most inexpensive methods to immobilize an enzyme is by silica granulation and this technique is used in detergent formulations that release the enzyme into the washing liquid during washing.⁹⁸ The enzyme bound nanoparticles show Brownian movement when dispersed in aqueous solutions, showing that the enzymatic activities are comparatively better than that of the unbound enzyme.⁹⁹ Magnetic nanoparticles possess additional advantage, can be separated easily using an external magnetic field.¹⁰⁰

iii) DNA- and protein-based scaffolds

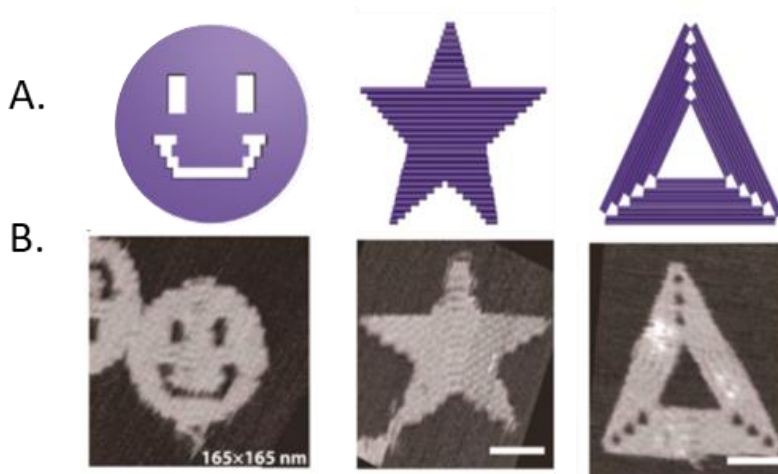


Figure 1.6 Design and assembly of DNA origami. (A) Targeted shape for DNA origami. (B) The AFM image of a representative assembled DNA origami structure (Figures are adapted and modified from Ref. 101 with permission from Springer Nature and Copyright Clearance Center, see appendix on page 126)¹⁰¹

Attaching proteins onto DNA scaffolds can be achieved in a few different ways. By modifying the protein with a DNA oligonucleotide one can use the base complementarity of DNA bases to position the protein. In 2006, Paul Rothumend was the first to report the DNA origami technique. He described the assembly process of several single-layered, planar structures, which ranged from simple triangular, five-point star shapes to complex smiley faces, each with a unique size, roughly 100 nm in diameter (**Figure 1.6**). Zhilei Ge et.al. reported the assembly of a DNA origami-templated enzymatic cascade (glucose oxidase and horseradish peroxidase) on gold electrodes. They used a monolayer of DNA origami that was anchored on gold electrodes via Au–S chemistry, to create programmable, electrochemically driven biomimetic device containing both biochemical and electronic components. They reported that upon posing of a specific electrical potential, substrates/products flow through the enzyme pair and the end-product transferred electrons to the electrode. The steady state flux of the distance-dependent enzymatic cascade reactions was translated into a steady state current signal that recorded the overall enzyme activity.¹⁰² Protein-based scaffolds are also used for enzyme immobilization. Designing protein-based scaffolds to have a desired architecture is a challenge given the complexity of protein–protein binding interfaces.¹⁰³⁻¹⁰⁵ A 9.8 kDa proteins was synthesized from *Salmonella enterica* to build a self-assembling protein scaffolding system for enzyme co-immobilization. Hexamers generated from those protein monomers spontaneously aggregated into supramolecular protein structures (scaffolds). Immobilization of two cascade enzymes alcohol dehydrogenase and amine dehydrogenase on that protein scaffold for the conversion of (S)-2-hexanol to (R)-2-amino-hexane showed improved reaction rate of the cascade.¹⁰⁶ Moreover, the surface of immobilization platforms can provide a pH microenvironment that can influence the activities of immobilized enzymes (Zhang, Wang, & Hess, 2017). Protein scaffolds with different surface charges could provide optimal/adverse conditions for different enzyme cascades. Hence, care must be taken to choose a protein scaffold whether it has negative effect on enzyme activity.

Viruses and virus like particles-based scaffolds

Virus-based scaffolds for enzyme immobilization enable the genetically encoded spatial organization of single or multiple enzymes cascade platform. Viruses are intrinsically attractive scaffolds due to their ability to self-assemble into highly stable symmetrical assemblies. Composed of multiple copies of protein monomers, virus capsids can be readily modified (either chemically or genetically) and functionalized, making them highly versatile and tunable scaffolds. While their natural function is the storage and transport of genetic material, they have been applied as scaffolds for mineralization and as containers for the encapsulation of inorganic compounds as well as enzymes.¹⁰⁷⁻¹⁰⁹ The reproductive power of viruses has been used to develop multipurpose analytical methods, such as phage display, for the selection and identification of target compounds. Shapes of viruses are predominantly of two kinds: rods (or filaments) having a linear structure composed of nucleic acid and repeated protein subunits (that surround the nucleic acid); and spheres, which are 20-sided (icosahedral) polygons. Depending of their size and shape, virus particles have been used as very attractive nanoscale building blocks for many fields of applications including biosensors and in nano-biotechnology.¹¹⁰⁻¹¹³ Plant viruses, virus-like particle (VLP), and bacteriophages are most commonly used for enzyme scaffolding for the immobilization on or as nano-cages for the storage of organic materials as well as single or multiple enzymes. Tobacco mosaic virus was the first plant virus described and is among the best-studied viruses (Koch et al., 2016). The viral capsid proteins are covalently functionalized, genetically engineered or immune-decorated with many copies of single or multiple enzymes. These nano-sized constructs work as nano-reactors, nano-nets, and enzyme aggregates that potentially increase the catalytic activity of corresponding enzyme in compare while enzymes are in the solution. For example, Mariana et.al. showed that the self-assembly of genetically engineered M13 bacteriophages that bind enzymes to magnetic beads ensures high and localized enzymatic activity. These phage-decorated colloids provide a proteinaceous environment for directed enzyme immobilization. The magnetic properties of the colloidal carrier particle permit repeated enzyme recovery from a reaction solution, while the enzymatic activity is retained. Moreover, localizing the phage based construct with a magnetic field in a micro-container allows the enzyme–phage–colloids to function as an enzymatic micropump, where the enzymatic reaction generates a fluid flow.¹¹⁴ This system shows

the fastest fluid flow reported to date by a biocompatible enzymatic micropump. Enzymes are also immobilized on the bacteriophage surface through phage display technology.^{34,115,116} In these cases the genetic information of the enzyme is stored inside the attached phage which allows further production of phage immobilized enzymes bearing unique characteristics with less effort.

1.4.2 Strategies of enzyme immobilization for industrial use

Enzyme immobilization on a support matrix can provide increased resistance to changes in environments such as pH or temperature. It also allows easy separation from the products, and therefore can be reused and so is widely used in industry for enzyme-catalyzed reactions. Various enzyme immobilization techniques, especially scaffolding-based approaches, have been developed over the past few decades.¹¹⁷ Immobilization of enzymes results in the confinement of enzymes to a particular space, such as either displayed on, or encapsulated within, solid support materials, creating a heterogeneous biocatalyst system while retaining enzyme specificity and at certain level of activity.¹¹⁸ Interestingly, nanoscale localizing enzymes on the scaffolding carriers may significantly improve enzymes' catalytic performance and structural stability in certain scenarios due to macromolecular crowding.^{119,120} Nevertheless, in some cases, enzyme immobilization can impair the functionality of enzymes as a result of unfavorable conformational changes in enzymes and restricted substrate access in comparison to their soluble counterpart.¹²¹⁻¹²⁴ The most common procedures of enzyme immobilization are: i) binding to a support, ii) entrapment in a polymer network, and iii) cross-linking (**Figure 1.7**).

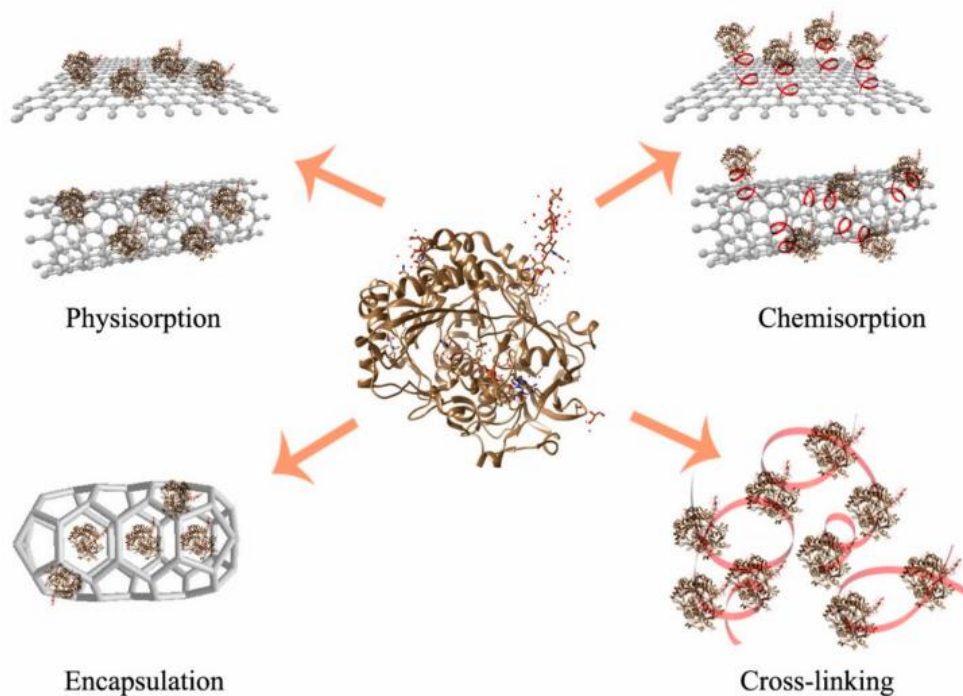


Figure 1.7 Schematic of different enzyme immobilization techniques. Physical and covalent immobilization techniques are shown on flat graphene sheet and carbon nanotube respectively. Schematic of encapsulation is shown to a porous geometry, while cross-linking is illustrated to show the distance between two individual GOx (Adapted from Ref. 125, it is an open access journal) . ^{125,126}

The solid supports for enzyme immobilization can be a synthetic resin, a biopolymer or an inorganic polymer such as (mesoporous) silica or a zeolite, nanoparticles, biological materials (e.g., protein, deoxyribonucleic acid or virus particles). The enzymes can be attached by interactions ranging from reversible physical adsorption (such as van der Waals and hydrophobic interactions), ionic linkages and affinity binding, to the irreversible but stable covalent bonds that are present through ether, thio-ether, amide or carbamate bonds. Enzymes are usually encapsulated in a gel lattice, such as an organic polymer or a silica sol-gel, or a membrane device such as a hollow fiber or a microcapsule. This kind of immobilization is suitable for use in processes involving low molecular weight substrates and products. However, larger substrate molecules have difficulty to approach the catalytic sites of the entrapped enzymes. Enzymes have been entrapped in natural

polymers like agar, agarose, gelatin, etc.¹²⁷ A number of synthetic polymers like polyvinyl alcohol hydrogel,¹²⁸ polyacrylamide¹²⁹ have also been investigated. Besides immobilization on a carrier, there is an increasing interest in carrier-free immobilized enzymes, such as cross-linked enzyme crystals (CLECs) and cross-linked enzyme aggregates (CLEAs). Both of them offer the advantages of high stability combined with highly concentrated enzyme activity and low production costs.²¹ The enzymes have been usually crosslinked in the presence of an inert protein like gelatin, albumin, or collagen. Crosslinked enzyme aggregates (CLEAs) are produced by simple precipitation of the enzyme from aqueous solution, as physical aggregates of protein molecules, by the addition of salts, or water miscible organic solvents or non-ionic polymers. These physical aggregates are held together by non-covalent bonding without disruption of their tertiary structure. CLEAs are very attractive biocatalysts, owing to their facile, inexpensive, effective production method, can readily be reused and exhibit improved stability and performance.¹³⁰ Application to penicillin acylase used in antibiotic synthesis showed large improvements over other type of biocatalysts.¹³¹

Besides the above-mentioned enzyme immobilization methods, enzymes have been attached to the scaffolds by affinity-based interactions. For example, streptavidin, a tetrameric protein, binds very tightly to the vitamin biotin with one of the strongest non-covalent interactions known in nature reported to (binding affinity is $\sim 10^{15} \text{ molL}^{-1}$). This is one of the strongest non-covalent interactions¹³² and is far beyond the normal protein–ligand binding strength.^{30,31} This high affinity of streptavidin for biotin means that the streptavidin-biotin complex is widely used in various biological tools, including for affinity tags, detection, and immobilization of proteins and has been widely used in biochemical sensing applications, especially in the identification of possible new drug targets.³² For example, M13 bacteriophage was genetically modified to express AviTag, a biotinylatable 15 amino acid (GLNDIFEAQKIEWHE) protein tag as a fusion to the p3 and p7 coat proteins. AviTag phages were then biotinylated by biotin ligase and the phages are subsequently crosslinked with streptavidin forming the end-to-end virus nanonets. The enzyme urease was immobilized on the nanonets via the phage major coat protein p8 via sulfo-SIAB. Urease activity and stability was tracked by a colorimetric activity assay. It

was shown that the bacteriophage nanonets form a promising platform for heterogeneous enzyme biocatalysis that exhibited high activity while allowing for enzyme recovery and reuse.¹³³ Another example of based affinity-based enzyme to scaffold binding is via antigen-antibody. As an example, functional GOx-fd nanoarrays were constructed using fd bacteriophage that were functionalized with the enzyme glucose oxidase (GOx), using an antigen-antibody assembly strategy, directly on a gold electrode support. The conjugation was mediated via a primary antibody against the fd-phage's coat protein p8 and the secondary antibody tagged with GOx. They reported the enhancement of the enzymatic activity due to scaffolding on a filamentous viral particle via phage-antibody.¹³⁴

1.5 Influencing enzyme activity by nano/micro-environment engineering

A nano/micro-environment is a nano- or micro-scale physicochemical environment around an enzyme or a group of enzymes (e.g., enzyme cascade) catalyzing chemical reactions. Recent studies have shown that engineering a favorable microenvironment for enzymes is an effective approach for optimizing enzymatic reactions.²⁶ The goal of microenvironment engineering is not radically different from those of traditional enzyme immobilization; it mostly focuses on the local environment of freely diffusing enzymes and enzyme complexes rather than engineering the support and enzyme attachment strategies. The physicochemical conditions such as concentrations of reactants, pH, and temperature in the microenvironment can be altered locally by encapsulation in nano- or micro-compartments, immobilization on carriers, conjugation with polymers, aggregation into complexes, adding additives in the reaction, and so forth.^{135,136} Mostly, microenvironment engineering is the combination of protein engineering and immobilization because both of these events create altered nanoscale distribution around the enzyme (**Figure 1.8**).

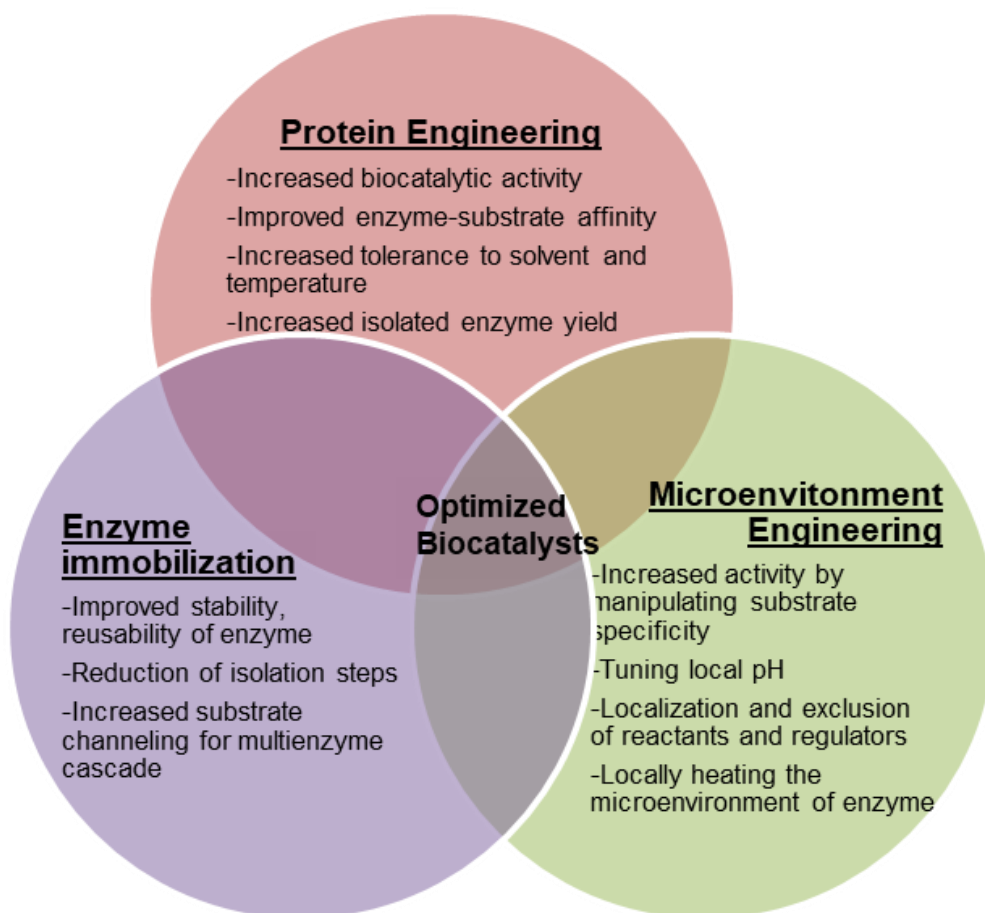


Figure 1.8 Schematic representation of a multidisciplinary approach aimed to create optimal biocatalysts. Implementation of biocatalysts in industrial technologies will have to not only consider optimization of the enzyme functionality but further, lead to increase in enzyme operational stability at the interface with supports used for immobilization.

1.5.1 Concentrating and Eliminating of Reactants and Regulators

The engineering of enzyme kinetics to improve kinetic parameters (e.g., K_M and k_{cat}) can be achieved by rational tuning of intermolecular interactions between the enzyme and its substrates. This strategy is based on the assumption that inserting beneficial interactions between an enzyme and its substrate molecule can increase the local molarity of a substrate, which in turn might enhance reaction rate and consequently enhance catalytic efficiency (k_{cat}/K_M).¹³⁷⁻¹³⁹ In enzymology, the Michaelis-Menten constant, K_M describes the

substrate concentration at which half the enzyme's active sites are occupied by substrate. It gives the information of the affinity of an enzyme towards a particular substrate. The k_{cat} (also termed turnover number) is defined as the number of chemical conversions of substrate molecules per second that a single catalytic site will accomplish for a given enzyme concentration.

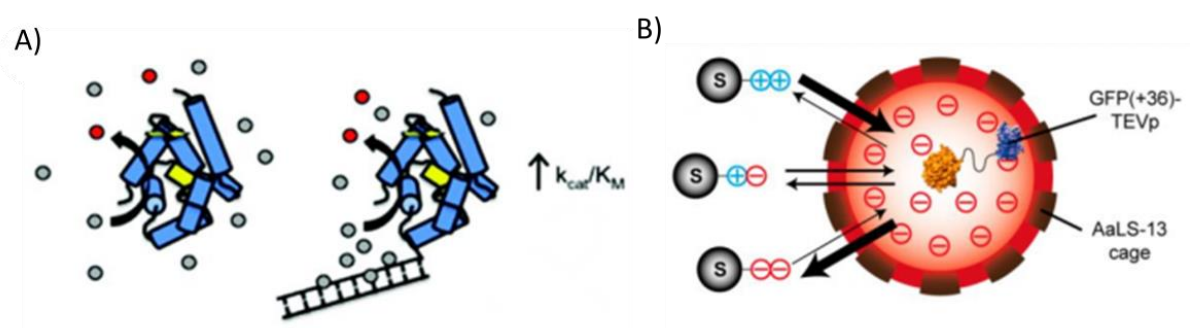


Figure 1.9 Schematic of stimulating interactions between enzyme and substrates. (A) Substrate–DNA interactions attract the substrates around an enzyme and hence increase the local concentration of substrates. The gray circles represent substrate molecules and the red ones represent products.¹⁴⁰ (B) A supercharged nano-reactor regulates the substrate specificity through electrostatic interactions (Adapted from Ref. 140 and 141 with permission from American chemical society, see appendix on page 127).¹⁴¹

Researchers have explored strategies to increase the local substrate concentration, which in turn might enhance catalytic efficiency. For instance, superoxide dismutase (SOD) is one of the fastest known enzymes that exploit electrostatic interactions between a charged substrate and oppositely charged residues on it. Positively charged patches on its surface attracted the negatively charged superoxide substrate towards the opening of the active site, hence enhanced catalytic efficiency.¹⁴²

Alternatively, charged molecules conjugated to the enzyme can induce electrostatic interactions between the enzyme and a charged substrate. To do this, a negatively-charged DNA was conjugated with HRP outside its active site, which captured substrate molecules and directed them to the active site, resulted enhanced substrate–enzyme interactions and reduced apparent K_M and higher catalytic rates at low bulk substrate concentrations (**Figure 1.9A**).¹⁴³ Similarly, trypsin was covalently immobilized on an insoluble polyanionic polymer that showed lower K_M value than the free enzyme toward its positively charged substrate benzoyl-L-arginine amide.¹⁴⁴ A similar reduction in K_M was also observed in the cases of lysozyme¹⁴⁵ and α -chymotrypsin.¹⁴⁶ In these cases, enzymes were assembled with different polyelectrolytes when the polyelectrolytes were oppositely charged to their substrates. It is also possible that the strong interactions between the substrates and the scaffolds also may hinder the enzymatic activity.¹⁴⁷

Compartmentalization is also an effective way to localize and/or exclude reactants and regulators. Some examples of *in vitro* compartmentalization are polyionic complex micelles¹⁴⁸, layer-by-layer assembled capsules,¹⁴⁹ viral capsids,¹⁵⁰ liposomes,¹⁵¹ polymersomes,¹⁵² etc. with different partitioning efficiency and permeation selectivity. Compartmentalization typically allows only specific molecules to diffuse in and out. An HRP-encapsulated polymersome was prepared from an amphiphilic block copolymer where cysteine double mutant of outer membrane protein F (OmpF) porins were incorporated into polymersome to induce redox responsiveness to the membrane. Located in the pore of OmpF, these two cysteine residues can serve as a gate by forming/cleaving disulfide bonds with other thiol compounds controlled by the environmental redox potential. Such a construction controls the enzymatic reaction in terms of both substrate molecular weight and redox stimulus.¹⁵³ The electrostatic interactions are also effective in improving the substrate specificity of enzymes in charged nanoreactors. A negatively supercharged protein cage was made of Aquifex aeolicus lumazine synthase (AaLS -13), which can spontaneously encapsulate a protease from Tobacco Etch virus (TEV) fused to a supercharged green fluorescent protein, GFP(+36) -TEVp (**Figure 1.9B**). The encapsulated protease preferentially takes up and hydrolyzes cationic peptides over the anionic and zwitterionic peptides. The cationic peptides are

supposed to be localized in the negatively charged lumen of the nanoreactor, leading to a decrease in K_M and increase in k_{cat}/K_M compared with the unencapsulated protease.¹⁴¹

Microenvironmental partitioning also plays an important role in enhancing multienzyme cascade throughput by accumulating substrates and saving unstable intermediates.⁴² Enhancing cascade throughput requires optimization of the diffusive resistance of the compartment for the transport of substrate, intermediate and product molecules. Compartmentalization with selective permeability enables enzyme cascades to work at a higher efficiency.⁴³ For example, the synthesis of cytidine-5'-monophosphate-5-N-acetylneuraminic acid (CMP-Neu5Ac) by a cascade composed of N-acyl-D-glucosamine 2-epimerase (AGE), N-acetylneuraminate lyase (NAL), and CMP-sialic acid synthetase (CSS) is hampered by strong inhibition of the first enzyme AGE by the substrate, cytidine triphosphate (CTP), of the third enzyme (i.e., CSS). Therefore, they compartmentalized AGE inside a polymersome that incorporated with a selective channel protein capable of blocking CTP outside, while securing the other two enzymes NAL and CSS on the outer surface. This construction protects the activity of AGE in a microenvironment by avoiding cross-inhibition in cascade reactions, resulting in increased production of CMP - Neu5Ac.⁴⁴ Moreover, interactions between intermediate substrates and scaffolds/modifiers prevent the loss of intermediate substrates to some extent. By linking two cascade enzymes together through a cationic peptide that electrostatically attract the anionic intermediates.^{154,155}

1.5.2 Regulating Microenvironmental pH:

Regulating local pH of an enzyme reaction is another approach of micro-environmental engineering to control pH dependent enzyme activity. The pH dependence of an enzyme is usually dominated by the protonation/deprotonation of the key residues at the active site.¹⁵⁶

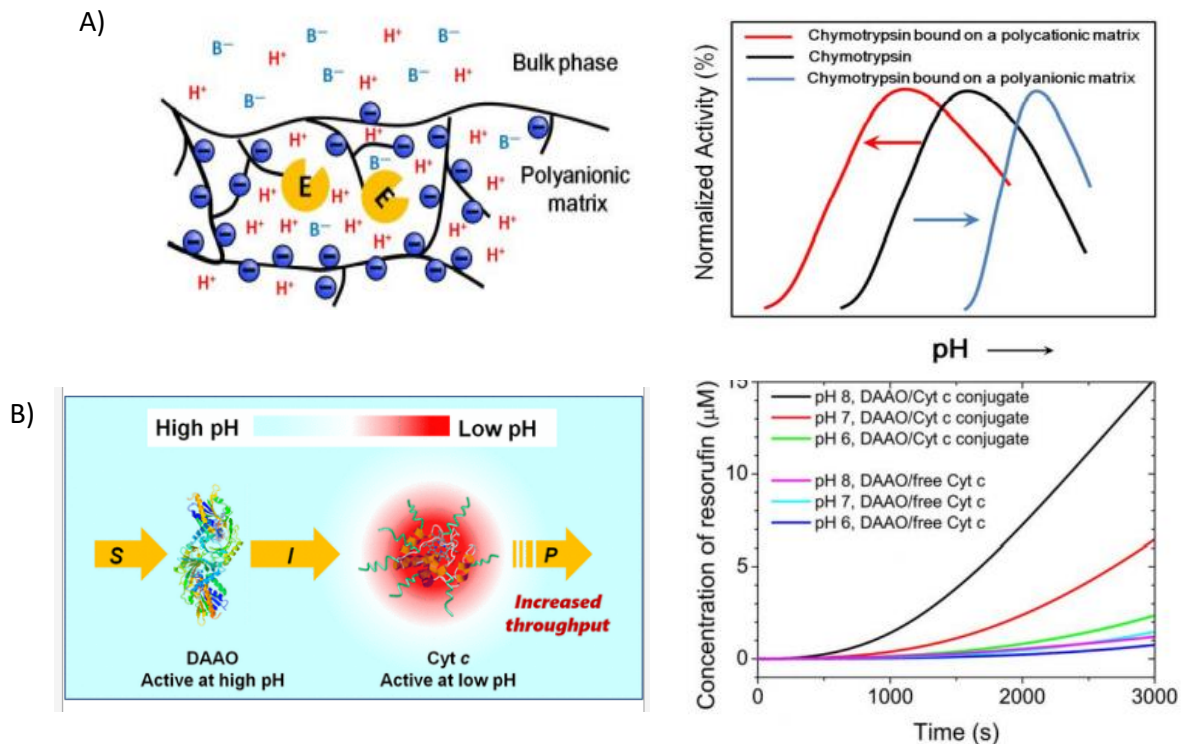


Figure 1.10 Microenvironmental pH effects on single enzymes and multiple enzymes. (A) Schematic representation of the proton distribution between a polyanionic matrix and the bulk solution (upper left panel), and an illustration of the shifts in the pH-activity profile of chymotrypsin bound on a polyanionic or polycationic matrices (upper right panel).^{24,157} (B) Activity enhancement in the DAAO -Cyt c cascade by creating a more acidic pH microenvironment for Cyt c (Adapted from Ref. 24 and 158 with permission from Elsevier and Copyright Clearance Center and American chemical society, see appendix on page 128 and 129).¹⁵⁸

Chymotrypsin (ChT) is a proteolytic enzyme and used protease for protein degradation applications. Substrate specificity towards charged peptides and its use at low pH (pH 5 and below) has recently been explored through engineering the local environment (**Figure 1.10A**). Attaching a positively-charged polymer onto the enzyme's free lysine residues (ChT has 14 surface lysines) created a dense cationic shell around the enzyme. The reaction mechanism of proteolytic cleavage is dependent on the stabilization of peptide substrates in the catalytic triad, serine, aspartic acid, and histidine. The

protonation state of the histidine is problematic; it must be deprotonated for the reaction to proceed.¹⁵⁹ The cationic shell of ChT-pQA effectively reduces the pK_a of the histidine, increasing catalytic activity at lower pH. The polymer-modified enzyme was also determined to be more thermostable, exhibit higher activity towards negatively charged substrates.¹³⁸

Immobilization provides an alternative approach to tuning the operating pH conditions of an enzyme, because the pH-activity profile of an enzyme often shifts after immobilization due to the nature of the carriers. If the enzymes are immobilized on poly-anionic or -cationic carriers the pH-activity profiles of enzymes shifted toward more alkaline or acidic pH ranges respectively compared to the native enzymes.^{138,160,161} Enzyme/polymer modifications have also been used to engineer pH-activity profiles of multi-step reaction cascades. As example, in a two-enzyme cascade reaction catalyzed by D-amino acid oxidase (DAAO) and cytochrome C (Cyt C) for the oxidation of alanine and the removal of coproduced hydrogen peroxide (by DAAO and Cyt C, respectively) faces challenges because they optimal pH for these enzymes are different (**Figure 1.10B**). DAAO exhibits optimum activity at basic pH, while Cyt C is active under slightly acidic conditions. Conjugation of negatively charged poly(methacrylic acid) to Cyt C created an anion shell around the protein that maintained a local environment of low pH. The engineered cascade achieved higher rates than the unmodified enzymes.¹⁵⁸

Nucleic acid-based nanostructures with various shapes and conjugation sites are capable of arranging multiple enzymes in nanometer precision. Cascade enzymes exhibited several-fold enhancement in overall activity while tethered on DNA scaffolds¹⁶²⁻¹⁶⁴ or on protein scaffolds^{165,166} compared to the untethered counterparts. The enhancement was often attributed to the proximity channeling that facilitated the transfer of intermediate substrates from the first enzyme to the next. In a demonstration for a model cascade system composed of glucose oxidase (GOx) and HRP conjugated them with the DNA-scaffold showed that the highly negatively charged DNA nanostructures can create a relatively more acidic pH microenvironment for the enzymes than the bulk solution which facilitate the rate enhancement.³⁶ This example also resembling the effect of polyelectrolyte carriers on immobilized enzymes described above.

1.5.3 Tuning the micro environmental temperature:

Locally heating the microenvironment of enzymes can control enzyme activity in a nano-/micro-scale without affecting the enzyme's structure. The folding state of an enzyme is sensitive to the surrounding temperature. A relatively high temperature (e.g., usually above 40 °C for most animal-derived enzymes) can lead to inactivation and even denaturation of enzymes.¹⁶⁷ However, heating the entire reaction system is energetically inefficient due to the high specific heat capacity of water.

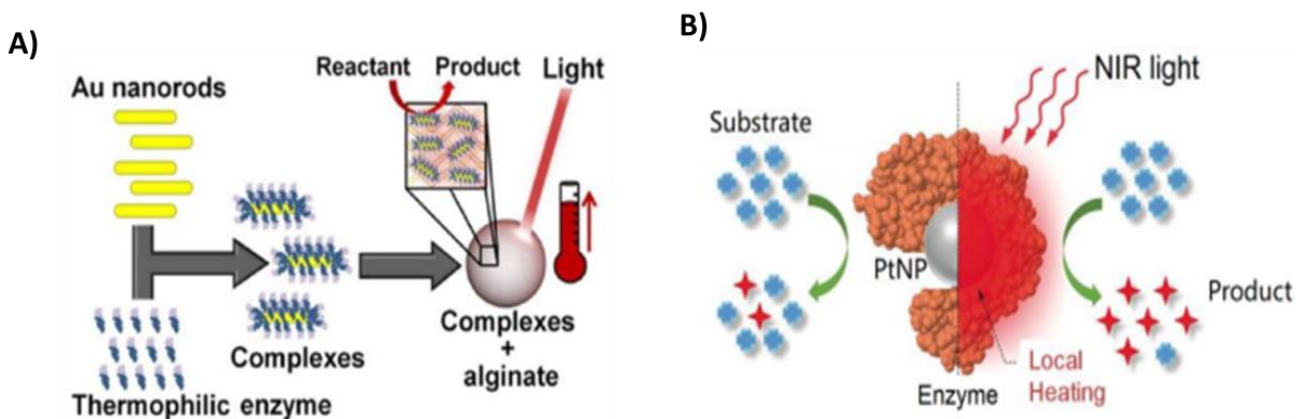


Figure 1.11 Two proposed strategies to increase the local temperature around enzymes. (A) Immobilization of enzymes on gold nanorods followed by encapsulation in Ca-alginate beads.¹⁶⁸ (B) Incorporation of platinum nanoparticles inside enzymes. The average diameter size of PtNP was 2.54 ± 0.31 nm.¹⁶⁹ (Adapted from ref. 168 and 169 with permission from John Wiley and Sons and Copyright Clearance Center and American chemical society, see appendix on page 129 and 130)

Thus, locally increasing the temperature near the enzymes becomes appealing for enhancing and controlling the activity of enzymes. Plasmonic nanoparticles with photothermal effects can act as nano-heaters for this task. For instance, thermophilic *A. pernix* glucokinase was immobilized on gold nanorods, which were subsequently encapsulated in calcium-alginate beads. Irradiation with 800 nm near-infrared light caused the temperature inside the beads to increase by 20 °C, while only a 2 °C difference was observed in the bulk (**Figure 1.11A**).¹⁶⁸ Similarly, platinum nanoparticles (Pt-NPs)

are also efficient thermoplasmonic light-to-heat converter that can generate a locally high temperature upon near-infrared irradiation. The enzymes (such as glucoamylase, glucose oxidase, catalase, and proteinase K) embedded with Pt-NPs exhibit higher activity enhancement after receiving pulsed near-infrared irradiation (**Figure 1.11B**). During the irradiation, the bulk temperature in solutions remained stable.¹⁶⁹ In addition to the temperature-induced activity increase, conjugation of Pt-NPs embedded enzyme with thermo-responsive materials, e.g., copolymer of acrylamide and acrylonitrile [poly(AAm-co-AN)] formed microscale aggregates at a temperature below the upper critical solution temperature (UCST). Upon near-infrared irradiation, the photothermal heating by platinum nanoparticles increased the local temperature above the UCST and then the aggregates became soluble, exposing enzymes to their substrates and enhances reaction rate.¹⁷⁰ These examples evidenced microenvironmental temperature engineering that regulate the apparent enzyme performance without requiring an engineering of the intrinsic enzyme properties.

1.6 Enzyme cascade

Enzyme cascade reactions are multi-step chemical reactions catalyzed by a series of enzymes. The product of each enzyme is consumed by the next enzyme, and so on (**Figure 1.12**). Most biological processes are in fact accomplished by such complex multi-enzyme synthetic pathways. For instance, the metabolism of glucose by the glycolytic pathway involves the participation of ten enzymes that work sequentially and efficiently.¹⁷¹ Similarly, the multistep citric acid cycle is a metabolic pathway that connects carbohydrate, fat, and protein metabolism, and a complete cycle involves eight enzymes.¹⁷² Inspired by multi-enzyme reaction systems in nature, researchers have devoted efforts to reconstitute those cascade reaction systems in vitro with precise engineering designs. Combination of enzyme reactions into a multistep one-pot biocatalytic process brings additional benefits, including the fact that intermediates need not be isolated as they are directly transferred to the next step of the reaction sequence.^{12-14,173-177} Generally, this can reduce cost, time, effort, and increase final yield of product.¹⁷⁸

Moreover, enzyme cascade reactions can be accelerated by local nanoscale confinement of the enzymes, and theories to explain this include providing a more favorable micro-environment for catalysis and/or by promoting mass transfer of intermediates from one enzyme to another.¹⁷⁹ Nature accomplishes this by compartmentalization, such as within cells or sub-cellular compartments.¹⁸⁰

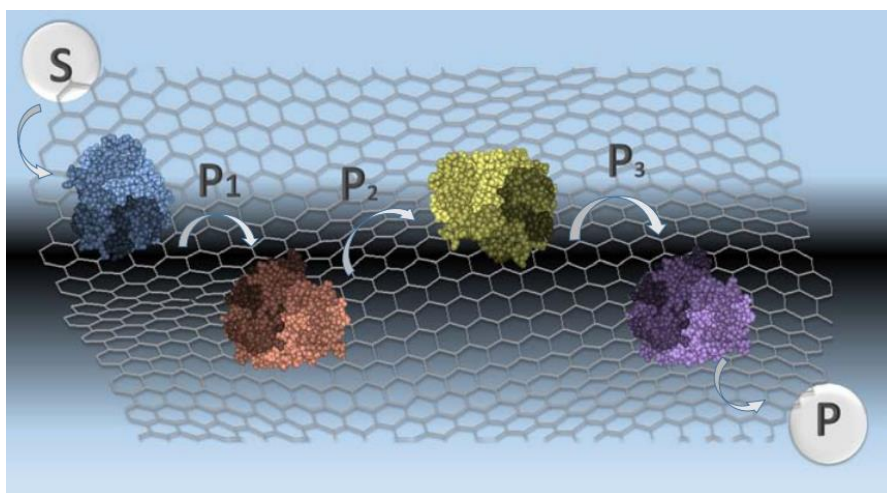


Figure 1.12 A Schematically Represented Cascade Reaction comprising four enzymes. S represents the initial substrate added to the reaction, while P represents the final product of the cascade process. P1, P2, and P3 are the intermediate products released by each enzyme, which are then used as substrates for the following enzyme. The cascade reaction proceeds until the final desired product is formed.¹⁸¹ (Adapted from Ref. 181 with permission from Elsevier and Copyright Clearance Center, see appendix on page 130)

Multienzyme Co-immobilization onto nano-supports for cascade reactions have gained importance in biotransformation and biomedical engineering and are regarded as an alternative for the production of pharmaceuticals, biofuels, and fine chemicals.¹⁸² The synthesis of carbohydrates,^{183,184} polymers,¹⁸⁵ chiral alcohols,¹⁸⁶ and β -glucosidase¹⁸⁷ are some examples of multienzyme reactions in one pot.

Substrate channeling is an advantage arising from enzyme complexes. This involves direct transfer of the product as a substrate from an enzyme to the next enzyme with the bulk phase without equilibration, as shown in **Figure 1.13**

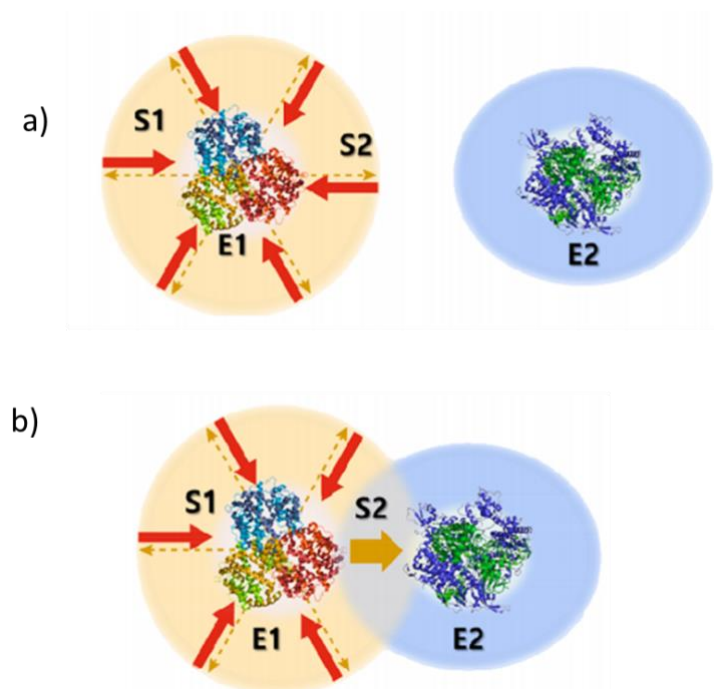


Figure 1.13 Schematic illustration of the substrate (S1 and S2) channeling effect between (a) two free-floating enzymes (E1 and E2) and (b) two proximate enzymes (E1/E2).¹⁸² (Adapted from Ref. 182 with permission from American Chemical Society, see appendix on page 131)

Such phenomena take place only when the distance between two active sites is short. In addition, overall reaction rates can be increased in an efficient way^{188,189} though some other group claimed there might be other reasons than proximity that enhances substrate channeling. Idan et. al. immobilized two enzymes on DNA scaffold in various distances. No proximity effect was detected in the closer distance than the farther one. They suggested that the reason for the activity enhancement of enzymes localized by DNA scaffolds is that the pH near the surface of the negatively charged DNA nanostructures is lower than that in the bulk solution, creating a more optimal pH environment for the anchored enzymes.³⁶

Multienzyme cascade approach has been emulated artificially using inorganic nanoparticles,¹⁹⁰ polymersomes,¹⁹¹ or by tethering the enzymes to a scaffold (e.g., DNA origami, other proteins, or even viruses).^{108,192}

1.7 Michaelis-Menten (steady-state) Kinetics

In biochemistry, Michaelis–Menten kinetics is one of the best-known models of enzyme kinetics.¹⁹³ It is named after German biochemist Leonor Michaelis and Canadian physician Maud Menten. The model takes the form of an equation describing the rate of enzymatic reactions, by relating reaction rate v (rate of formation of product $[P]$ to $[S]$ (the concentration of a substrate S). The formula is given by

$$v = \frac{d[P]}{dt} = \frac{V_{max} \cdot [S]}{K_M + [S]}$$

Here, V_{max} represents the maximum rate achieved by the system, happening at saturating substrate concentration for a given enzyme concentration.

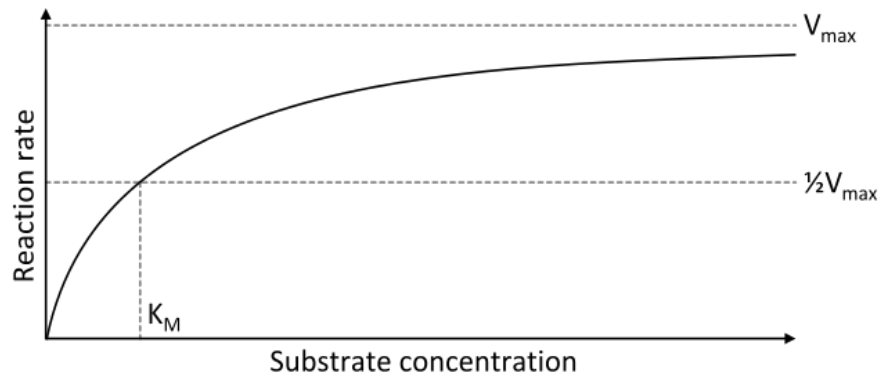
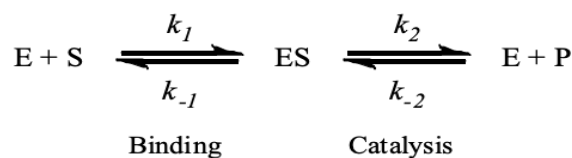


Figure 1.14 Michaelis–Menten saturation curve for an enzyme reaction showing the relation between the substrate concentration and reaction rate.

Here we show the derivation of Michaelis-Menten (steady-state) Kinetics:

The Michaelis-Menten model for enzyme kinetics presumes a simple two-step reaction:



Step 1: Binding – the substrate binds to the enzyme

Step 2: Catalysis – the substrate is converted to product and released

Several simplifying assumptions allow for the derivation of the Michaelis-Menten equation:

1. The binding step ($E + S \rightleftharpoons ES$) is fast, allowing the reaction to quickly reach equilibrium ratios of $[E]$, $[S]$, and $[ES]$. The catalytic step ($ES \rightleftharpoons E + P$) is slower, and thus rate-limiting.
2. At early time points, where initial velocity (V_o) is measured, $[P] \approx 0$.
3. ES immediately comes to steady state, so $[ES]$ is constant (throughout the measured portion of the reaction).
4. $[S] \gg [ET]$, so the fraction of S that binds to E (to form ES) is negligible, and $[S]$ is constant at early time points.
5. The enzyme exists in only two forms: free (E), and substrate-bound (ES). Thus, the total enzyme concentration (ET) is the sum of the free and substrate-bound concentrations: $[ET] = [E] + [ES]$

A derivation of the Michaelis-Menten equation shows how to use the above assumptions to describe the rate of the enzyme-catalyzed reaction in terms of measurable quantities:

From (1), we know the overall rate of the reaction is determined by the rate of the catalytic

step: $V_o = k_2[ES] - k_{-2}[E][P]$

From (2): $V_o = k_2[ES]$

$[S]$ is known, from (4). To express $[ES]$ in terms of $[S]$, we can start from (3):

Rate of formation of ES = Rate of breakdown of ES , therefore,

$$k_1[E][S] + k_{-2}[E][P] = k_{-1}[ES] + k_2[ES]$$

From (2) this simplifies to: $k_1[E][S] = k_{-1}[ES] + k_2[ES]$

We can factor out [ES] and group the rate constants:

$$k_1[E][S] = [ES]\{k_{-1} + k_2\}$$

$$[E][S] = [ES] \left\{ \frac{k_{-1} + k_2}{k_1} \right\}$$

This ratio of rate constants is defined as the Michaelis Constant, K_m :

$$K_m = \frac{k_{-1} + k_2}{k_1}$$

Substituting in K_m for the rate-constant ratio gives: $[E][S] = [ES]K_m$

Just as [ES] is not easy to measure, [E] is also not easy to measure. However, $[E_T]$ is known. Rearranging (5) for [E] and substituting, we get:

$$\{[E_T] - [ES]\} [S] = [ES] K_m$$

Here we can multiply, rearrange, factor, and divide, to get [ES] in terms of [ET], [S], and K_m :

$$[E_T] [S] - [ES][S] = [ES] K_m$$

$$[E_T] [S] = [ES] K_m + [ES][S]$$

$$[E_T] [S] = \{[ES] K_m + [S]\}$$

$$[E_T] [S] = \{[ES] K_m + [S]\}$$

$$\frac{[E_T] [S]}{K_m + [S]} = [ES]$$

Now we can substitute our expression for [ES] into the rate equation:

$$V_o = k_2[ES] = \frac{k_2[E_T][S]}{K_m + [S]}$$

At high [S] (when [S] \gg K_m), nearly all enzyme will have substrate bound, and [ES] approaches [E_T]. This is when V_o approaches V_{max} . Since $V_o = k_2[ES]$, (Or, mathematically, when [S] \gg K_m , K_m is negligible, and the equation simplifies to):

$$V_{max} = k_2[E_T]$$

$$\left(V_{max} = \frac{k_2[E_T][S]}{[S]} = k_2[E_T] \right)$$

Substituting V_{max} in to the rate equation gives the Michaelis-Menten equation:

$$V_o = \frac{V_{max}[S]}{K_m + [S]}$$

1.8 Conclusion

From the literature review above, important points can be made:

-Enzymes are natural biocatalysts that accelerate many biochemical reactions, thus are widely used in healthcare and manufacturing. The widespread industrial use of enzymes can be hampered by their lack of long-term stability (towards solvent, pH and temperature) and by the sometimes-burdensome recovery of enzyme/products.

-Recent advances in biotechnology have provided the basis for the efficient development of enzymes with improved properties. Tailoring enzyme properties by active site engineering is an approach to improve catalytic efficiency of an enzyme. It also facilitates to increase tolerance to harsh pH, increase substrate acceptance, increase substrate selectivity.

-Enzyme engineering by rational design significantly reduces the effort and time is required for the screening of the library, nonetheless this method is applicable only when there is detailed knowledge of enzyme's structural features of the active site and their contribution to function is available.

-Enzyme engineering by directed evolution has become the most widely used approach to optimize performance, because it can be accomplished without in-depth knowledge of structure/ function relationships. The challenges for this method are choosing the appropriate screening strategy to find the most active enzyme from the huge library.

-Immobilized enzymes are more robust and more resistant to environmental changes compared to free enzymes in solution. The diversity of the immobilized enzyme systems allows an easy recovery of enzymes and products, recycling of enzymes, continuous operation of enzymatic processes, and rapid termination of reactions.

-Another approach to increase catalytic activity is by microenvironment engineering. This approach also enhances catalytic efficiency of an enzyme by placing it in a more favorable local environment for catalysis.

-The microenvironment can be altered locally by encapsulation in nano- or micro-compartments, immobilization on carriers, conjugation with polymers, aggregation into complexes, adding additives, and so forth.

- The development of new multienzyme complex structures by immobilization has received attention for several years, and new strategies for stabilizing enzymes with improved enzymatic cascade activity and operational stability have been achieved by classical immobilization methods with specific strategies, such as random co-immobilization, compartmentalization, and positional co-immobilization.

1.9 Objectives of the thesis

Within the context of the research above on manipulating the catalytic properties of enzymes, the objective of this thesis is to investigate microenvironmental effects experienced by enzymes displayed on a phage. Understanding microenvironmental

effects caused by attachment to a phage would be important when screening enzymes by phage display techniques, and equally have relevance when using phage as an immobilization scaffold for conveniently handling the enzyme.

The specific objectives of this thesis are:

- 1) To display *Bacillus subtilis* lipase A on a phagemid and explore the effect of this templating on its catalytic properties, and the influence of this template on nanoscale distribution in solution.
- 2) Having seen that nanoscale distribution has an important effect on activity, the second objective is to further explore the potential of nanoscale distribution, by controlled oligomerization of enzymes templated on a nanoscale template. Moreover, the influence of nanoscale distribution on the communication between enzymes was explored.
- 3) To develop analytical technique suitable for the analysis of complex substrates, and suitable for use with the complex nanoscale immobilized enzymes from above.

1.10 Overview of the scientific content of this thesis

To achieve this overarching objective, the remainder of this thesis is divided into Chapters as follows:

In **Chapter 2**, a phagemid platform was engineered to display BSLA on the p3 minor coat protein. The catalytic properties of the phage-displayed and free BSLA were compared in a number of different conditions to understand differences between the two. This study concludes that the phage promotes the interaction between the displayed BSLA and substrate-rich micelles, which enhances activity.

In **Chapter 3**, three different enzymes (BSLA, GOx, and HRP) are immobilized onto a phagemid to explore whether such grafting would promote the communication between these enzymes and enhance a multi-step reaction. By varying the degree of enzyme grafting and by exploring intra- and inter-phage crosslinking, this study concludes that the phage enhances the rate of the cascade by providing a more favorable microenvironment

to the slowest enzymes in the cascade. Inter-phage crosslinking had the most pronounced effect, as this parameter is expected to promote enzyme/phage interactions.

The chapter above revealed that elucidating physical mechanisms influencing catalysis is complex, and tools that would facilitate monitoring enzyme kinetics in a label-free fashion would be highly valuable for this. As such, in **Chapter 4** we explore the use of a THz emission technology for the quantitative and label-free analysis of complex enzyme catalyzed reactions. This technology was utilized to monitor the catalytic activity of BSLA towards several different optically-inactive substrates and towards a complex substrate, cow milk. This technique could be very useful for facilitating the analysis of individual enzymes within complex systems, such as those explored earlier in this thesis.

In **Chapter 5**, a discussion is provided that presents the most significant finding of this thesis, its major limitation, what makes this work different from the work of others, what remains to be done, and how this thesis will benefit society.

CHAPTER 2

The phage display of *Bacillus subtilis* Lipase A significantly enhances catalytic activity due to altered nanoscale distribution in colloidal solution

Preface:

As mentioned in the previous section, our first objective was to display *Bacillus subtilis* lipase A (BSLA) on a phage and explore the effect of this templating on its catalytic properties. To achieve this objective phagemid based phage display platform was chosen to display BSLA on p3 coat protein of M13 phage. BSLA display was characterized by western blot and by measuring its catalytic activity. Interestingly, significant enhanced catalytic activity was detected for BSLA while it was attached to the phage in compare to the free BSLA in solution. To explore the mechanism to the enhancement of activity, we characterized the i) stability of the phage displayed enzyme towards pH and temperature ii) nanoscale distribution within the heterogeneous assay buffer. To characterize the nanoscale distribution of the enzyme in the reaction solution, the effect of additives (e.g., salt, poly(ethylene glycol) and wild type M13 phage) to the assay buffer was examined. The experimental findings for both phage bound BSLA and free BSLA was compared.

Note: A version of this chapter has been published in Biotechnology and Bioengineering

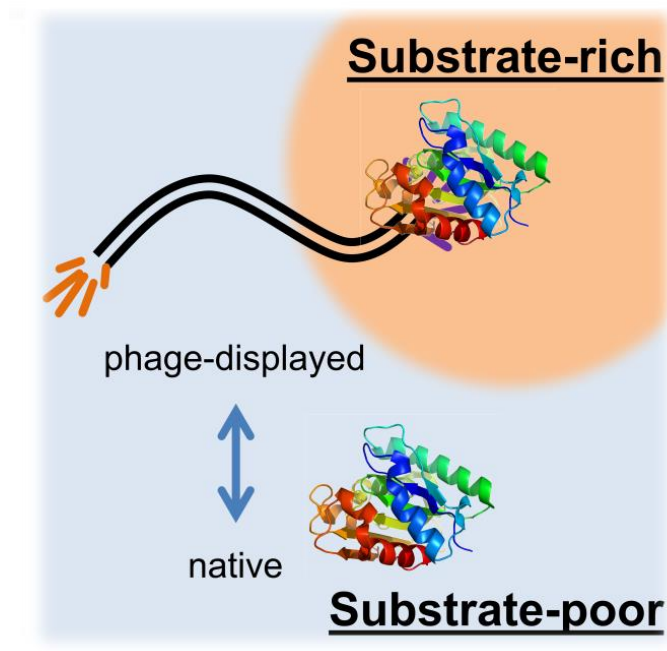
COMMUNICATION TO THE EDITOR

The phage display of *Bacillus subtilis* Lipase A significantly enhances catalytic activity due to altered nanoscale distribution in colloidal solution

Sharifun Nahar, Esen Sokullu, Marc A. Gauthier ✉

First published: 23 November 2019 | <https://doi.org/10.1002/bit.27229>

Graphical Abstract:



Abstract:

Screening libraries of mutant proteins by phage display is now relatively common. However, one unknown factor is how the bacteriophage scaffold itself influences the properties of the displayed protein. This chapter evaluates the effect of solution parameters on the catalytic activity of phage displayed *Bacillus subtilis* Lipase A (BSLA), compared to the free enzyme in solution. While the pH- and temperature-activity profiles of BSLA were not intrinsically affected by phage display, the nanoscale distribution of BSLA within the micellar assay buffer was. This leads to a pronounced increase of activity of phage–BSLA relative to the free enzyme, owing to the accumulation of phage–BSLA at the substrate-rich micelles. Considering this result obtained for BSLA, caution is warranted and similar effects should be considered when selecting other enzymes/proteins by phage display, as the activity of the displayed protein may differ from that of the free protein.

2.1 Introduction

Proteins are economically important biomolecules because of the specificity with which they bind target molecules (e.g., monoclonal antibodies), catalyze chemical reactions (e.g., enzymes), and can be used to modulate biological processes (etc.).^{194,195} The identification of new proteins and their optimization for a given application are thus active areas of research in the manufacturing and healthcare sectors. This, however, is challenging because proteins are complex molecules and it is difficult to computationally predict how modifications to their amino acid sequence will influence their properties. To reconcile this challenge, the field has developed approaches, such as directed or random mutagenesis (to generate ultra-diverse protein libraries) as well as strategies to screen these libraries and select hits. One of the most commonly used selection strategies is phage display, in which the protein of interest is displayed on a coat protein of a bacteriophage, and its amino acid sequence is encoded by the DNA contained within.⁷² Phage display has been used to screen libraries of proteins based on their ability to bind

to a target of interest,^{196,197} to select peptide mimotopes for use in vaccines,^{198,199} to investigate immune responses,^{200,201} to evaluate peptides for drug candidates, etc.^{202,203} However, while phage display is now relatively common, one unknown factor is how the bacteriophage scaffolds itself influence the functional properties of the displayed protein. Indeed, because of its highly repetitive structure, the bacteriophage may create a local microenvironment that is different from bulk solution. For instance, our group and others have demonstrated that pH-responsive polymers can alter the properties of proteins by locally altering solution pH.^{158,204} moreover, the bacteriophage scaffold may itself be influenced by solution parameters such as salts, concentration, surfactants, or crowding agents, which may in turn influence the activity the displayed protein. Thus, the selection of hits by phage display may – under certain circumstances – be inappropriate because the activity of the displayed protein may differ from those of the free protein. This issue may be particularly problematic when screening catalytic proteins (enzymes) for the manufacturing sector, owing to the use of concentrated or complex solutions for production processes (as opposed to simple dilute solutions). To investigate this scientific question, our work evaluates the effect of solution parameters on the catalytic activity of a phage displayed enzyme, *Bacillus subtilis* Lipase A (BSLA), compared to the free BSLA in solution. Of the enzymes that have been studied by phage display in the literature,²⁰⁵⁻²⁰⁹ lipase is an excellent model because of its industrial importance in the hydrolysis/synthesis of esters in the food (for flavor and aroma), pharmaceutical, cosmetic, detergent, fuel industries, etc.^{210,211} Moreover, considering that many of these reactions occur in organic–aqueous emulsions, BSLA is an excellent model to investigate the influence of the phage scaffold on enzyme activity in complex colloidal solutions.

2.2. Materials/methods

2.2.1. Materials: Plasmid, bacterial strain, helper phage and culture media

XL10-Gold Ultracompetent Cells (*TetrD(mcrA)183 D(mcrCB-hsdSMR-mrr)173 endA1 supE44 thi-1 recA1 gyrA96 relA1 lac Hte [F' proAB lacIqZDM15 Tn10 (Tetr) Amy Camr]*) were purchased from Agilent Technologies, USA. The plasmid pADL-20c Phagemid and

CM13 Interference-Resistant Helper Phage were purchased from Antibody Design Laboratories. NZY Broth contained: NZ amine (casein hydrolysate) (1% w/v), Bacto yeast extract (0.5% w/v), sodium chloride (0.5% w/v) and magnesium sulfate (0.2% w/v). 2x YT medium contained: Bactotryptone (1.6% w/v), Bacto yeast extract (1% w/v), and sodium chloride (0.5% w/v); LB medium contained: Bactotrypton (1% w/v), Bacto yeast extract (0.5% w/v), and sodium chloride (0.5% w/v). All of the ingredients for culture medium were purchased from BioShop Canada Inc. The antibiotics ampicillin and kanamycin were purchased from Sigma and were used at 100 µg/mL and 50 µg/mL, respectively. Chemicals used for enzyme assay: polyethylene glycol (PEG), NaCl, EDTA, Triton X-100 was purchased from BioShop Canada Inc. Gum Arabic, 4-Nitrophenyl octanoate and 4-Nitrophenol was purchased from Sigma-Aldrich.

2.2.2 Genomic DNA and enzymes

The genomic DNA of *Bacillus subtilis* (ATCC® Number: 23857D-5™) and native Lipase A from *Bacillus subtilis* were purchased from Cedarlane (Canada). Restriction enzymes Bgl I, Sfi I, Phusion High-Fidelity DNA polymerase (for PCR), and Shrimp Alkaline Phosphatase (rSAP) were purchased from New England BioLabs. 4-Nitrophenyl octanoate was purchased from Sigma Aldrich.

2.2.3 Primer Design and PeIB Leader Sequence (Oligonucleotides)

The DNA sequence of *LipA* was acquired from genomic DNA of *B. subtilis* by using the forward and reverse primer as following: LIPF-5' ATAT ***GGCC CAGC C GGCC***ATG GCG ATG AAA TTT GTA AAA AGA 3' (Sfi I), LIPR-5' ATAT ***GGCC TCCCG GGCC*** TTA ATT CGT ATT CTG GCC 3' (Sfi I). Restriction sites are mentioned in italic bold.

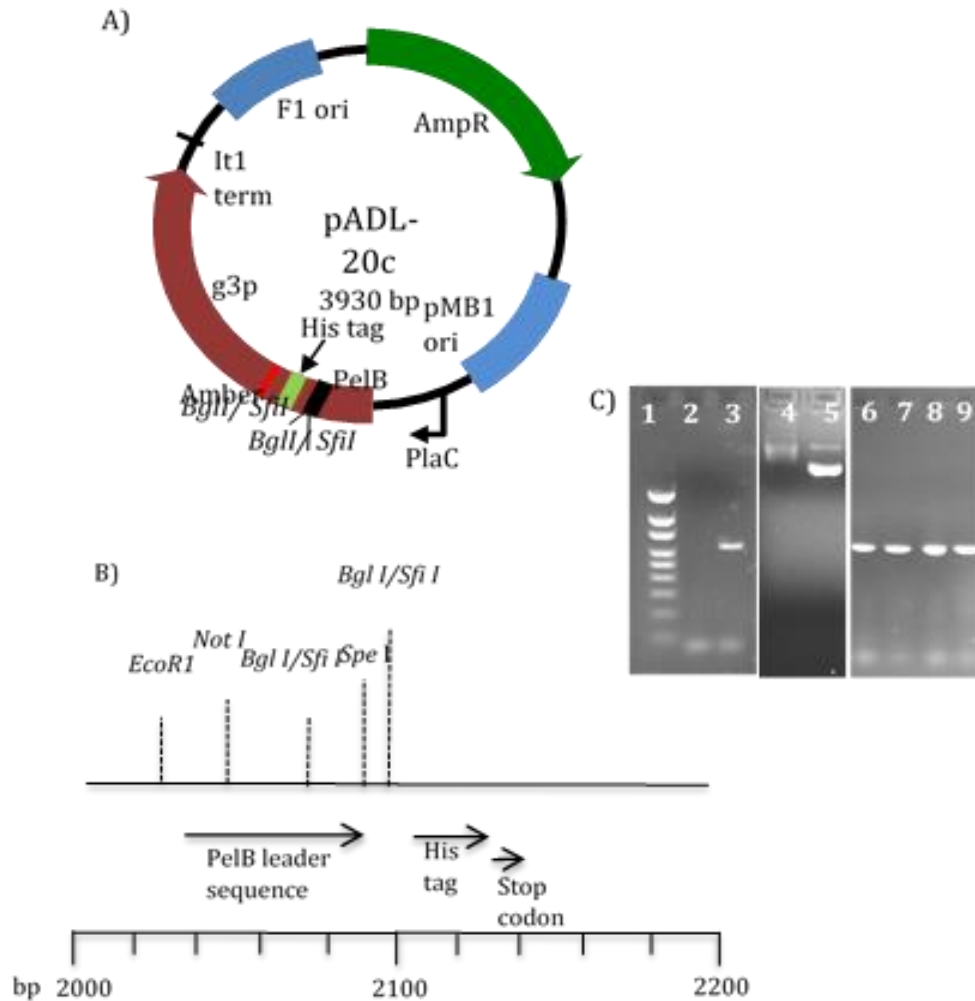


Figure 2.1 A) The phagemid pADL-20c map and B) schematic representation of the molecular structure of the vector used for the cloning of *lipA* gene. After *Sfi* I and *Bgl* I digestion, the *lipA* gene was cloned in *E. coli* into the *Sfi* I and *Bgl* I sites of the phagemid pADL-20c. C) Agarose gel electrophoresis of Lipase A DNA. Lane 1: 1 kb DNA ladder; 2: negative control of PCR (no DNA); 3: *lipA* DNA PCR product using LIPF & LIPR primers; 4: uncut phagemid; 5: cut phagemid after digestion with *Sfi*I; 6–9: colony PCR after transforming to *E.coli* with LIPF and LIPR primers.

A complete PelB leader sequence *MKYLLPTAAAGLLLLAAQPAMA* is necessary for export the synthesized proteins to the periplasm and proper removal of the leader peptide by host proteases. To design the LIPF primer, the short hexanucleotide *ATGGCN* was introduced immediately to the first *Sfi* I site to obtain a complete PelB leader encoding

sequence. The custom designed primers were purchased from Integrated DNA Technologies.

2.2.4 Construction of the plasmids

The phagemid pADL-20c was used to construct the recombinant plasmid. The map of the phagemid is shown in **Figure 2.1a** and the schematic representation mentioning the positions of the restriction sites in the DNA sequence is shown in **Figure 2.1b**. The 639-bp encoding gene for BSLA (**Figure 2.1c**) was cloned in the pADLTM-20c cloning site downstream of the *pelB* leader sequence and upstream of the His-tag and amber codon. The histidine residues can be used for the purification of fusion proteins. The amber codon is useful to produce soluble enzyme when a non-suppressor *E. coli* strain is used. The *SfiI* restriction enzyme requires two copies of its recognition sequence for cleavage to occur. Since pADLTM-20c has two sites very close to each other, so cut is done in-trans (in two different DNA) and digestion might thus not be complete. Therefore, opening of the phagemid was done with an alternative restriction enzyme, *BglI*, which cuts the shorter sequence (6 bases) and generates identical overhangs. The *lipA* sequence was amplified from the genomic DNA of *B. subtilis* 168 using the LIPF and LIPR primers. PCR was performed using Phusion HF DNA polymerase. To obtain high yields of PCR product, the following PCR protocol was used: 30 s 98 °C, 35 cycles of 10 s 98 °C, and 15 s 72 °C. At the end, DNA production was finished for 10 min at 72 °C. The amplified gene fragment (**Figure 2.1C**) was purified using QIAquick PCR purification kit (QIAGEN) digested with *SfiI*. Opening of pADL-20c was done with the *BglI* restriction enzyme followed by de-phosphorylation by shrimp alkaline phosphatase. The digested phagemid was purified from the gel using a QIAquick Gel Extraction kit. The purified digested insert DNA and phagemid were ligated using T4 ligase and transformed into XL10-Gold ultra-competent cells using the manufacturer's protocol. Prior to phage display, the transformed cell (referred to as *EpADL20LIPA*) was sequenced to verify the correct base pair sequence (Plate-forme d'Analyses Génomiques, Université Laval, Québec). The stock of *EpADL20LIPA* was preserved at -80 °C with 50% glycerol until used.

2.2.5 Phage display of BSLA

EpADL20LIPA (phagemid-containing bacteria) was inoculated in a LB agar plate and incubated overnight at 37°C. A single colony was cultured in 3 mL of 2× YT media containing 1% (w/v) glucose and 100 µg/mL ampicillin at 37°C in a shaker incubator overnight. The next morning, PCR was performed with LIPF and LIPR primers and only PCR-positive tubes were further diluted (1:20 v/v) and allowed to grow until an OD of 0.5 at 600 nm was reached. In this exponential growth phase of the bacteria, 1 µL of helper phage (from a stock 2.0×10^{12} pfu/mL) was added to each 1 mL of bacterial culture (at a final concentration of 2×10^9 phage/mL). After 16 h of growth at 30 °C (shaker incubator) in glucose depleted 2× TY medium containing ampicillin (100 µg/mL) and kanamycin (50 µg/mL), the culture was centrifuged at 13,000g for 5 minutes. The supernatant containing phage was transferred carefully to another tube, leaving the bacteria in the pellet, and phage were precipitated by addition of PEG/NaCl containing 20% w/v polyethylene glycol (8 kDa)/2.5 M NaCl (one fourth volume of phage solution). After centrifugation, the pelleted phage was re-suspended in 0.5 mL 10 mM Tris-HCl buffer (pH 7.4) containing 1 mM EDTA.

2.2.6. Electrophoresis

Sodium dodecyl sulfate polyacrylamide gel electrophoresis (SDS-PAGE) was performed using Mini-PROTEAN® TGX™ Precast Gels (Bio-Rad). After electrophoresis, proteins were blotted to nitrocellulose and immunostained with an anti-M13 p3 monoclonal antibody (mouse isotype IgG2a) (New England Biolabs Ltd.). Detection of the antibody was performed with anti-mouse IgG (H+L) to which is conjugated horseradish peroxidase (Promega, North America).

2.2.7 Counting phage lipase

The number of phage particles in suspension was determined spectrophotometrically. The method is based on the relationship between the length of the viral DNA and the

amount of proteins, which, together, are the major contributors of the absorption spectrum in the UV range at 269 nm.²¹² Each phage particle contains a fixed amount of g3p, g6p, g7p and g9p (i.e., 6×10^{-16} mg per phage particle).²⁰⁶ The amount of g8p depends on the size of the DNA that is packed. A EpADL20LIPA phage particle (4569 nt) weighs approximately 2.0×10^{-14} mg. The relationship between virion number and absorption was calculated by using the equation:

$$\text{Virions/mL} = (A_{269} - A_{320}) \times (6 \times 10^{16}) \div 4569 \quad \text{eq. 1}$$

2.2.8 Nanoparticle Tracking Analysis

NTA measurements were performed using a NanoSight NS300 instrument (Malvern Panalytical, UK), which is a laser based light scattering system. Phage samples (in water or enzyme assay buffer; *vide infra*) were diluted with sterile water to reach a particle concentration suitable for analysis ($\sim 1 \times 10^7$ to 1×10^9 particles/mL) and ran (300 μ L) through the flow cell with a 1 mL sterile syringe controlled with a syringe pump at a speed 100 (arbitrary units). Each sample was run five times. The capture settings (shutter and gain) and analysis settings were manually set and then optimized for each sample. Sixty-second sample videos were recorded, which were then analyzed with the NTA 3.3 Analytical software.

2.2.9 Concentration of native BSLA

Prior to use, as-received BSLA was established to be 86% pure based on analysis by HPLC with detection at 280 nm. As such, lipase concentration calculated from its absorbance at 280 nm (extinction coefficient: $24,410 \text{ M}^{-1}\cdot\text{cm}^{-1}$) was corrected by this value. Note that none of the impurities displayed catalytic activity, and were not further characterized.

2.2.10 Composition of assay buffer

Assay buffer for measuring catalytic activity consisted of 50 mM sodium phosphate, pH 8, containing 0.36% Triton X-100 (v/v) and 0.1% (w/v) gum Arabic. This buffer was used for enzyme assays and modified when required to study the effect of additives (*vide infra*).

2.2.11 Lineweaver-Burke analysis

Enzymatic activity was determined spectrophotometrically via the hydrolysis of 4-nitrophenyl octanoate (4-NPO). A stock solution of 10 mM of 4-NPO in methanol was prepared. Reactions with various concentrations of the 4-NPO solution (0.05–2 mM) were prepared to 0.1 mL assay buffer in the presence of 1.9 µg/mL lipase or 5×10^{12} phage particles/mL and the absorbance was measured at 410 nm for the production of 4-nitrophenol (molar extinction coefficient $18,000 \text{ M}^{-1}\cdot\text{cm}^{-1}$). One unit (U) is defined as the amount of enzyme that hydrolyzes 1 µmol 4-NPO per min. The Michaelis-Menten constant (K_M), maximum velocity (V_{max}), and turn-over number (k_{cat}) of the native and phage-bound lipase were determined using substrate concentrations ranging from 0.05 mM to 2 mM. In all cases, the background hydrolysis of the substrate in controls without enzyme (blanks) was subtracted from the sample data. Reactions were repeated in triplicate.

2.2.12 Effect of additives effect on enzyme activity

Effect of pH on lipase activity

To evaluate the effect of pH on catalytic activity, 50 mM sodium phosphate having different pH (pH 4–12) were prepared separately, then 0.36% Triton X-100 (v/v) and 0.1% (w/v) gum arabic were added. The final reaction mixture contained 0.2 mM of 4-NPO and 1.2 µg/mL of native lipase or 1×10^{12} phage/mL of phage lipase. Enzyme activity was also measured in equivalent solutions containing 0.5 mM of NaCl. Reactions were repeated in triplicate.

Enzyme activity in the presence of salt

Different amounts of solid NaCl crystals were added to the assay buffer to reach final concentrations of 0–2000 mM, and enzyme activity was measured with 0.2 mM 4-NPO for either native or phage-displayed lipase A (1.2 µg/mL or 1×10^{12} phage/mL respectively). Reactions were repeated in triplicate.

Enzyme activity in the presence of PEG and wild-type M13

The effect of PEG or wild-type M13 phage as crowding agents on the catalytic activity of native and phage-BSLA was evaluated. Various concentrations (in percent) of PEG (8 kDa; 0–20% wt %) were added to the assay buffer. One hundred-µL of these buffers were used to measure enzyme activity for native (1.2 µg/mL) and phage-BSLA (1×10^{12} phage particle) with 0.2 mM 4-NPO. To observe the effect of wild-type M13, a stock solution of M13 (3×10^{15} phage/mL) was prepared in 1× TBE buffer (10 mM Tris-HCl buffer, pH 7.4, containing 1 mM EDTA) and 0.12 µL or 1.2 µL of this solution was added to 100 µL of assay buffer to obtain 0.069 or 0.697 mg/mL of phage. The concentration of phage in solution was calculated by using the molecular weight of M13 (1.2×10^7 Da). These mixes were used for enzymatic reaction containing native (1.2 µg/mL) and phage lipase A (1×10^{12} phage particle/mL) with 0.2 mM 4-NPO. Reactions were repeated in triplicate.

Temperature effect on lipase activity

Native (1.2 µg/mL) and phage-BSLA (1×10^{12} phage particle/mL) activity was measured in assay buffer with 0.2 mM 4-NPO at various temperatures (24 – 70 °C). Alternatively, native and phage-displayed BSLA were incubated at temperatures from 24 – 80 °C for 20 minutes, then activity measured at room temperature. Heat-treated phage-displayed lipase particles were also analyzed by NTA as indicated at the section 2.6.3. Reactions were repeated in triplicate.

2.2.13 Statistical analysis

Comparison of means was performed by One-way analysis of variance (ANOVA), followed by a Tukey post-hoc test with a level of significance of $p < 0.05$.

2.3 Result and discussion

M13 was chosen to display BSLA, as it is the most commonly used filamentous phage used for phage display. However, considering that large proteins fused to the p3 coat protein can interfere with capsid assembly, a phagemid system was adopted rather than wild-type M13. In general, phagemid systems display between 0–1 copies of the fusion protein per phage,^{65,66} which is advantageous herein because it allows for the analysis of individual BSLA molecules on a given phage particle, and thus effects resulting from multiple enzymes co-displayed on the same phage can be neglected. Unfortunately, variable display levels of BSLA on the phagemid make it difficult to estimate enzyme concentration for these samples.

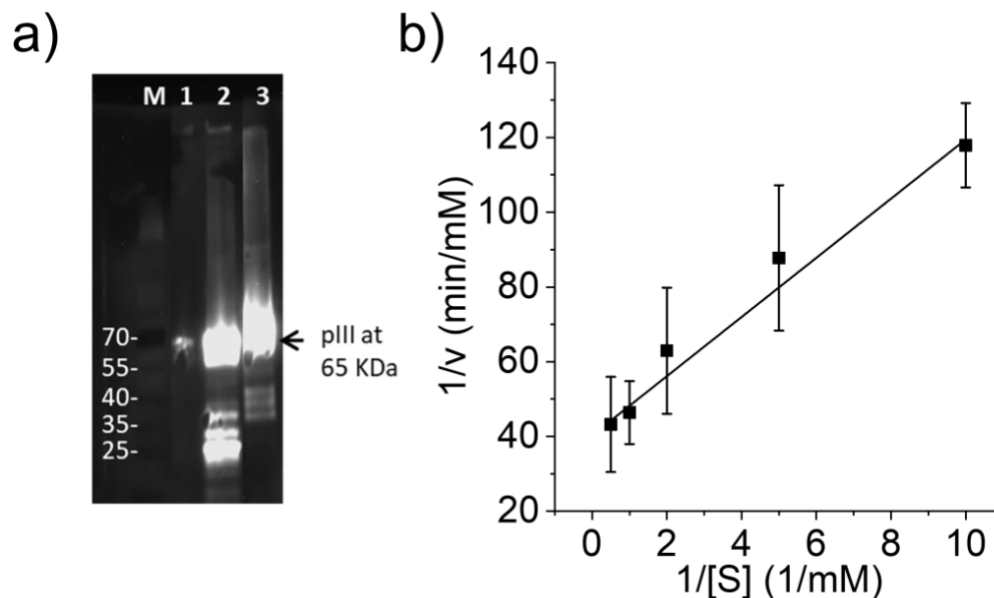


Figure 2.2 Characterization of phage displayed BSLA. (a) Western Blot analysis immunostained with mouse anti-M13 p3 monoclonal antibody (M: molecular weight ladder, Lane 1: phage displayed BSLA, Lane 2: wild-type M13, Lane 3: M13KO7 helper phage). (b) Lineweaver-Burke plot to determine K_M of phage displayed BSLA. Data presented as Mean \pm SD (n = 3).

Analysis of p3-containing proteins from phage displayed BSLA by Western Blot revealed a strong signal for wild-type p3 and no apparent band for BSLA-p3, in line with expectations of low levels of display (**Figure 2.2a**). Nanoparticle tracking analysis (NTA) of phage-BSLA in buffer revealed a major population of species with diameter 100–200 nm **Figure 2.3a,b**, corresponding to the phagemid adopting a flexible random coil conformation in solution. This result is consistent with the observations of Zhou et al. for tobacco mosaic virus.²¹³ As such, phage-BSLA is mostly monomeric in solution, with small populations of oligomers. Moreover, no obvious presence of large cell debris was observed. When the experiment was repeated in assay buffer, a small distribution at ~50 nm was also observed due to mixed micelles formed with gum Arabic and Triton-X100 (to solubilize the hydrophobic substrate; **Figure 2.3c**).

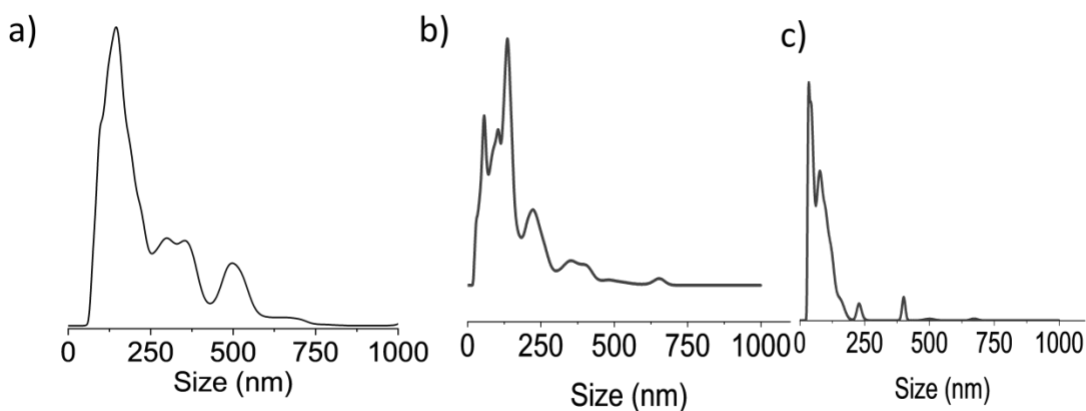


Figure 2.3 Nanoparticle tracking analysis of phage–BSLA in water (a), phage–BSLA in enzyme assay buffer (b), and the assay buffer alone (c)

To characterize the BSLA–p3 fusion, the steady-state hydrolysis of 4-nitrophenyloctanoate (4-NPO) by native BSLA and phage–BSLA was analyzed. From the Lineweaver-Burke plot **Figure 2.2b** the Michaelis constant K_M , could be determined. K_M is independent of enzyme concentration (when substrate concentration is much higher than enzyme concentration) and was not statistically different between native BSLA (0.42 ± 0.06 mM) and phage–BSLA (0.4 ± 0.1 mM). These values are similar to other published data,²⁰⁹ and suggest that BSLA fusion on the phage capsid did not influence substrate affinity and that BSLA is correctly folded. However, because the concentration of BSLA in the phage samples was difficult to estimate (due to variable display level), the concentration of native and phage attached BSLA were adjusted empirically to yield similar rates of reaction that were convenient for analysis. Thereafter, the values of V_{max} determined from this analysis were converted into turnover numbers k_{cat} (mole product formed per mole BSLA per second), to compare enzymatic activity on a molar basis. For phage–BSLA, k_{cat} is reported relative to the number of phage in solution, which overestimates enzyme concentration. The k_{cat} was found to be 1.28 s⁻¹ and 5.6 s⁻¹ for BSLA and phage–BSLA, respectively. A similar increase of k_{cat} was observed by Dröge et al. (18 s⁻¹ and 84 s⁻¹, respectively, for free and phage displayed lipase).²⁰⁹ Thus, in

conjunction with Western Blot analysis, the increase of k_{cat} in these phage samples, when normalized to the molar concentration of BSLA or phage, suggests that phage displayed BSLA is substantially more active than its free form in solution. To better understand these differences, experiments were performed to assess the effect of phage display on the enzyme's pH- and temperature-activity profiles, as well as its nanoscale distribution within the colloidal assay buffer.

To examine the existence of potential micro-environmental effects caused by the display of BSLA on a phage, catalytic activity was monitored as a function of pH. Lesuisse et al. have observed that optimum activity of lipase from *Bacillus subtilis* 168 strain is pH 10, while an optimal pH of 8–9 has been reported for lipases from some *Bacillus* species.²¹⁴⁻

218

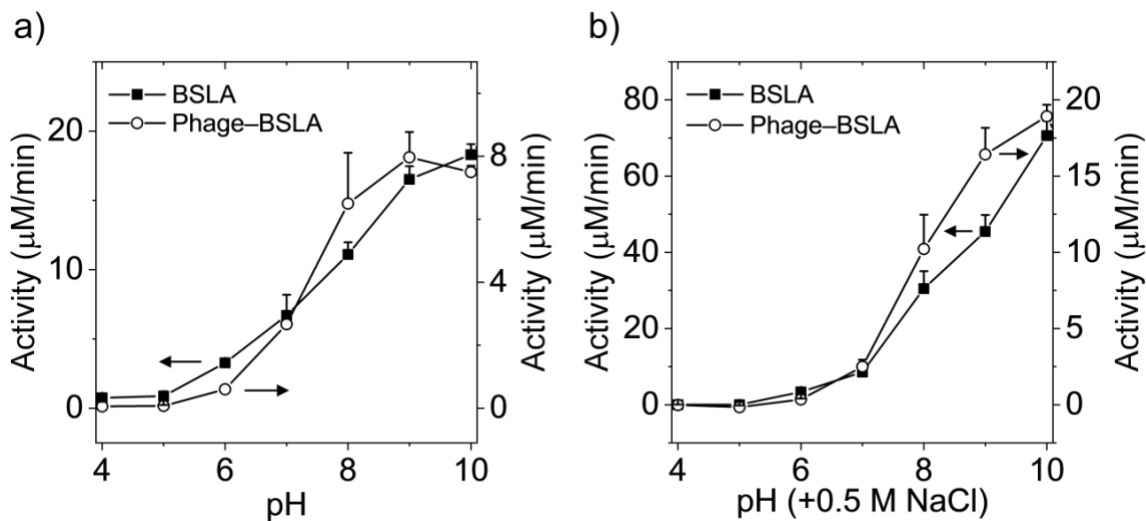


Figure 2.4 pH-activity profiles for BSLA and phage-BSLA. Activity was measured either in assay buffer (a) or in assay buffer supplemented with 0.5M NaCl (b). Data presented as mean+SD (n=3). BSLA, *Bacillus subtilis* Lipase A

As illustrated in **Figure 2.4a**, both free and phage attached BSLA possess optimal activities in this pH range. The activity of BSLA increased over the pH range examined

with a sigmoidal-type profile and very few differences, if any, were observed compared to phage displayed BSLA. At acidic pH, both forms of BSLA were inactive, and activity increased progressively as a function of pH. The increase of activity observed between pH ~6–8 was more abrupt for the phage displayed BSLA compared to native BSLA, and activity plateaued above pH ~8. Higher pH values were not examined because non-enzymatic hydrolysis of the substrate began to interfere with analysis. The addition of 0.5 M NaCl to these solutions yielded similar conclusions, though the absolute values of activity increased by a factor of 2–4, and the activity no longer plateaued above pH 8 for phage–BSLA (**Figure 2.4b**). Globally, despite the presence of multiple pH-responsive functional groups from phage coat proteins, these do not appear to be exerting a pronounced effect on the pH–activity profile of displayed BSLA.

To investigate whether display of BSLA on the phage altered the stability of the enzyme, catalytic activity was measured at different temperatures, as well as at room temperature following a pre-incubation at a given temperature for 20 min. As illustrated in **Figure 2.5a**, activity increased as a function of temperature for both forms of BSLA, and a 2–3-fold increase in activity was observed between room temperature and 65 °C for both samples. Considering that enzyme activity was calculated from the initial rate of hydrolysis (5 min), thermal denaturation of BSLA during this timeframe was neglected. No important effect of phage display on the temperature-dependent activity was observed, which may be important for downstream applications. Thereafter, the enzymes were incubated for 20 min at various temperatures, and then activity measured (**Figure 2.5b**). The results show that both forms of BSLA begin to lose activity at 30 °C, and activity decreased progressively with temperature. No obvious differences were observed between BSLA and phage–BSLA, albeit inactivation appeared to occur a slightly lower temperature for the phage–BSLA under the conditions examined. Overall, the phage display of BSLA appeared neither to stabilize nor destabilize the enzyme to a large extent relative to its free form. To further characterize heat-treated phage–BSLA, NTA was employed.

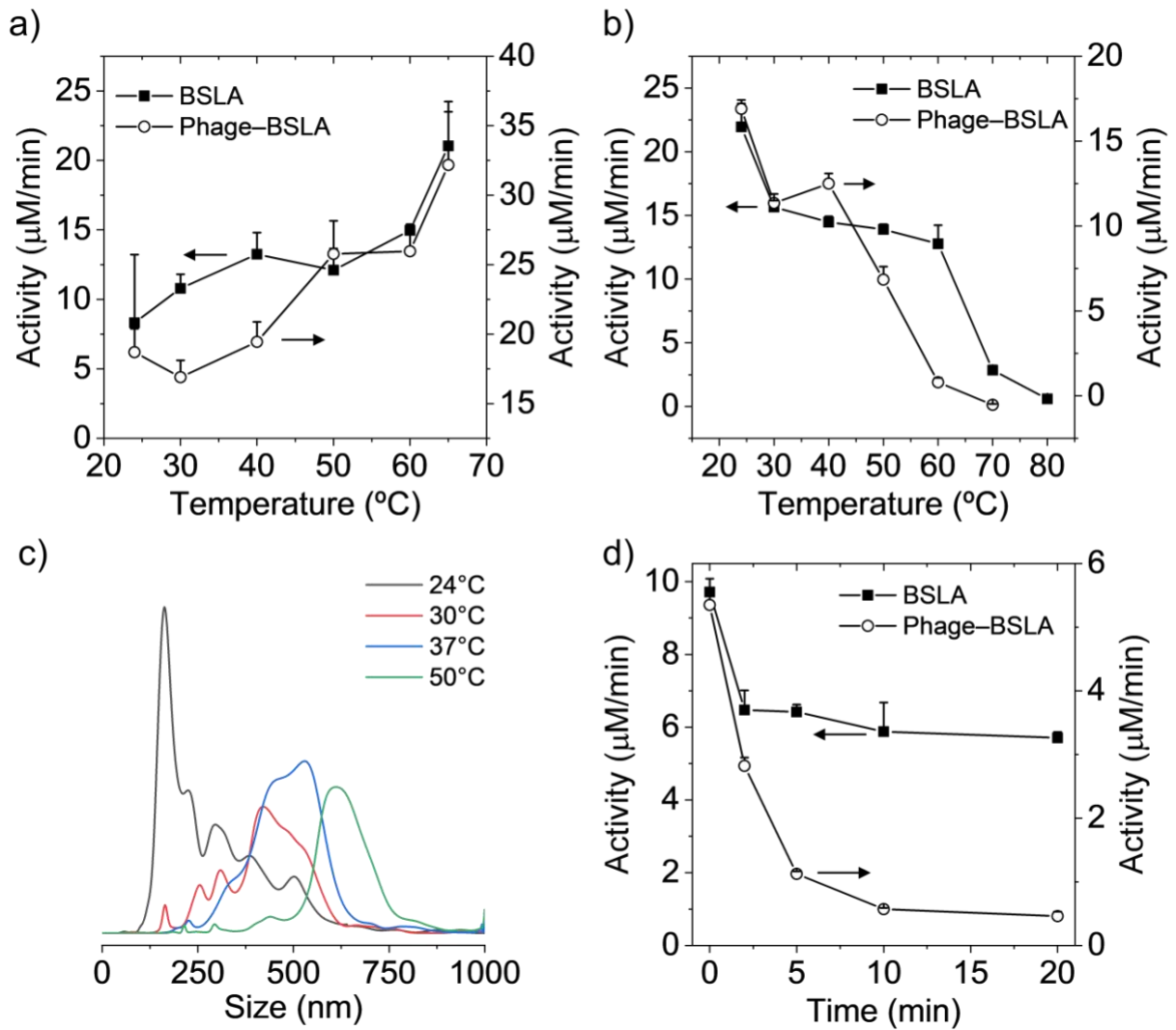


Figure 2.5 Thermal stability of BSLA and phage-BSLA (a) Catalytic activity measured as a function of temperature. (b) Catalytic activity measured at r.t., following pre-incubation at variable temperature for 30min. (c) Nanoparticle analysis of phage-BSLA samples following 30min incubation at different temperatures. (d) Catalytic activity measured at r.t. following pre-incubation at 65°C for different times. For panels a, b, and d, data are presented as mean+SD (n=3). BSLA, *Bacillus subtilis* Lipase A; r.t., room temperature

As illustrated in **Figure 2.5c**, the size associated with phage–BSLA increased from 100–500 nm to 400–800 nm, suggesting that oligomerization could contribute to the decrease of activity, alongside potential denaturation. Regarding stability at high temperature, BSLA and phage–BSLA were incubated at 65 °C for different times, then activity assessed at r.t. (**Figure 2.5d**). Results shows that native BSLA loses ~33% activity within two minutes, though remained stable thereafter. In contrast, phage–BSLA lost most of its activity within 10 min, suggesting an alternative mechanism of loss of activity may be at play.

Considering that phage display appeared neither to affect the local environment or stability of BSLA, the enhanced activity of phage–BSLA relative to free BSLA could result from a different nanoscale distribution within the heterogeneous assay buffer. For instance, accumulation near the substrate-rich micelles may result in increased activity. To characterize this possibility, the effect of salt concentration on enzyme activity was assessed while maintaining a constant pH of eight. Interestingly, the activity of BSLA increased by a factor of ~16 over the salt concentration range examined, while the mean activity of the phage–BSLA remained constant over this same range (**Figure 2.6a**, ANOVA, Tukey, $p > 0.05$). This result suggests that BSLA and phage–BSLA are in nanoscale environments that respond very differently to salt, which may be at the origin of the higher apparent activity of phage–BSLA versus native BSLA. Indeed, one possible explanation for this observation is that phage–BSLA may be partially associated with the gum Arabic/Triton-X micelles (that contain the hydrophobic substrate 4-NPO) and that BSLA presence is rather predominant in the aqueous phase where substrate concentration is much lower.

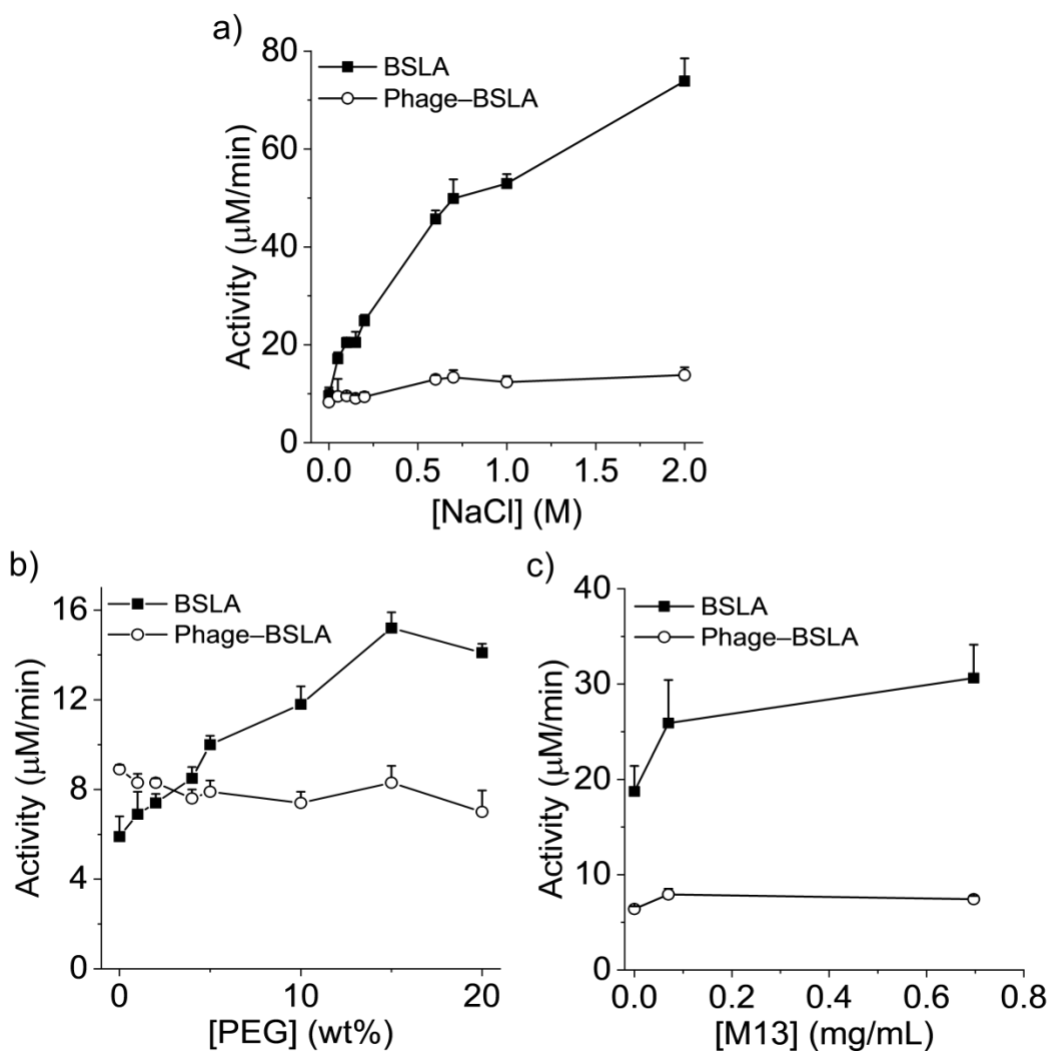


Figure 2.6 Effect of salt, PEG, and wild-type phage on catalytic activity. Influence of NaCl (a), PEG 8kDa (b), and wild-type M13 (c) on the catalytic activity of BSLA and phage-BSLA. Data presented as mean+SD (n=3). BSLA, *Bacillus subtilis* Lipase A; PEG, poly(ethylene glycol)

As such, increasing salt concentration would drive BSLA from the water phase towards the micelles, akin to a salting-out effect. To validate this hypothesis, poly(ethylene glycol) (PEG, 8 kDa) was added to the assay buffer, owing to its known ability to exert an excluded-volume effect on proteins in solution. The addition 8 kDa PEG to the solution is expected to drive proteins and phage out of the aqueous phase (this is the premise for PEG-induced protein and phage precipitation), and potentially towards the interface of

the micelles. As illustrated in **Figure 2.6b**, the activity of BSLA progressively increased to 3-fold its initial value upon addition of PEG, suggesting re-distribution of BSLA towards substrate-rich micelles. In contrast, similar to the results obtained with NaCl, the activity of phage–BSLA was not affected by the presence of PEG (ANOVA, Tukey, $p > 0.05$). These combined results suggest that the difference in activity between BSLA and phage–BSLA lies mainly in the preferential association of phage–BSLA with substrate micelles. Finally, to validate that the phage themselves were not somehow affecting activity by e.g., altering the structure of the substrate-containing micelles, wild-type M13 phage was added to assay buffer. Indeed, while a rapid increase of activity of free BSLA was observed upon addition of a small amount of phage, the overall increase of activity was small ($< \sim 1.5$ -fold increase) and rapidly plateaued at higher phage concentration (**Figure 2.6c**).

Overall, this work illustrates that the microenvironment and stability of BSLA did not appear to be intrinsically affected by phage display, though the phage modified the nanoscale distribution of BSLA within the micellar assay buffer. As such, caution should be exerted when selecting enzymes by phage display, and the effect observed herein for BSLA should be considered on a case-by-case basis for other proteins, particularly when the foreseen application involves complex solutions (e.g., colloidal or other).

CHAPTER 3

Enhancement of enzyme cascade reactions on M13 bacteriophage and oligomers thereof

Preface:

After verifying the templated effect of phage on enzyme activity as well as its nanoscale distribution in heterogeneous assay buffer, our second objective was to further explore the potential of nanoscale distribution by controlled inter-phage oligomerization of enzyme templated phage. Furthermore, the influence of nanoscale distribution on the communication between multiple enzymes in a three-enzyme based cascade reaction was explored. More specifically, i) Two other enzymes, glucose oxidase and horseradish peroxidase were immobilized on BSLA–phage while these three enzymes together participate in a cascade reaction. ii) Enzyme grafting was characterized nanoparticle tracking analysis. iii) Michaelis–Menten kinetics of the individual enzyme reaction was monitored before and after immobilization to see the effect of phage template on enzyme kinetics. iv) This phage-templated cascade model was exposed at various nanoscale platforms by inter-phages crosslinking, and then effect of oligomerization on enzyme kinetics of individual enzyme reaction as well as the cascade reaction was monitored and compared with the data obtained with enzymes free in solution.

Abstract:

This study explores whether a model three-enzyme cascade system, templated onto M13 phage, yields an advantageous acceleration of the overall reaction relative to the free enzymes in solution. BSLA was displayed on the P3 minor coat protein of the phage, while glucose oxidase and horseradish peroxidase were immobilized onto the P8 major

coat protein. Phages were crosslinked by biotin–streptavidin interactions. The dominant parameter influencing the rate of final product formation was inter-phage crosslinking, which appeared to create a more favorable microenvironment for GOx, and to a lesser extent HRP. Intra-phage crosslinking and immobilization onto the phage itself influenced the cascade reaction to a lesser degree. The low number of enzymes per phage template is consistent with what is achievable using phagemid technology, suggesting that such cascades could be biologically produced without the need for supplemental conjugations steps. Ultimately, this proof-of-concept study suggests that phage-templated enzyme cascade systems may be promising platforms for green manufacturing, though predicting the effect of microenvironmental effects on all the enzymes remains a challenge.

3.1. Introduction

Enzyme cascade reactions are multi-step chemical reactions catalyzed by a series of enzymes. The product of each enzyme is consumed by the next enzyme, and so on. Most biological processes are in fact accomplished by such complex multi-enzyme synthetic pathways. For instance, the metabolism of glucose by the glycolytic pathway involves the participation of ten enzymes that work sequentially and efficiently.¹⁷¹ Similarly, the multistep citric acid cycle is a metabolic pathway that connects carbohydrate, fat, and protein metabolism, and a complete cycle involves eight enzymes.¹⁷² Mimicking these natural systems, some groups have been able to design up to 10-step enzyme artificial cascade reactions. For instance, Zhou et al. have prepared an artificial 9-step enzyme cascade and metabolic pathway for the synthesis of benzylamine from L-phenylalanine.⁴⁵ Industrially, grouping enzyme reactions into a multistep one-pot bio-catalytic process brings additional benefits, including the fact that intermediates need not be isolated as they are directly transferred to the next step of the reaction sequence.^{12-14,173-177} Globally, this can reduce cost, time, effort, and increase final yield of product.¹⁷⁸ Moreover, enzyme cascade reactions can be accelerated by local nanoscale confinement of the enzymes, and theories to explain this include providing a more favorable micro-environment for catalysis and/or by promoting mass transfer of intermediates from one enzyme to

another.¹⁷⁹ Nature accomplishes this by compartmentalization, such as within cells or sub-cellular compartments.¹⁸⁰ This approach has been emulated artificially using inorganic nanoparticles, liposomes, polymersomes, or by tethering the enzymes to a scaffold (e.g., DNA origami, other proteins, or even viruses).^{108,192} In fact, some of these nanoscale scaffolds allow for precisely positioning and orienting enzymes relative to one another, which has been used to study the transfer of molecules from one enzyme to another. Another approach used to reduce the cost, time, and effort associated with enzyme catalyzed-reactions is to immobilize the latter on macroscopic supports (polymeric or other) for convenience of recovery from solution and reuse.²¹⁹ Of course, with such macroscopic templates it is generally difficult to control the nanoscale positioning of the enzymes. Overall, the design and preparation of enzyme cascade systems can become increasingly complicated and costly to implement as one seeks nanoscale precision, because of the need for bioconjugation or loading steps, self-assembly, etc.²²⁰ Simultaneously, greater nanoscale precision is generally achieved at the compromise of the convenience of handling (e.g., macroscopic supports).

One opportunity to prepare a nanoscale-templated enzyme cascade systems without the need for bioconjugation steps could be to exploit phage display technology. Indeed, phages are nanoscale templates that can be genetically engineered to display different enzymes on their coat proteins, and yet maintain the handling properties of macroscopic supports. This includes the possibility of removing them from solution by centrifugation or precipitation.^{134,221-224} Moreover, the propagation of phages is straightforward and considered a green manufacturing process.²²⁵ This study will explore whether a model three-enzyme cascade system, templated onto M13 phage, yields an advantageous acceleration of the overall reaction relative to the free enzymes in solution. The intrinsic influence of immobilization of the enzyme on the phage will be examined, as well as the influence of phage oligomerization (achieved by crosslinking) and the density of enzymes on the bacteriophage template.

3.2 Materials and Methods

3.2.1 Materials

Anti-P8–HRP (Antibodies-online Inc.), GOx–biotin (Rockland Antibodies and Assays), BSLA (Cedarlane), anti-P8–biotin (OriGene Technologies Inc.), 6-O-acetyl-D-glucose (Carbosynth, USA) were purchased at the highest purity available and used as received. HRP, hydrogen peroxide, oPD, and streptavidin were purchased from Sigma-Aldrich. D-Glucose, KCl, KH₂PO₄, NaCl, and Na₂HPO₄ were purchased from BioShop Canada Inc.

3.2.2 SDS-PAGE

Pre-cast polyacrylamide PROTEAN TGX Stain-Free Protein Gels (4–15%) and Precision Plus Protein Standard (10–250 kDa) were purchased from BioRad Inc. 5 µg of each sample to be analyzed was dissolved in 10 µL of milliQ water, reduced with 5 µL loading buffer containing 2-mercaptoethanol (5% in the final mix), and heated to 80 °C for 10 min. Gels were run at 70 V for 70 minutes. Subsequently, gels were imaged using a UV trans-illuminator.

3.2.3 Nanoparticle Tracking Analysis (NTA)

NTA measurements were performed using a NanoSight NS300 instrument (Malvern Panalytical, UK), which is a laser based light scattering system. Streptavidin, anti-P8–biotin, BSLA–phage, streptavidin + anti-P8–biotin + GOx–biotin, Sample **2**, or Sample **3** was diluted with sterile water to reach a particle concentration suitable for analysis (ca. 10⁷–10⁹ particles/mL). These solutions were run through the flow cell using a 1-mL syringe controlled with a syringe pump. Each sample was run at least five times. The capture settings (shutter and gain) and analysis settings were manually set and then optimized for each sample. Sixty-second sample videos were recorded, which were then analyzed with the NTA 3.3 Analytical software to extract size distributions.

3.2.4 Assembly of cascade samples

Stock solutions were prepared in 10 mM phosphate buffer pH 7.4 at the following concentrations: 6.25×10^{13} BSLA-phage/mL (~104 nM considering a molecular weight of 1.17×10^7 Da for each phage); 0.66 μ M anti-P8-biotin; 6.66 μ M GOx-biotin; 3.16 μ M anti-P8-HRP; 1.66 μ M streptavidin; 2.8 μ M BSLA. **Sample 1:** GOx-biotin (0.63 μ L), anti-P8-HRP (1.3 μ L), and BSLA (0.8 μ L) were added to 247 μ L phosphate buffer (10 mM, pH 7.4). **Sample 2:** GOx-biotin (0.63 μ L) and anti-P8-biotin (6.25 μ L) were added to 200 μ L phosphate buffer (10 mM, pH 7.4), followed by the addition of streptavidin (2.5 μ L). The solution was incubated for 2 hours at room temperature on an orbital agitator. Then, anti-P8-HRP (1.3 μ L) was added, mixed, and followed by BSLA-phage (40 μ L). The solution was incubated for 2 hours at room temperature on a rotary agitator. **Sample 3:** GOx-biotin (0.63 μ L) and anti-P8-biotin (12.5 μ L) were added to 193 μ L phosphate buffer (10 mM, pH 7.4), followed by the addition of streptavidin (2.5 μ L). The solution was incubated for 2 hours at room temperature on an orbital agitator. Then anti-P8-HRP (1.3 μ L) was added, mixed, and followed by BSLA-phage (40 μ L). The solution was incubated for 2 hours at room temperature on a rotary agitator. **Sample 4:** GOx-biotin (0.63 μ L) and anti-P8-biotin (31.25 μ L) were added to 172 μ L phosphate buffer (10 mM, pH 7.4), followed by the addition of streptavidin (5 μ L). The solution was incubated for 2 hours at room temperature on an orbital agitator. Then, anti-P8-HRP (1.3 μ L) was added, mixed, and followed by BSLA-phage (40 μ L). The solution was incubated for 2 hours at room temperature on an orbital agitator. **5:** GOx-biotin (0.63 μ L) and anti-P8-biotin (125 μ L) were added to 58 μ L phosphate buffer (10 mM, pH 7.4), followed by the addition of streptavidin (25 μ L). The solution was incubated for 2 hours at room temperature on a rotary agitator. Then, anti-P8-HRP (1.3 μ L) was added, mixed, and followed by BSLA-phage (40 μ L). The solution was incubated for 2 hours at room temperature on an orbital agitator. **6 (control for 7):** GOx-biotin (2.75 μ L), anti-P8-HRP (6 μ L), BSLA (0.72 μ L) and were added to 208 μ L phosphate buffer (10 mM, pH 7.4). **7:** GOx-biotin (2.75 μ L) and anti-P8-biotin (55 μ L) were added to 115.5 μ L phosphate buffer (10 mM, pH 7.4), followed by the addition of streptavidin (11 μ L). The solution was incubated for 2 hours at room temperature on an orbital agitator. Then, anti-P8-HRP (6 μ L) was added, mixed, and

followed by BSLA–phage (29.5 μL). The solution was incubated for 2 hours at room temperature on a rotary agitator. The final composition of the stock solutions of samples **1–7** is compiled in **Table 3.1**.

Table 3.1 Concentration of all compounds used to prepared cascade samples described in the section 3.2.4 Assembly of cascade samples

Sample	BSLA (nM)	BSLA–phage (nM)	GOx–biotin (nM)	Anti-P8–biotin (nM)	Streptavidin (nM)	Anti-P8–HRP (nM)
1	8.96		16.78			16.43
2		16.64	16.78	16.5	16.6	16.43
3		16.64	16.78	33	16.6	16.43
4		16.64	16.78	82.5	33.2	16.43
5		16.64	16.78	330	166	16.43
6	8.96		83.25			86.18
7		16.64	83.25	165	83	86.18

3.2.5 Catalytic activity of BSLA

To measure the activity of BSLA without recourse to the other enzymes (i.e., for Michaelis-Menten analysis), enzymatic activity was determined spectrophotometrically via the hydrolysis of 4-NPO. A stock solution of 10 mM of 4-NPO in methanol was prepared. Reactions with various concentrations of the 4-NPO solution (0.05–4 mM) were prepared in 0.1 mL assay buffer (50 mM phosphate buffer containing 0.1% gum Arabic and 0.36% Triton X-100). The reaction was initiated by enzymes at a final concentration of 343 nM of BSLA or 64 nM of phage–BSLA and the absorbance was measured at 410 nm for the production of 4-nitrophenol (molar extinction coefficient $18,000 \text{ M}^{-1} \cdot \text{cm}^{-1}$). The Michaelis-Menten constant (K_M), maximum velocity (V_{max}), and turn-over number (k_{cat}) of the phage-bound BSLA were determined using substrate concentrations ranging from 0.1 mM to 4 mM and between 0.1–0.8 mM for native BSLA because the reaction rate was insensitive to substrate concentration at higher concentrations. In all cases, the background

hydrolysis of the substrate in controls without enzyme (blanks) was subtracted from the sample data. The final composition of these solutions can be found in **Table 3.5**

To measure the catalytic activity of BSLA→GOx→HRP of the cascade samples **1–7**, solutions containing 25 μL of oPD (from a 0.1 M stock in PBS) and 25 μL of 6-O-acetyl-D-glucose (from a stock of 0.2 M in PBS) were prepared. Catalysis was initiated by addition of 50 μL of the stock solutions of **1–7**. The production of DAP was measured at 415nm as a function of time. Control samples not containing enzyme was subtracted from the sample data to account for substrate degradation. Reactions were repeated in triplicate. The final composition of these solutions can be found in **Table 3.2**.

Table 3.2 Concentration of all compounds used to measure catalytic activity of BSLA→GOx→HRP described in the section 3.2.5 and to generate Figure 3.4c.

Sample	BSLA (nM)	BSLA–phage (nM)	GOx–biotin (nM)	Anti-P8–biotin (nM)	Streptavidin (nM)	Anti-P8–HRP (nM)	6-O-Acetyl glucose (mM)	D-Glucose (mM)	H ₂ O ₂	oPD (mM)
1	4.48		8.39			8.21	50			25
2		8.32	8.39	8.25	8.3	8.21	50			25
3		8.32	8.39	16.5	8.3	8.21	50			25
4		8.32	8.39	41.25	16.6	8.21	50			25
5		8.32	8.39	165	83	8.21	50			25
6	4.48		41.6			43	50			25
7		8.32	41.6	82.5	41.5	43	50			25

3.2.6 Catalytic activity of GOx

To perform a Michaelis-Menten analysis of GOx, the catalytic activity of GOx was measured in the presence of excess anti-p8–HRP, so that GOx activity was the rate-limiting step of the reaction. Under the conditions examined below, a 3-fold excess of anti-P8–HRP was used so that the reaction rate became independent of HRP concentration. A cascade sample (named ‘Gox on phage’) was prepared in 10 mM phosphate buffer pH 7.4 containing 6.7 nM anti-P8–biotin, 2 nM streptavidin, 6.7 nM GOx–biotin, 25 nM anti-P8–HRP on 8.3 nM phage–BSLA. Similar concentration of GOx–biotin and anti-P8–HRP were used to prepare ‘GOx in solution’ where anti-P8–biotin, streptavidin and phage–BSLA were absent. To measure reaction kinetics, D-glucose was used in a range of 10–70 mM while oPD concentration was fixed (30 mM). As a representative example, for 10 mM of D-glucose reaction, 10 μ L of D-glucose (from 0.1 mM), 30 μ L of oPD (from 0.1 mM) were added to 50 μ L of 10 mM phosphate buffer pH 7.4. Finally 10 μ L of stock solutions of GOx–biotin, or GOx–biotin immobilized on phage from above was added to the mixture to start the reaction (the final volume was 0.1 mL). The production of DAP was measured at 415 nm ($\epsilon_{415} = 16,700 \text{ M}^{-1}\cdot\text{cm}^{-1}$) as a function of time in a BioTek microplate reader. The final composition of these solutions can be found in **Table 3.5**

To measure the activity of samples **1–7**, reaction solutions were prepared with 5 μ L of oPD (from a 0.1 M stock in PBS), 10 μ L of D-glucose (from a stock of 0.1 M) in 75 μ L of PBS, finally 10 μ L of the stock solutions of **1–7** (Section 5.4) were added to start the reaction. In all cases above, the background of the substrate in controls without enzymes (blanks) was subtracted from the corresponding sample data. Reactions were repeated in triplicate. The final composition of these solutions can be found in **Table 3.3**.

Table 3.3 Concentration of all compounds used to measure catalytic activity of GOx→HRP described in the section 3.2.6 and to generate Figure 3.4b.

Sample	BSLA (nM)	BSLA-phage (nM)	GOx-biotin (nM)	Anti-P8-biotin (nM)	Streptavidin (nM)	Anti-P8-HRP (nM)	6-O-Acetyl glucose (mM)	D-Glucose (mM)	H ₂ O ₂ (mM)	oPD (mM)
1	0.8		1.69			1.64		10		5
2		1.66	1.69	1.65	1.66	1.64		10		5
3		1.66	1.69	3.35	1.66	1.64		10		5
4		1.66	1.69	8.25	3.32	1.64		10		5
5		1.66	1.69	33	16.6	1.64		10		5
6	0.8		8.3			8.6		10		5
7		1.66	8.3	16.5	8.3	8.6		10		5

3.2.7 Catalytic activity of HRP

To perform a Michaelis-Menten analysis of HRP, stock solutions of HRP (5 nM) and anti-P8-HRP (5 nM) with phage-BSLA (8.3 nM) were prepared in 10 mM phosphate buffer pH 7.4. For Michaelis-Menten kinetics, oPD concentration was varied in the range of 0.03–2 mM while H₂O₂ concentration was fixed at 1 mM. As a representative example, 2 μL of oPD solution (from a 10 mM stock) and 1 μL of the H₂O₂ solution (from a 100 mM stock) were added to 87 μL of PBS. Finally, 10 μL of the anti-P8-HRP solution (either with or without phage) was added to start the reaction (the final volume was 0.1 mL). The production of DAP was measured at 415 nm ($\epsilon_{415} = 16,700 \text{ M}^{-1} \cdot \text{cm}^{-1}$) as a function of time in a BioTek microplate reader. The final composition of these solutions can be found in

Table 3.5

For the HRP activity of **1–5**, reaction solutions were prepared with 5 μL of oPD (from a 0.1 M stock in PBS), 1 μL of H₂O₂ (from a stock of 0.1 M) in 84 μL of PBS finally 10 μL of the stock solutions of **1–5** (Section 5.4) were added to start the reaction. In all cases above, the background of the substrate in controls without enzymes (blanks) was subtracted from the corresponding sample data. Reactions were repeated in triplicate. The final composition of these solutions can be found in **Table 3.4**

Table 3.4 Concentration of all compounds used to measure catalytic activity of HRP described in the section 3.2.7 and to generate Figure 3.4a

Sample	BSLA (nM)	BSLA-phage (nM)	GOx-biotin (nM)	Anti-P8-biotin (nM)	Streptavidin (nM)	Anti-P8-HRP (nM)	6-O-Acetyl glucose (mM)	D-Glucose (mM)	H ₂ O ₂ (mM)	oPD (mM)
1	0.8		1.69			1.64			1	5
2		1.66	1.69	1.65	1.66	1.64			1	5
3		1.66	1.69	3.35	1.66	1.64			1	5
4		1.66	1.69	8.25	3.32	1.64			1	5
5		1.66	1.69	33	16.6	1.64			1	5

3.3 Results

3.3.1 Design and concept

M13 phage was chosen as nanoscale template as it is the most commonly used filamentous phage for phage display. However, considering that proteins of a certain size are generally difficult to display on the coat proteins of M13, a phagemid platform was chosen as the nanoscale template rather than wild-type M13. A phagemid is a plasmid carrying the viral gene encoding the fusion coat protein, phage origin of replication, and a phage-packaging signal. The genes required for phage assembly, including the wild-type coat protein, are provided by packaging-defective helper phage. Upon coinfection of bacteria by phagemid and helper phage, wild-type proteins and fusion coat proteins are co-synthesized and preferentially assembled around the phagemid DNA, which has lower copy number than helper phage DNA. This results in hybrid phages displaying only a few copies of the fusion coat protein. By appropriate genetic engineering, these strategies can be used to introduce different enzymes onto either P3 or P8 coat proteins, and thus phages bearing multiple enzymes could, in principle, be directly produced in a green fashion without the need for conjugation steps. Nevertheless, to illustrate this point and yet maintain some degree of control over the relative display level of the different enzymes in this proof-of-concept study, a hybrid approach was rather adopted. As illustrated in **Figure 3.1a**, *Bacillus subtilis* Lipase A (BSLA) was displayed on the P3 minor coat protein

using the phagemid approach, while the two other enzymes, glucose oxidase (GOx) and horseradish peroxidase (HRP), were attached to the phage template using a high-affinity non-covalent interactions. More specifically, HRP was immobilized onto the P8 major coat protein in the form of an anti-P8–HRP antibody conjugate.

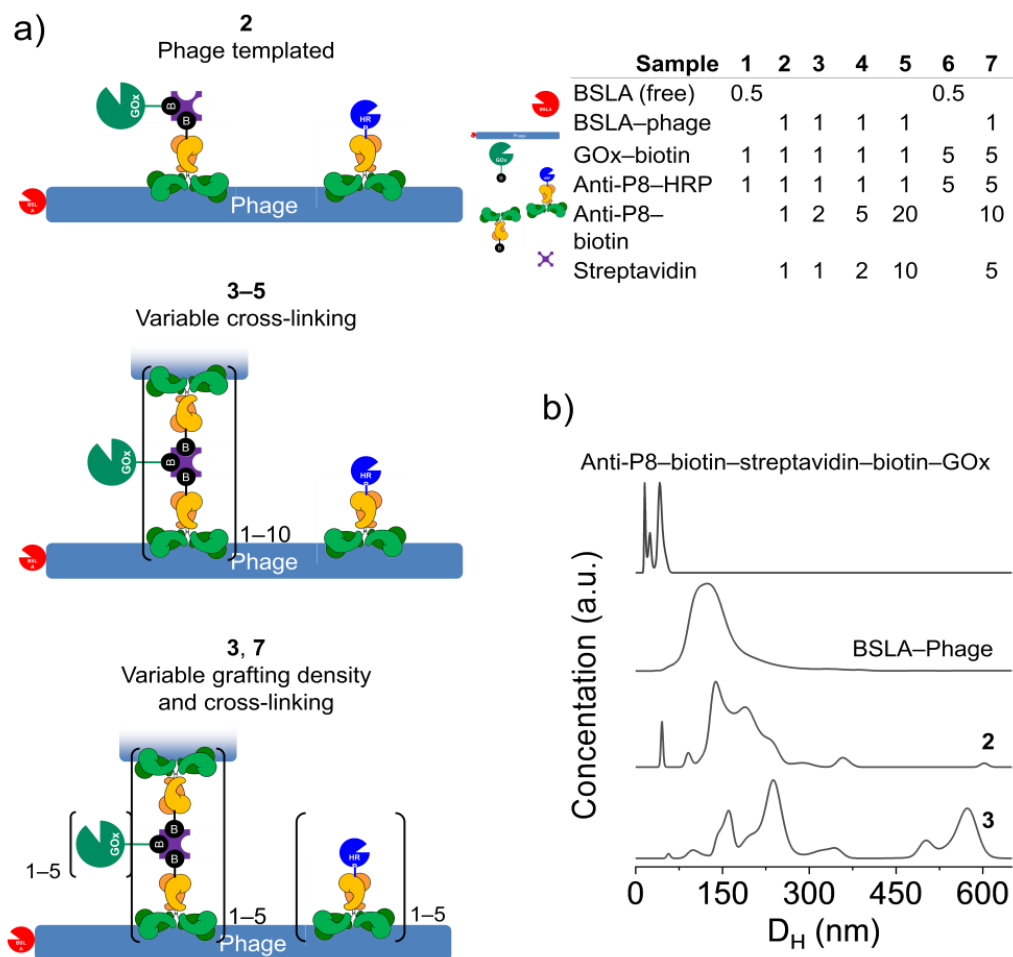


Figure 3.1 Design and assembly of phage-templated enzyme cascade. (a) The relative stoichiometry of the components enables independent control of the degree of crosslinking as well as the density of enzymes grafted onto the phage. (b) Representative characterization of the self-assembly of selected components by nanoparticle tracking analysis.

In contrast, GOx–biotin was immobilized to the P8 major coat protein via an anti-P8–biotin conjugate and a streptavidin linker. This platform was seen as ideal for investigating the opportunities and limitations of phage-templated cascade reactions, because of the convenience of varying the ratio of enzymes and controlling the degree of phage crosslinking via the relative amounts streptavidin and anti-P8–biotin. These parameters could ultimately be adjusted by other means when all the enzymes are to be directly expressed as fusions of phage coat proteins. The first enzyme of the cascade, BSLA, hydrolyzes 6-O-acetyl glucose to produce D-glucose, which is then oxidized by GOx to produce hydrogen peroxide. HRP then uses this hydrogen peroxide to convert o-phenyl diamine (oPD) to 2,3-diaminophenazine (DAP), the concentration of which can be measured spectroscopically (**Figure 3.2**). This cascade system, in particular the GOx→HRP pair,²²⁶ is well documented and will serve to benchmark the influence of the phage template relative to other templates in the literature.

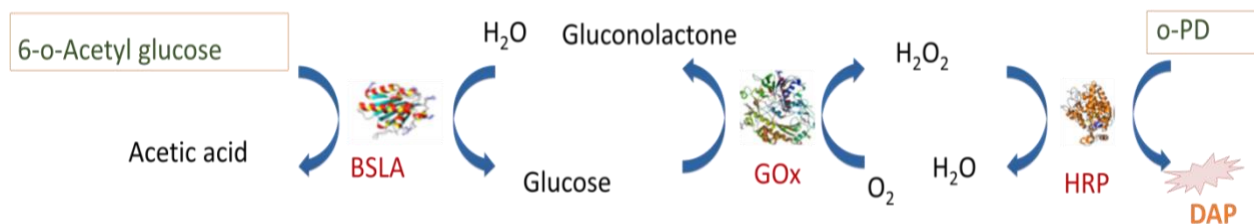


Figure 3.2 Schematic of three-enzyme cascade reaction. To monitor HRP reaction o-PD and H₂O₂ are used as substrates. For GOx→HRP reaction, D-Glucose and o-PD were added as substrates. For BSLA→GOx→HRP reaction, 6-O-acetyl glucose and o-PD were added as substrates. In all cases DAP was measured as end product.

3.3.2 Cascade assembly and characterization

The molar concentration of phage (i.e., the number of phage particles in suspension) was established by nanoparticle tracking analysis. A control sample was also prepared by replacing BSLA–phage with free BSLA. In general, phagemid systems display between 0 and 1 copies of the P3 fusion proteins per phage.⁶⁶ As reported previously by our group, the expression level of BSLA on the phage was difficult to quantify because it was indeed low (no evidence for P3–BSLA by Western Blot, which is complicated by the high abundance of other phage coat proteins), and the intrinsic catalytic activity of the enzyme could not be used to accurately estimate concentration because it was influenced by display on the phage.²²⁷ These prior observations, combined by the fact that similar reaction rates (*vide infra*) were emulated with less of the native BSLA indeed reflect that the level of expression of BSLA is below one copy per phage, and this enzyme is thus the stoichiometrically limiting component in the cascade.

The three-enzyme cascade systems illustrated as samples **1–7** in **Figure 3.1a** were assembled in one-pot by first mixing GOx–biotin, anti-P8–biotin, and streptavidin to yield an anti-P8–biotin–streptavidin–GOx–biotin complex. Then, to this solution was added anti-P8–HRP and BSLA–phage. Based on the relative ratios of anti-P8–biotin, streptavidin, and BSLA–phage, the systems were expected to either be non-crosslinked, have a variable degree of crosslinking (intra and/or inter-phage), or to have different densities of GOx and HRP on the phage. The low number of enzyme per phage (i.e., 1–5 per phage) was chosen to replicate the expected low level of fusion protein expression using the phagemid system. Moreover, the levels of crosslinking were chosen to obtain nanoscale colloids, rather than a macroscopic gel. Indeed, macroscopic gelation was observed for degrees of crosslinking greater than that used for **5** (data not shown), and were thus not pursued.

The cascade solutions were analyzed by nanoparticle tracking analysis (**Figure 3.1b**) to characterize the self-assembly of the components. The solution containing anti-P8–biotin, streptavidin, and biotin–GOx displayed a major peaks a ~50 nm, alongside two minor peaks a lower size (25–50 nm). Considering the expected sizes of the individual

components (D_H: immunoglobulin G ~13 nm,^{228,229} GOx ~12 nm,^{230,231} HRP ~4 nm,²³² streptavidin ~5 nm²³³); the major peak was attributed to the foreseen complex. Owing to the excess of streptavidin binding sites in this solution (i.e., there are four biotin-binding sites per streptavidin molecule), the minor peaks likely reflect un-biotinylated contaminants present in the starting materials. The BSLA–phage particles behaved as a monomodal population of species in solution, with a size centered at ~130 nm, reflecting the flexible nature of the phage and its ability to adopt a random coil conformation in solution. Sample **2** (non-crosslinked) showed several populations of species, with major populations at ~140 nm, 190 nm, and 230 nm. The increase in size compared to the free phage occurs in increments of 40–50 nm, which approximately reflects the addition of one or two equivalents of the streptavidin complex (~50 nm; above) and other components to the phage. Very little residual ‘free’ components were observed in this solution. Moreover, the absence of a significant number of species with sizes greater than 230 nm suggest that the phage remain mostly monomeric, with very low amounts of inter-phage crosslinking (small populations at 350 and 600 nm). For sample **3**, which can crosslink, two major populations at ~250 nm and 500–575 nm were observed (**Figure 3.1b**), suggesting the presence of crosslinked monomers (intra-phage crosslinking) and dimers (inter-phage crosslinking). Samples containing greater amounts of crosslinking agents (**4, 5, 7**) could not be analyzed by this technique because of the presence of particles >1000 nm, indicative of greater levels of inter-phage crosslinking. These were qualitatively observed during nanoparticle tracking analysis, but could not be analyzed due to multiple scattering.

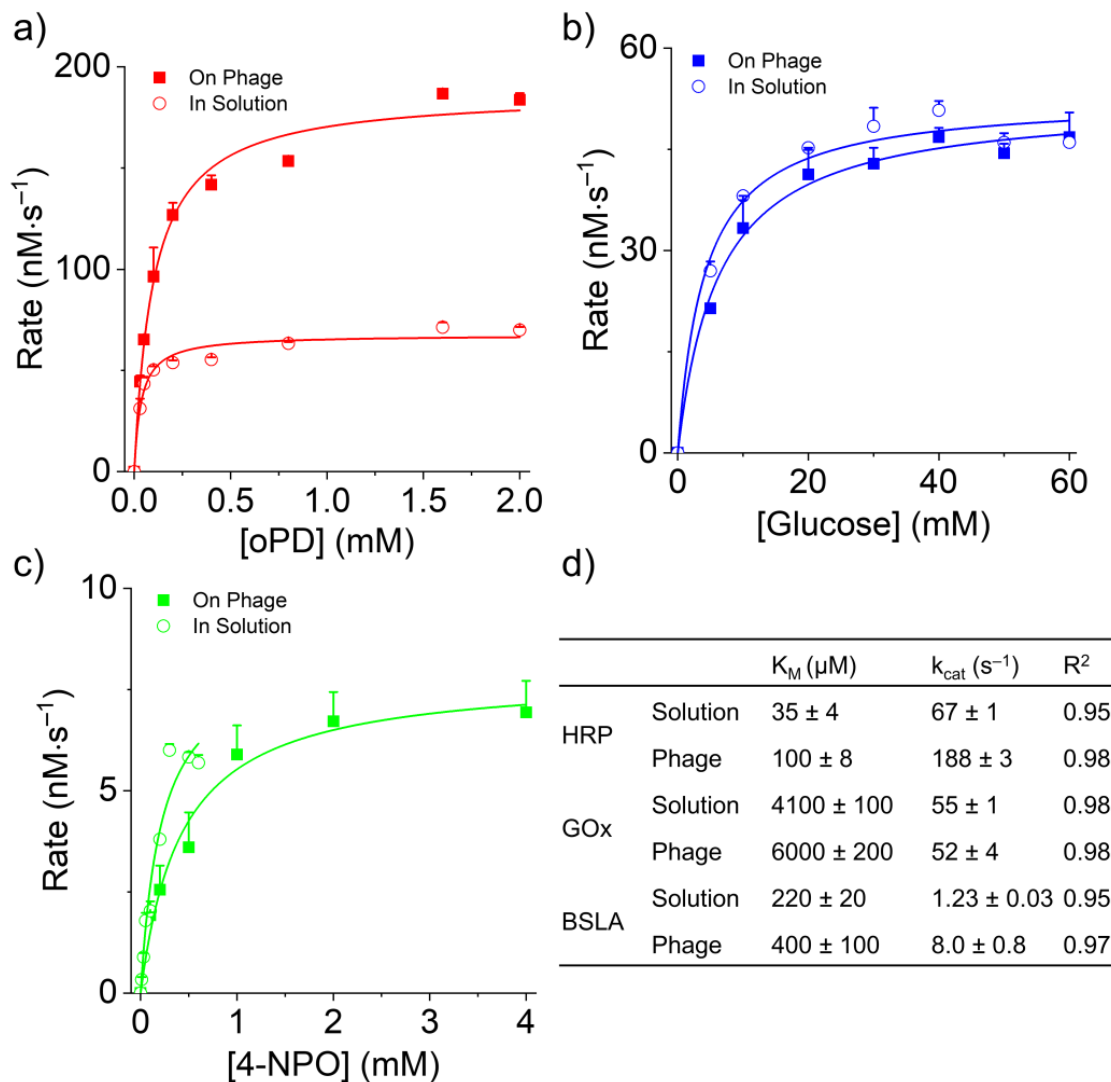


Figure 3.3 individual characterizations of the properties of the three enzymes immobilized on the phage template. Michaelis-Menten plots for (a) HRP (0.5 nM anti-P8–HRP (solution or immobilized), 1 mM H₂O₂, variable oPD), (b) GOx (0.7 nM GOx–biotin (solution or immobilized), 2.5 nM anti-P8–HRP (solution or immobilized), 30 mM oPD, variable glucose), and (c) BSLA in solution and immobilized on phage (343 nM BSLA (solution), 64 nM BSLA–phage (immobilized), variable 4-NPO). (d) Michaelis-Menten parameters. Note that plots a–c are normalized to an enzyme concentration of 1 nM, for ease of comparison. Data presented as Mean + or \pm SD (n = 3). The composition of all solutions tested is provided in Table 3.5

3.3.3 Direct effect of phage immobilization

To assess the intrinsic effect of immobilization of the enzymes on the phage template, a Michaelis-Menten analysis was undertaken. As chromogenic substrates exist for both HRP and BSLA, these were used to analyze the activity of these enzymes independently. For GOx, a three-fold excess of anti-P8–HRP was added to the solution to measure activity optically via the GOx→HRP coupled reaction.

As can be seen in **Figure 3.3** the experimental data were reliably fit with the Michaelis-Menten kinetic model and the k_{cat} and K_{M} could be extracted for comparison. In general, the immobilization of the enzymes on the phage template had an intrinsic effect on the activity of all the enzymes, as indicated by a small increase of K_{M} . This could possibly suggest a small structural perturbation of the protein leading to distortion of the catalytic site. The values obtained are similar to those found in the literature for these enzymes/substrates.^{28,33,34} Moreover, a ~3-fold increase of k_{cat} was observed for HRP, while the k_{cat} of GOx was not altered by immobilization on the phage. A ~6-fold increase of k_{cat} was observed for BSLA, which is consistent with prior observations when using micellar solutions of 4-nitrophenyl octanoate (4-NPO) as substrate.³⁴ Increased k_{cat} was rationalized by a preferential interaction of BSLA–phage with the substrate micelles, compared to BSLA alone. Differences between experimental and literature values reflect intrinsic differences between batches of proteins from different sources, conjugated with other ligands (e.g., immunoglobulin or biotin), different substrates, experimental conditions, and possibly also the difficulty of quantifying the expression level of BSLA on the phage, all of which have an effect on k_{cat} .

3.3.4 Effect of phage crosslinking and grafting density

To best understand the influence of phage templating on the enzymes for the seven different cascade systems in **Figure 3.1**, different substrates were employed to initiate the cascade at different steps along the way. In this manner, the catalytic properties of HRP were assessed by addition of oPD and H₂O₂, while the GOx→HRP couple was assessed by addition of glucose and oPD. Finally, the entire cascade was analyzed by

addition of 6-O-acetyl glucose and oPD. Importantly, considering that the rate at which the final product, DAP, was produced decreased significantly with the number of steps in the cascade, the experimental conditions (including enzyme concentration) needed to be adapted so that kinetics could be monitored over a convenient timeframe. Absolute reaction rates can be found in **Figure 3.4**. **Tables 3.2–3.4** show the detail specific component of all solutions analyzed.

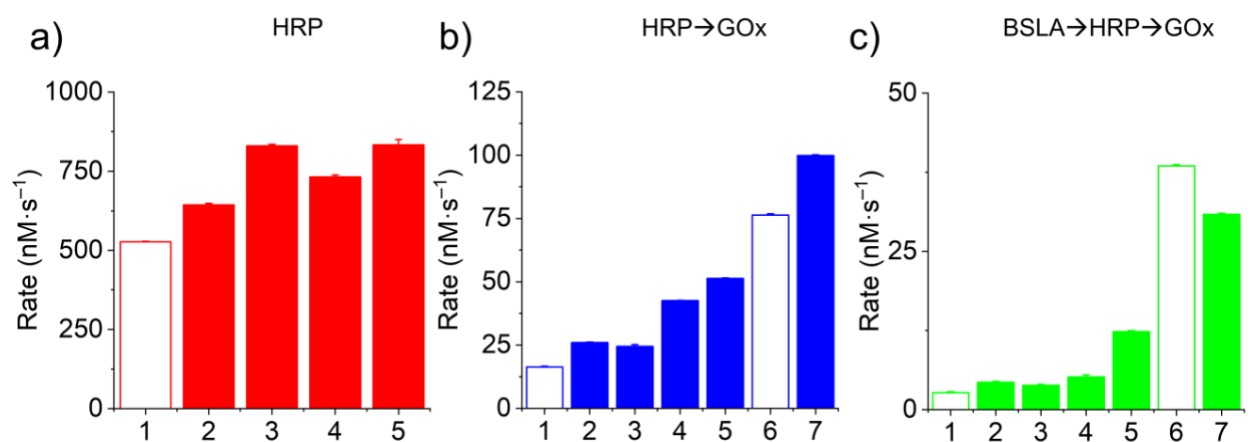


Figure 3.4 Influence of cascade parameters on the rate of (a) HRP, (b) GOx→HRP, and (c) BSLA→GOx→HRP. Data presented as Mean + SD ($n = 3$). Sample 1 is the control for sample 2-5 where only three enzymes are present, no conjugation linker (anti p8-bio) and scaffold (phage) are present. The ratio of BSLA:GOx:HRP = 1:1:1; The ratio of enzyme and conjugation linker varies in sample 2-5 as: sample 2 (1:1), sample 3 (1:2), sample 4 (1:5), sample 5(1:20). In all cases the ratio of enzyme and scaffold was same (1:1). sample 6 is the control for sample 7 where no conjugation linker (anti p8-bio) and scaffold (phage) are present. Sample 7 consists of ratio of BSLA:GOx:HRP = 1:5:5 and its contains 10 conjugation linker.

Table 3.5 Concentration of all compounds used to generate MM data

	BSLA (nM)	BSLA- phage (nM)	GOx- biotin (nM)	Anti-P8- biotin (nM)	Streptavidin (nM)	Anti-P8-HRP (nM)	4-NPO (mM)	D-Glucose (mM)	H ₂ O ₂ (mM)	oPD (mM)
HRP										
In solution						0.5			1	0.03–2
On phage		0.83				0.5			1	0.03–2
GOx										
In solution			0.7			2.5		10–70		30
On phage		0.83	0.7	0.7	0.8	2.5		10–70		30
BSLA										
In solution	343								0.1–0.8	
On phage		64							0.1–4	

As illustrated in **Figure 3.5a**, increasing the degree of crosslinking (Samples **2–5**) produced a 1.2–1.6-fold increase of the activity of HRP compared to Sample **1** (solution). This enhancement was only slightly dependent on crosslinking density. Considering the large copy number and negative charge of the P8 major coat protein, these results could suggest that the enhancement remains an intrinsic effect of immobilization on HRP activity,³⁵ possibly due to local acidification as suspected to arise on other negatively-charged templates.³⁶

Analysis of the GOx→HRP pair using D-glucose as substrate to initiate the cascade led to the observation that the rate of DAP production decreased compared to when HRP was used alone (**Figure 3.5b**). This suggests that GOx is the slowest enzyme amongst the two and thus is rate limiting for the cascade. The un-crosslinked (**2**) and intra-phage crosslinked (**3**) samples showed only a 1.5-fold increase of the rate of catalysis, while inter-phage crosslinking led to up to a 3-fold enhancement of the rate of catalysis (Sample **5**) compared to the free enzymes in solution (**Figure 3.5b**). The kinetic curves shown in this figure show that the productions of the chromophore DAP is not immediately linear at early time points, indicating a small transient phase before steady-state catalytic activity is achieved. This supports the idea the GOx is having difficulty supplying HRP with H₂O₂.

Considering that mass transport cannot explain enhanced activity under steady-state conditions, the higher rates of catalysis observed upon inter-phage crosslinking (**4** and **5**) again suggest that the microenvironment experienced by GOx is more acidic, due to greater proximity of the enzyme to the negatively-charged phage template (caused by crosslinking). Increasing the degree of grafting of both GOx and HRP onto the phage template (Sample **7**) leads to an increase in the absolute rate of catalysis (**Figure 3.5b**) and to the disappearance of the transient phase before attaining steady state kinetics. Under these higher grafting conditions, a ~1.3-fold increase of activity is maintained compared to the control in solution (**6**).

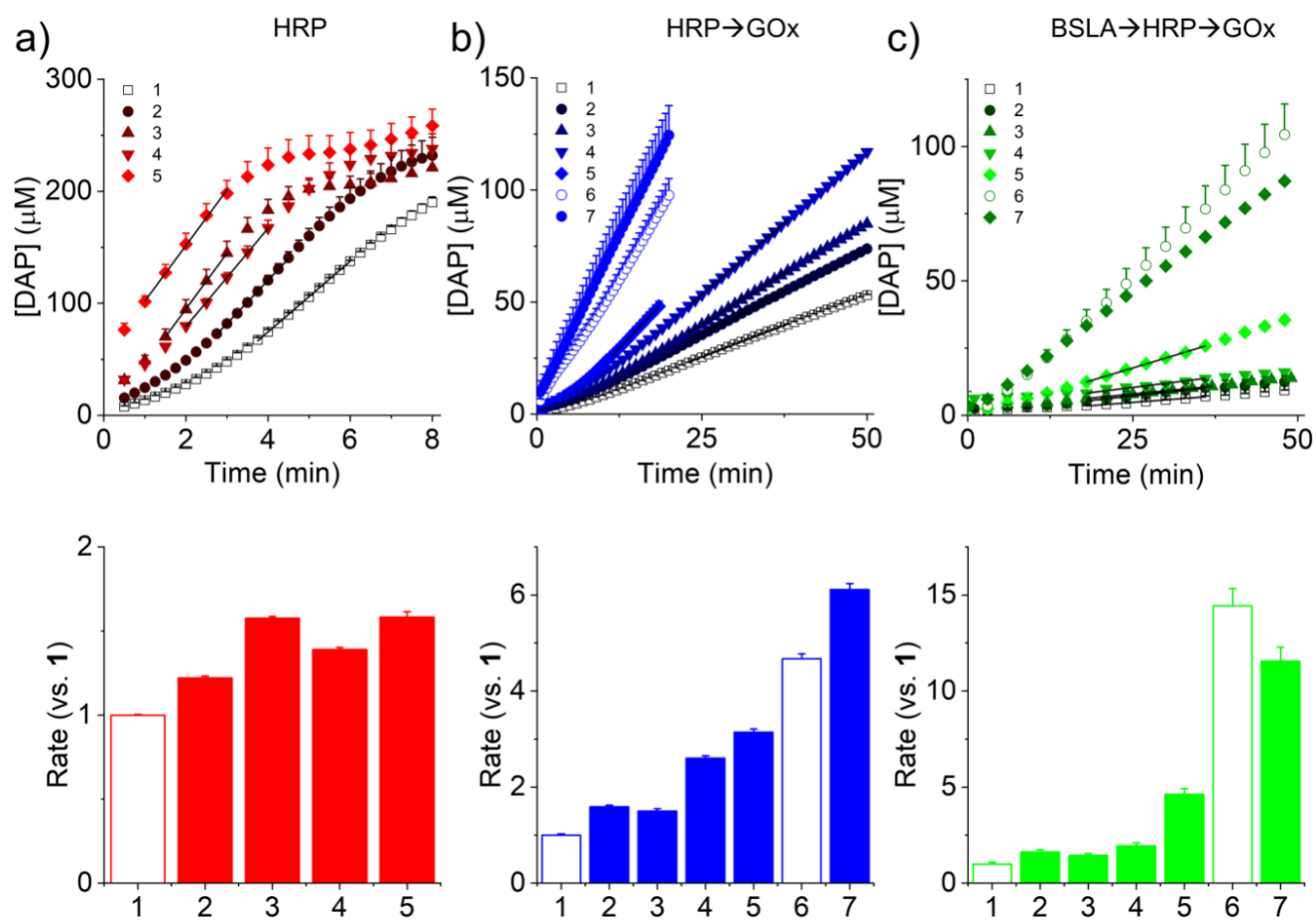


Figure 3.5 Influence of cascade parameters on the rate of (a) HRP, (b) GOx→HRP, and (c) BSLA→GOx→HRP. Data presented as Mean + SD (n = 3). Absolute values for the rate of DAP production can be found in Figure 3.3.

Analysis of the BSLA→GOx→HRP cascade using 6-O-acetyl glucose to initiate the entire cascade (**Figure 3.5c**) revealed a further deceleration in the rate of production of DAP, which suggested at first that BSLA might be the rate limiting enzyme within the cascade. However, increasing the concentration of GOx and HRP (in solution and on the phage, Samples **6** and **7**, respectively) yielded an increase in the rate of catalysis beyond that expected based on simple stoichiometry, which indicated that this was not the case. Indeed, while BSLA was expected to be the slowest enzyme at high substrate concentration, the K_M of GOx is substantially higher than that of the other two enzymes and may thus be functioning sub-optimally because of the slow supply of D-glucose from BSLA. Thus, the observed increase of catalysis might reflect not only effects on GOx, but also BSLA. For Samples **2–4**, an enhancement of catalytic activity by ~1.4–1.9-fold was observed that was independent of crosslinking density. However, Sample **5** displayed a 4.6-fold increase of activity, indicating that inter-phage crosslinking has a beneficial effect on the cascade.

The kinetic plots obtained for **1–5** (**Figure 3.5c**) show a substantial transient phase before attaining steady-state kinetics, corroborating the idea that the initial reaction in the cascade is slow and unable to supply the other enzymes downstream. Intriguingly, increasing the density of GOx and HRP in solution (**6**) or on the phage template (**7**), while leading to an overall acceleration of the reaction, showed that the immobilized cascade was slower than the cascade formed by enzymes in solution. Indeed, this decrease of activity could partially reflect a less beneficial microenvironment for GOx and HRP compared to when the degree of grafting is lower, as seen above for GOx→HRP. Moreover, considering the absence of lag phase in the kinetic plots (**Figure 3.5c**), this reduction of activity could also possibly be explained by a microenvironmental effect that negatively influences BSLA activity, yet remains challenging to elucidate. Indeed, in addition to pH, salt and molecular crowding agents (e.g., phage concentration) have also

been shown to have large to moderate to positive effects on the activity of free BSLA (with lower or no effect on BSLA–page), which could also explain these observations.³⁴

3.5 Discussion

Immobilization strategies have been widely employed to enhance the stability and catalytic performance of enzymes,²² sometimes by providing a microenvironment for the enzyme that is different from that of the bulk solution. Various parameters such as reactant concentration, pH, and possibly even temperature in the microenvironment can be significantly different from bulk conditions due to carrier immobilization, conjugation to polymers, encapsulation in nano-/micro-compartments, aggregation into complexes, presence of additives and so forth.^{25,140,158,169} In general, such parameters can be adjusted to yield a several-fold enhancement of the output of an enzyme cascade reaction.^{162,163,234-236} In this context, the GOx→HRP cascade has been one of the most widely investigated systems to screen approaches for enhancing catalysis, such as by promoting mass transfer (e.g., substrate channelling), altering the local environment (e.g., pH), promoting stability, etc. Considering the diversity of strategies explored in the literature as well as the intrinsic variability in the properties of different lots of biomacromolecules, results between studies are somewhat divergent and a general consensus regarding the mechanism(s) underlying increased/decreased activity does not exist. In an insightful study from the Hess group,³⁶ GOx and HRP were chemically conjugated to one another to investigate the mechanism of substrate tunnelling between the enzymes. The authors of this study conclude that proximity between the enzymes does not contribute to enhancement of the cascade, because of the rapidly diffusing nature of the intermediate (H₂O₂). They further suggest that similar conclusions could be applicable to other cascade systems involving small molecule intermediates. As such, the rate of final product generation of such cascade systems reflects the rate of the slowest enzyme within the cascade. In this same study, the authors suggest that acceleration/deceleration of the GOx→HRP pair is caused by micro-environmental

effects. More specifically, they suggest that local acidification caused by negatively-charged templates enhance the activity.

In the present study, the grafting density of the three different enzymes is low and, considering the overall dimensions of the phagemid template (**Figure 3.1b**), the average distance between these molecules is quite large compared to those tested by others to evaluate substrate channeling.³⁶ Thus, the results from the Hess group in addition to the conditions of this present work, appear to preclude substrate channelling as responsible for the activity enhancement observed due to immobilization on phage, intra-phage crosslinking, or inter-phage crosslinking. Rather, the results from **Figure 3.4** appear to reflect changes to microenvironment caused by the latter parameters. In particular, immobilization of phage and intra-phage crosslinking had only a minor effect on cascade activity, while inter-phage crosslinking had a more substantial impact, especially on GOx. Intriguingly, the degree of GOx and HRP grafting decreased somewhat the positive effect of crosslinking on GOx activity, and the phage displayed BSLA→GOx→HRP cascade was even slower than the control with the free enzymes in solution. These results testify to the complexity of characterizing the microenvironment experienced by the slowest enzyme in the cascade, and predicting approaches to beneficially alter it to maximize reactivity.

3.6 Conclusions

The combined results of this study indicate that the three-enzyme cascade, BSLA→GOx→HRP, can indeed be enhanced compared to the free enzymes in solution by templating on a phage. The dominant parameter influencing the rate of final product formation was inter-phage crosslinking, which appeared to create a more favorable microenvironment for GOx, and to a lesser extent HRP. While the range of inter-phage crosslinking values tested was limited to maintain colloidal stability, future work might consider extending this range to evaluate gel-type materials. Intra-phage crosslinking and immobilization itself influenced the cascade reaction to a lesser degree, though overall

the level of enhancement achieved was comparable to that reported for other related cascade systems. The low number of enzymes per phage template is consistent with what is achievable using the phagemid technology, suggesting that such cascades can be biologically produced without the need for supplemental conjugations steps. Ultimately, this proof-of-concept study suggests that phage-templated enzyme cascade systems may be promising platforms for green manufacturing, though predicting the effect of microenvironmental effects on all the enzymes may be a challenge. Along this line, the ability to simultaneously co-engineer the properties of the P8 major coat protein (i.e., to modify the local charged environment of fused proteins) may provide interesting opportunities to tailor the microenvironment experienced by the displayed enzymes in future work.

CHAPTER 4

Non-invasive, label-free, and quantitative monitoring of lipase kinetics using Terahertz emission technology

Preface: To achieve better performance of enzyme, in addition of engineering of enzyme itself as well as its surrounding microenvironment, and immobilization on suitable supports; an appropriate technology to monitor enzyme kinetics towards natural sample is also desirable. Therefore, our third objective is to develop a detection platform to monitor the rapid changes of a chemical reaction, even for complex, opaque, or scattering samples. To accomplish this objective, Terahertz (THz) waves radiated from the sensing plate (made of Si/SiO₂ thin layer deposited on sapphire support) as a result of femtosecond laser illumination was recorded during the progression of enzymatic reaction. The generated THz wave is influenced by any chemical/electrical change happened on the surface of sensing plate where samples are placed. To explore this laser system, various kinds of enzymatic reactions was performed on the sensing plate while generated THz waves were continuously recorded as electric signal which later converted into molar concentration of the product molecule. Results were then compared with those obtained by proton NMR spectroscopy and UV visual spectroscopy.

More specifically, in this chapter:

- i) Michaelis-Menten kinetics of lipase was analyzed by THz emission system with two 'optically inactive' substrates, methyl butyrate and ethyl acetate and results were compared with those obtained by proton NMR spectroscopy.
- ii) Enzyme kinetics of lipase was also monitored with 'optically inactive' long chain ester (methyl octanoate) and aromatic ester (benzyl acetate). Results were compared with those obtained by proton NMR spectroscopy.
- iii) Enzyme kinetics of lipase was qualitatively monitored for a model 'complex' substrate, whole cow's milk.

iv) The hydrophobic nature of lipase endorses its adsorption on silicon surface of the sensing plate that ultimately influences on enzyme activity. Therefore we choose another enzyme, horseradish peroxidase (HRP), and monitored its activity by THz emission. Michaelis-Menten kinetics of HRP was tested towards o-phenylenediamine in the presence of H₂O₂. Kinetic parameters were compared with those obtained by optical absorbance.

Note: The work of this chapter is submitted to the 'Biotechnology and Bioengineering' journal for publication.

Non-invasive, label-free, and quantitative monitoring of lipase kinetics using Terahertz emission technology

Sharifun Nahar,^{1,#} Ahmed Mohamed,^{1,#} Xavier Ropagnol,^{1,2} Amir Hassanpour,¹ Toshihiko Kiwa,³ Tsuneyuki Ozaki,¹ and Marc A Gauthier^{1,*}

¹ Institut National de la Recherche Scientifique (INRS), EMT Research Center, Varennes, Quebec, Canada

² École de Technologie Supérieure (ETS), Département de Génie Électrique, Montréal, Québec, Canada

³ Graduate School of Interdisciplinary Science and Engineering in Health Systems, Okayama University, Japan

Abstract:

Enzymes are ubiquitous organic catalysts, and the analysis of the rate at which they catalyze chemical transformations is of great importance in many fields. Enzymatic reactions are typically monitored using surrogate substrates that produce quantifiable optical signals, owing to limitations associated with 'label-free' techniques that could be used to monitor the transformation of original substrate molecules. In this study, terahertz (THz) emission technology is used as a non-invasive and label-free technique to monitor the kinetics of lipase-induced hydrolysis of several substrate molecules (including the complex substrate whole cow's milk) and horseradish peroxidase-catalyzed oxidation of o-phenylenediamine in the presence of H₂O₂. This technique was found to be quantitative, and kinetic parameters are compared to those obtained by proton NMR spectroscopy or UV/vis spectroscopy. This study sets the stage for investigating THz emission technology as a tool for research and development involving enzymes, and for monitoring industrial processes in the food, cosmetic, detergent, pharmaceutical, and biodiesel sectors.

4.1. Introduction

Enzymes are ubiquitous organic catalysts that are involved in almost all metabolic processes in the cell and have enormous potential as industrial biocatalysts. Their ability to accelerate the rate of chemical reactions, combined with the ability to screen and engineer their catalytic properties make enzymes particularly interesting within the biotechnological and "green" manufacturing sectors. However, matching the right enzyme (or mutant thereof) to the right application is not always trivial, in part because monitoring of the reaction kinetics can be technically challenging. This holds particularly true when the starting material is complex (i.e., mixtures of substrates), heterogeneous, and absorbs/scatters light, or even when reaction kinetics are too fast to be monitored by conventional offline techniques (e.g., chromatography). Indeed, common techniques such as mass spectroscopy,²³⁷ Fourier-transform infrared spectroscopy,²³⁸ Raman spectroscopy,²³⁹ and nuclear magnetic resonance (NMR) spectroscopy²⁴⁰ have some limitations in such situations. Moreover, most chemical transformations do not produce or consume a chromophore, which makes it impossible to monitor the reaction in real-time

by conventional optical techniques. As a result, most enzymatic reactions are monitored using surrogate substrates that produce conveniently quantifiable (e.g., optical) signals in model reaction conditions that simplify the analysis. However, proceeding in this manner can lead to surprises when eventually working with the 'real' starting materials/substrates of interest. Overcoming this challenge would require the development of a label-free detection platform to monitor the rapid changes of a chemical reaction in real-time, even for complex, opaque, or scattering samples. To this end, Kiwa *et al.* has developed a non-contact analytical technique that uses terahertz (THz) emission to monitor the chemical composition of solutions. The central component of this technique is a 'sensing plate' made of a SiO₂/Si thin film deposited on a laser-grade sapphire substrate.²⁴¹ Due to defects near the SiO₂/Si boundary, a depletion layer is formed, resulting in a local electric field around this boundary. As illustrated in **Figure 4.1b**, when a femtosecond laser with photon energies larger than the bandgap of Si illuminates the sensing plate from the sapphire side, free carriers are generated in the Si film, which are then accelerated by this surface electric field. This acceleration generates an electromagnetic pulse in the THz regime, that can be detected in the direction of reflection (*i.e.*, out of the sapphire side). It has been shown that the peak electric field of this THz pulse is proportional to the local electric field in the depletion layer. When the chemical composition of a solution placed on the SiO₂ layer of the sensing plate changes, or when molecules interact with the SiO₂ layer, the electric potential at the surface changes. This in turn changes the electric field within the depletion layer, thus changing the peak electric field of the emitted THz pulse. Therefore, the changes to the type and concentration of molecules on the surface of the sensing plate can be quantitatively measured as a function of time by monitoring the peak electric field of the emitted THz pulse. This technique has been used to detect the binding interactions of antigens–antibodies,²⁴² avidin–biotin interactions,²⁴³ and to monitor pH within microfluidic chips.²⁴⁴

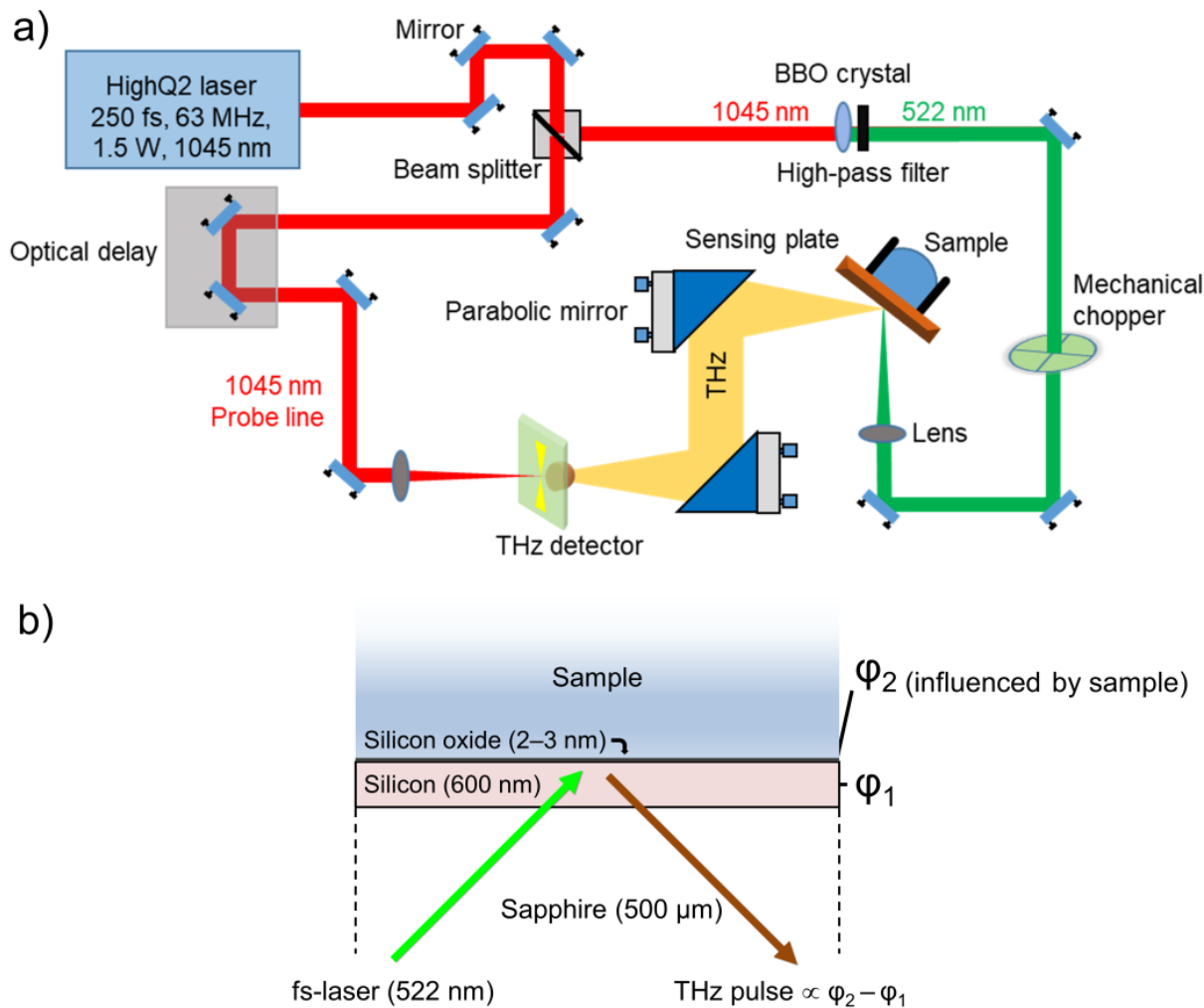


Figure 4.1 Optical setup used to monitor chemical reactions by THz emission. (a) A 522-nm femtosecond laser pulse is directed towards the sensing plate, resulting in THz emission that is detected by photoconductive sampling (using a 1045-nm probe line). (b) The sensing plate is composed of a SiO₂/Si film deposited on laser-grade sapphire substrate. A depletion layer is formed near the SiO₂/Si boundary due to band bending and gives rise to a local electric field ($\phi_2 - \phi_1$). When the femtosecond laser hits the sensing plate, carriers are generated in the Si film, which are then accelerated by this field. This generates a THz pulse that is detected in the specular direction of reflection. The amplitude of the THz signal is influenced by the sample, because the thinness of the SiO₂ layer makes ϕ_2 sensitive to the chemical composition of the sample.

Moreover, this technique has been adapted to raster the femtosecond laser along the sensing plate to generate images of THz emission (the so-called “THz Chemical

Microscope”) that are influenced by chemical reactions and adsorption of molecules/cells on the sensing plate.^{245,246} Therefore, monitoring THz signal amplitude could provide, in principle, real-time quantitative information about the progression of a chemical reaction occurring on the opposite surface of the sensing plate. Compared to other techniques, such as surface plasmon resonance or the quartz crystal microbalance, THz emission is more sensitive to changes involving small molecules, which facilitates the analysis of chemical reactions.^{247,248}

To build upon these achievements, this study explores whether THz emission technology can be used for quantitative real-time and label-free enzymology of a lipase towards four ‘optically inactive’ substrates including methyl butyrate (BuOMe), ethyl acetate (AcOEt), methyl octanoate (OcOMe), and benzyl acetate (AcOBn), as well as qualitatively for a model ‘complex’ substrate, whole cow’s milk. This technique was found to be quantitative for all substrates tested, albeit certain discrepancies were observed compared to the reference analytical technique, caused by adsorption of lipase to the sensing plate. These discrepancies were not observed for horseradish peroxidase, another enzyme tested. THz emission technology is therefore found to be a convenient and useful technique for research and development involving enzymes.

4.2. Materials and methods

4.2.1 Materials

Candida antarctica lipase B from *Candida* sp. (expressed in *Aspergillus niger*, also called Novozymes CALB; 1 band visible by sodium dodecyl sulfate gel electrophoresis (not shown)), BuOMe, AcOEt, AcOBn, OcOMe, deuterated phosphoric acid, deuterium oxide, NaOD (40 wt% in D₂O), gum Arabic, hydrogen peroxidase (HRP), hydrogen peroxide (H₂O₂), and o-phenylenediamine (oPD) were purchased from Sigma-Aldrich. Triton X-100, dimethyl sulfoxide (DMSO), sodium phosphate monobasic (H₂NaPO₄), dibasic (HNa₂PO₄), and D-glucose were purchased from BioShop Canada Inc. at the highest possible grade and were used as received. The sensing plate was purchased from MTI

Corporation, USA. Whole cow milk (3.25% milk fat) was purchased fresh from a local grocery store and stored at 4 °C until use.

4.2.2 Terahertz optical setup

As described in **Figure 4.1a**, solid-state ytterbium oscillator laser (HighQ-2 Spectra-Physics, USA) generating optical pulse with 250 fs pulse duration at a repetition rate of 63 MHz, a peak power of 1.6 W, and 24 nJ per pulse at a wavelength of 1045 nm was used to pump the THz emission setup. The fundamental beam (1045 nm) was frequency doubled using a BBO crystal to generate the second harmonic (522 nm). The conversion efficiency of the BBO crystal was around 50%, and the 522 nm power was around 650 mW. The key component of the THz optical setup is the sensing plate, composed of a Si layer (600 nm thickness) deposited on a 500 μm thick sapphire substrate. The topmost layer naturally oxidizes to SiO_2 (thickness of ~ 3 nm). The optical pump beam hits the sensing plate at an incidence angle of around 45° in air, from the sapphire side, allowing the sensing plate to be parallel to the optical table. The second harmonic power was reduced to around 300 mW using a gradient density filter. A plastic sample holder was fabricated by 3D printing and attached to the sensing plate with water-resistant adhesive. The THz radiation is generated through the Si layer by the acceleration of free carriers by the depletion field. The free-space THz radiation is emitted in transmission and in reflection of the Si layer. However, for simplicity, only the reflected THz beam was analyzed in our experiments. The THz beam is then collimated and focused onto the THz detector (Bowtie photoconductive antenna, BATOP, Germany) using a pair of off-axis parabolic mirrors. The Bowtie detector was probed using 20 mW, 1045 nm femtosecond laser pulses. Photoconductive sampling was performed to detect the THz peak profile, by tuning the time delay between the pump and probe laser pulses. Then, the delay was fixed to monitor the THz peak maximum with time. The pump beam was mechanically chopped at a frequency of 300 Hz, and lock-in detection was employed to improve the signal-to-noise ratio of the measurements with an integration time of 3 seconds. The optical delay was fixed at a specific time where the THz transient was maximum and the variations of electric field were monitored as a function of time during measurements.

4.2.3 Monitoring enzyme activity using the THz optical setup

Monitoring enzyme activity using the THz optical setup was done in a 50 mM phosphate buffer, pH 8, containing 0.1 vol% Triton X-100 and 0.36 wt% gum arabic. Triton X-100 and gum arabic act as detergents that emulsify the hydrophobic ester substrates. As a representative example, 168 μL of assay buffer was first placed on the sensing plate. The THz signal amplitude was recorded at 9 second intervals. Once the THz signal became stable (~ 2 minutes), 2.1 μL of BuOMe (to achieve a final concentration of 100 mM) was added to the sample well and mixed with the pipette tip while the THz amplitude was continuously recording. After equilibration, the THz signal became stable but was nonetheless monitored for 5 minutes to clearly visualize a stable signal. At this point, the enzyme reaction was initiated by adding 5 μL of CALB (from the stock 0.35 mM in assay buffer; concentration established using $\epsilon_{280} = 40,690 \text{ M}^{-1}\cdot\text{cm}^{-1}$)²⁴⁹ to achieve a final concentration of 9.7 μM . THz amplitude was monitored until the reaction finished (approximately 10 minutes). This process was adapted to achieve different substrate concentrations, and repeated for all other substrates. The concentration of CALB was adapted so that the reaction proceeded over a convenient time of analysis for the different substrates. This concentration was 19.5 μM for AcOEt, 4.85 μM for OcOMe, and 9.7 for AcOBn. To assess the effect of DMSO on enzyme activity, select experiments with BuOMe were repeated with assay buffer containing either 0.5 vol% or 1 vol% DMSO. All assays were performed in triplicate.

4.2.4 Monitoring enzyme activity by ^1H NMR spectroscopy

For ^1H NMR spectroscopy, the assay buffer was composed of 50 mM of deuterated phosphoric acid in D_2O (pH was adjusted to 8 by the addition of an appropriate amount of NaOD in D_2O), 0.1 vol% Triton X-100, and 0.36 wt% gum arabic. As a representative example, 673 μL of assay buffer was added to a 1.5 mL Eppendorf vial, followed by the addition of 7 μL of DMSO, and 17.5 μL of BuOMe (from a 1 M stock in assay buffer; to yield a final concentration of 25 mM). The solution was vortexed and then 6.9 μL of CALB (from a stock of 1 mM in assay buffer) was added to achieve a final concentration of 9.7

μM , the solution vortexed, a stopwatch started (to measure the dead time required to lock and shim the sample), and the solution rapidly transferred to an NMR tube using an NMR pipette. Proton NMR spectra were then recorded using a Bruker BioSpin GmbH spectrometer operating at 500.13 MHz for protons. The acquisition time for each spectrum was 4.08 s, and spectra were recorded over a period of 30 min. The integral of the peak of DMSO was used as an internal standard for concentration, and was used to convert the integrated area of substrate/product peaks into units of concentration. This process was adapted to achieve different substrate concentrations, and repeated for all other substrates. The concentration of CALB was adapted so that the reaction proceeded over a convenient time of analysis for the different substrates. This concentration was 19.5 μM for AcOEt, 4.85 μM for OcOMe, and 9.7 for AcOBn. All assays were performed in triplicate.

4.2.5 Monitoring lipase activity in whole milk

To monitor CALB activity in whole milk by THz emission technology, 176.4 μL of whole cow milk (3.25% milk fat) was first placed on the sensing plate. The THz signal amplitude was recorded at 9 second intervals. Once the THz signal became stable (~5 minutes), 3.6 μL of CALB (from the original stock of 4.87 mM to achieve a final concentration of 97.5 μM) was added to the milk and mixed with the pipette tip while the THz amplitude was continuously recording. THz signal amplitude was monitored with time to follow chemical changes to the sample. A separate identical sample was prepared to measure pH, so as not to generate artifacts in the THz emission data.

4.2.6 Monitoring horseradish peroxidase activity

Horseradish peroxidase is a bi-substrate enzyme that catalyzes the oxidation of a chromogenic substrate oPD by H_2O_2 to produce 2,3-diaminophenazine (DAP). For the THz emission measurement, stock solutions of horseradish peroxidase, H_2O_2 , and oPD were prepared in 10 mM phosphate buffer pH 7.4 at concentrations of 250 nM, 100 mM, and 10 mM, respectively. To begin, 171 μL of 10 mM phosphate buffer (pH 7.4) was placed on the sensing plate and THz amplitude recorded until a stable signal was obtained. Then, 1.8 μL of H_2O_2 and 3.6 μL of oPD stock solutions were added to the

buffer, and THz amplitude was recorded again until a stable signal was obtained (substrate plateau). Finally, the reaction was initiated by addition of 3.6 μL of the enzyme stock solution, and THz amplitude was recorded until a final plateau was reached (product plateau). The final concentrations of horseradish peroxidase, H_2O_2 , and oPD were 5 nM, 1 mM, and 0.2 mM, respectively. For analysis of horseradish peroxidase activity by optical absorption, a reaction solution was prepared with 2 μL of oPD (from a 10 mM stock in PBS), 1 μL of H_2O_2 (from a stock of 100 mM in PBS) in 95 μL of PBS. The reaction was initiated by adding 2 μL of horseradish peroxidase (from a stock of 250 nM in phosphate buffer). The formation of the chromogenic end-product DAP was monitored at 415 nm as a function of time in a BioTek microplate reader and converted to units of concentration ($\text{DAP}_{\epsilon_{415}} = 16700 \text{ M}^{-1}\cdot\text{cm}^{-1}$). All reactions were repeated in triplicate.

4.2.7 Conversion to THz signal to units of concentration (Lipase)

Reaction: Ester \rightarrow Acid + Alcohol; Type of reaction: $A \rightarrow B + C$

At time t , $THz_t = aA_t + bB_t + cC_t$ eq. 1

Capital letters represent molar concentration in mM, small case letters are proportionality constants ($\mu\text{V}/\text{mM}$). Due to stoichiometry of the reaction: $A_t = A_0 - B_t$;
 $C_t = B_t$

Therefore,

$$[B]_t = \frac{THz_t - a[A]_0}{b+c-a} = \frac{THz_t - THz_0}{2b' - a} = \frac{THz_t - THz_0}{\beta - \alpha} \quad \text{eq. 2}$$

Where b' is an effective proportionality constant ($\mu\text{V}/\text{mM}$), the average of b and c , used because B and C are produced in equimolar amounts and at the same rate, and α and β are the slopes of the substrate and product(s) calibration curve, respectively (Figure 4.3a, b).

4.2.8 Conversion to THz signal to units of concentration (Horseradish peroxidase)

Reaction(s): $\text{oPD} + \text{H}_2\text{O}_2 \rightarrow \frac{1}{2} \text{DAP}$; Type of reaction: $A + B \rightarrow C$

At time t , $THz_t = aA_t + bB_t + cC_t$

Capital letters represent molar concentration in mM, small case letters are proportionality constants ($\mu\text{V}/\text{mM}$).

Due to stoichiometry of the reaction: $A_t = A_0 - 2 \times C_t$; $B_t = A_0 - 2 \times C_t$;

Therefore,

$$[C]_t = \frac{THz_t - a[A]_0 - b[B]_0}{c - 2a - 2b} = \frac{THz_t - THz_0}{c - 2b'} = \frac{THz_t - THz_0}{\beta - 2\alpha} \quad \text{eq. 3}$$

Where b' is an effective proportionality constant ($\mu\text{V}/\text{mM}$), the average of a and b , used because B and C are consumed in equimolar amounts and at the same rate, and α/β are the proportionality factors between THz amplitude in the substrate(s)/product plateau and concentration, respectively.

4.3. Results and Discussion

Lipases are commonly used in the food, cosmetic, detergent, pharmaceutical, and biodiesel sectors,²⁵⁰ and a technique to analyze reaction kinetics for such complex starting materials would be very valuable. The enzyme chosen to establish this proof-of-concept is *Candida Antarctica* lipase B (CALB), which is one of the most commonly used industrial lipases owing to its high enantioselectivity, substrate promiscuity, and stability at high temperature and in organic solvents.²⁵¹

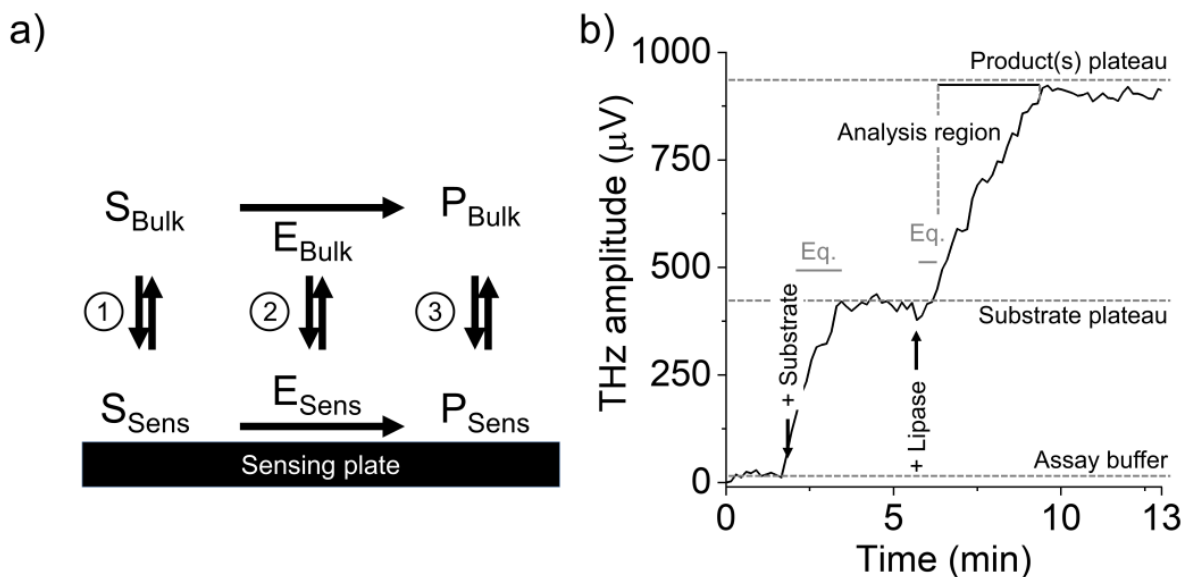


Figure 4.2 Influence of sample equilibria and chemical reactions on THz emission amplitude. (a) Equilibria involving substrate (S), enzyme (E), and products (P) as well as reactions with an effect on THz emission. THz amplitude is only sensitive to changes immediately above the sensing plate (“Sens”), corresponding to molecules within the first nanometers above the sensing plate, including those adsorbed to the latter. (b) Typical time-course of an experiment used to measure lipase activity towards BuOMe (description in text).

An illustrative experiment used to measure the catalytic activity of lipase towards BuOMe is presented in **Figure 4.2**. The initial signal (THz amplitude in μV) corresponding to assay buffer was stable with time and normalized to zero. Upon addition of substrate (BuOMe), a sharp increase was observed due to equilibration between BuOMe in bulk solution and those adsorbed onto the SiO_2 surface (“Eq.” in **Figure 4.2a**; governed by equilibrium 1). Thereafter, a plateau was reached whereby the chemical composition within the region affecting THz amplitude (‘sensing region’) reflects that of the bulk solution. Addition of lipase produced a second small but sharp change in the THz amplitude caused by adsorption of lipase (equilibrium 2) onto the SiO_2 film, the enzymatic reaction occurring at this location, and equilibrium of the resulting product between the sensing plate and the solution (equilibrium 3). Within the subsequent “analysis region”, the enzyme reaction

becomes the rate-limiting step of the system and the initial slope can be used for quantification. A final plateau is observed when no more substrate remains.

To convert THz amplitude (μV) into units of concentration, calibration curves for substrate and product(s) were established from the 'Substrate' and 'Product plateaus', respectively, by varying the initial concentration (25–150 mM) of starting material and assuming complete conversion of substrate to product(s) in the 'Product plateau' (**Figure 4.3a** for BuOMe and **4.3b** for AcOEt).

Table 4.1 Linear fit parameters for Figure 4.3a,b. Note that alterations to the THz emission setup, such as changing the sensing plate, can result in different values of slope. It is thus suggested to verify the calibration of the instrument when changes are made.

	MeOBu		AcOEt	
	Substrate	Product	Substrate	Product
Intercept (μV)	0 (fixed)	0 (fixed)	0 (fixed)	0 (fixed)
Slope ($\mu\text{V}\cdot\text{mM}^{-1}$)	5.1 ± 0.2	12.2 ± 0.6	7.8 ± 0.2	15.4 ± 0.5
R^2	0.98	0.99	0.99	0.99

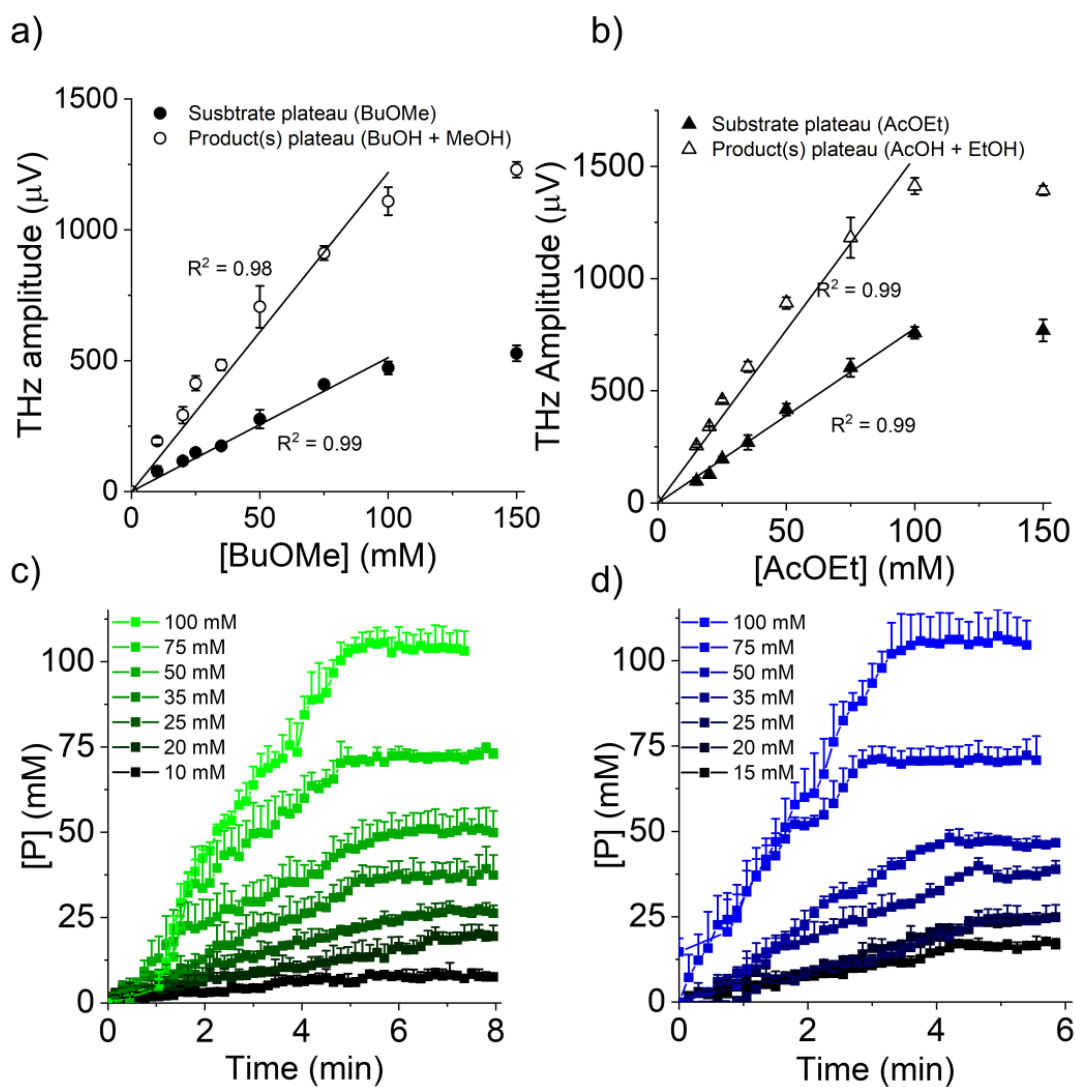


Figure 4.3 Analysis of lipase activity by THz emission technology. (a,b) Plots of THz amplitude measured at the “Substrate plateau” and “Product plateau” as a function of BuOMe (a) and AcOEt (b) concentration. These linear curves are used to convert THz amplitude into units of product concentration. Evolution of product concentration upon addition of lipase to the sample solution containing BuOMe (c) or AcOEt (d), calculated from raw THz amplitude. Time “zero” corresponds to the moment lipase was added. Data presented as Mean + SD, $n = 3$. Fit parameters in Table 4.1

The curves were linear between 0–100 mM, and show that the polar product molecules (acid + alcohol) more strongly influence THz signal amplitude compared to the ester substrate. Beyond 100 mM, THz amplitude deviated from linearity, likely due to saturation

of the sensing plate. The molar concentration of product molecules produced by lipase (i.e., either the acid or the alcohol; see eq. 1) at any given time can be extracted from raw THz amplitude as follows, so that reaction kinetics can be compared to other analytical techniques.

$$[P]_t = \frac{THz_t - \alpha[S]_0}{\beta - \alpha} \quad \text{eq. 4}$$

where, $[P]_t$ is product concentration at time t (in mM), THz_t is THz amplitude at time t (in μV), $[S]_0$ is the substrate concentration at time zero (in mM), α is the slope of the substrate calibration curve ($\mu\text{V}/\text{mM}$), and β is the slope of the product calibration curve ($\mu\text{V}/\text{mM}$). Note: this equation depends on the stoichiometry of the reaction (see eq. 2).

As illustrated in **Figure 4.3c, d**, the THz amplitude was converted into units of product concentration, to measure the initial reaction rate by linear regression. To avoid the small artifact caused by the mixing/equilibration step caused by the addition of lipase, analysis of the slope was performed beyond 30–60 s (to err on the side of caution). This process was repeated for several initial concentrations of BuOMe (**Figure 4.3c**) or AcOEt (**Figure 4.3d**).

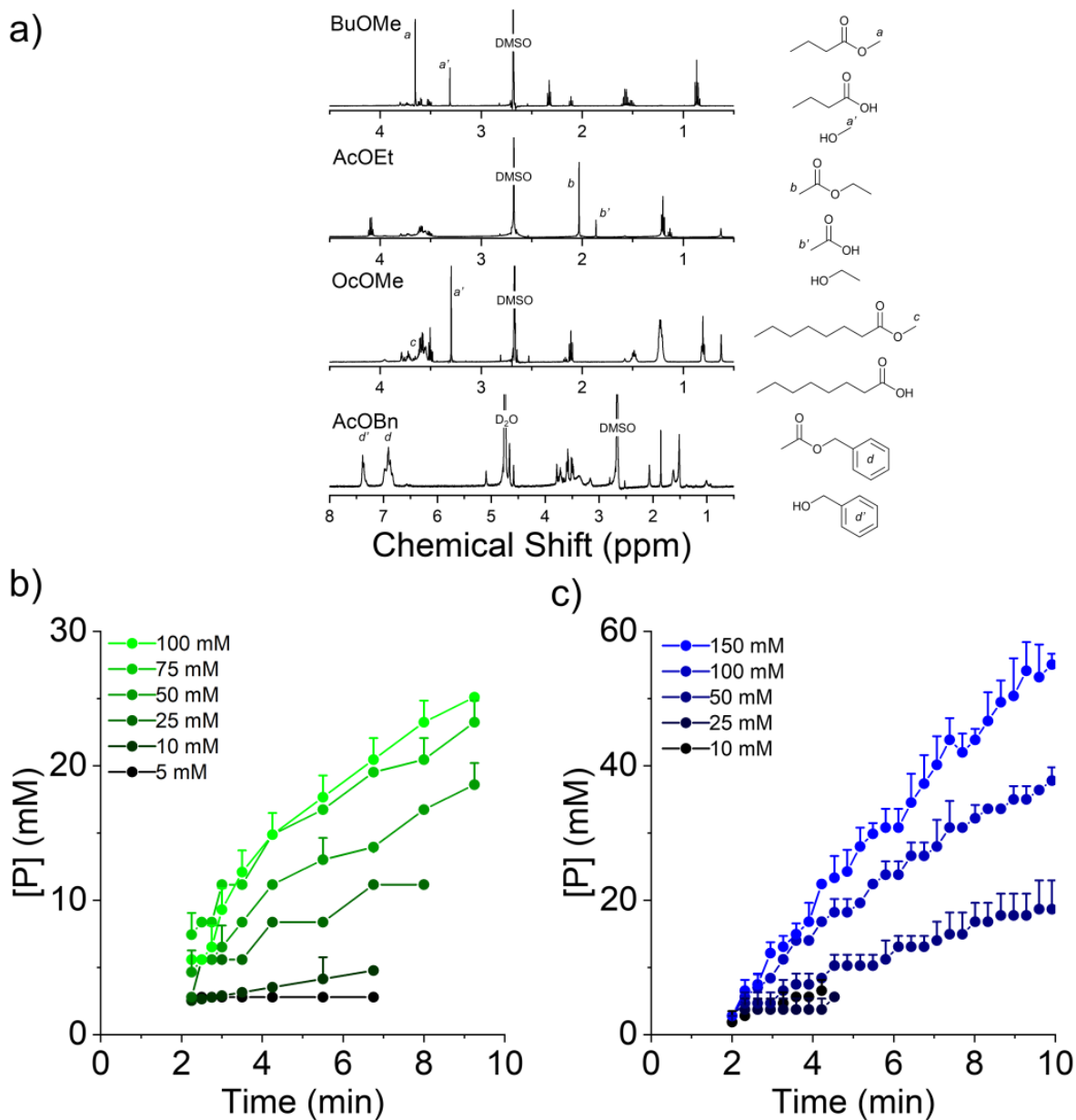


Figure 4.4 Analysis of lipase activity by ^1H NMR spectroscopy. (a) Representative spectra used to monitor the progress of CALB-catalyzed substrate (from top to bottom: BuOMe, AcOEt, OcOMe, or AcOBn) hydrolysis by ^1H NMR spectroscopy in deuterated phosphate buffer. Selected peaks associated with substrate and product peaks that were used for integration are assigned. DMSO is used as internal integration reference. (b,c) Evolution of product concentration upon addition of lipase to the sample solution containing BuOMe (b) or AcOEt (c). Time “zero” corresponds to the moment lipase was added. An approximate delay of 2 min was required to lock and shim the sample before spectra could be recorded. Data presented as Mean + SD, $n = 3$.

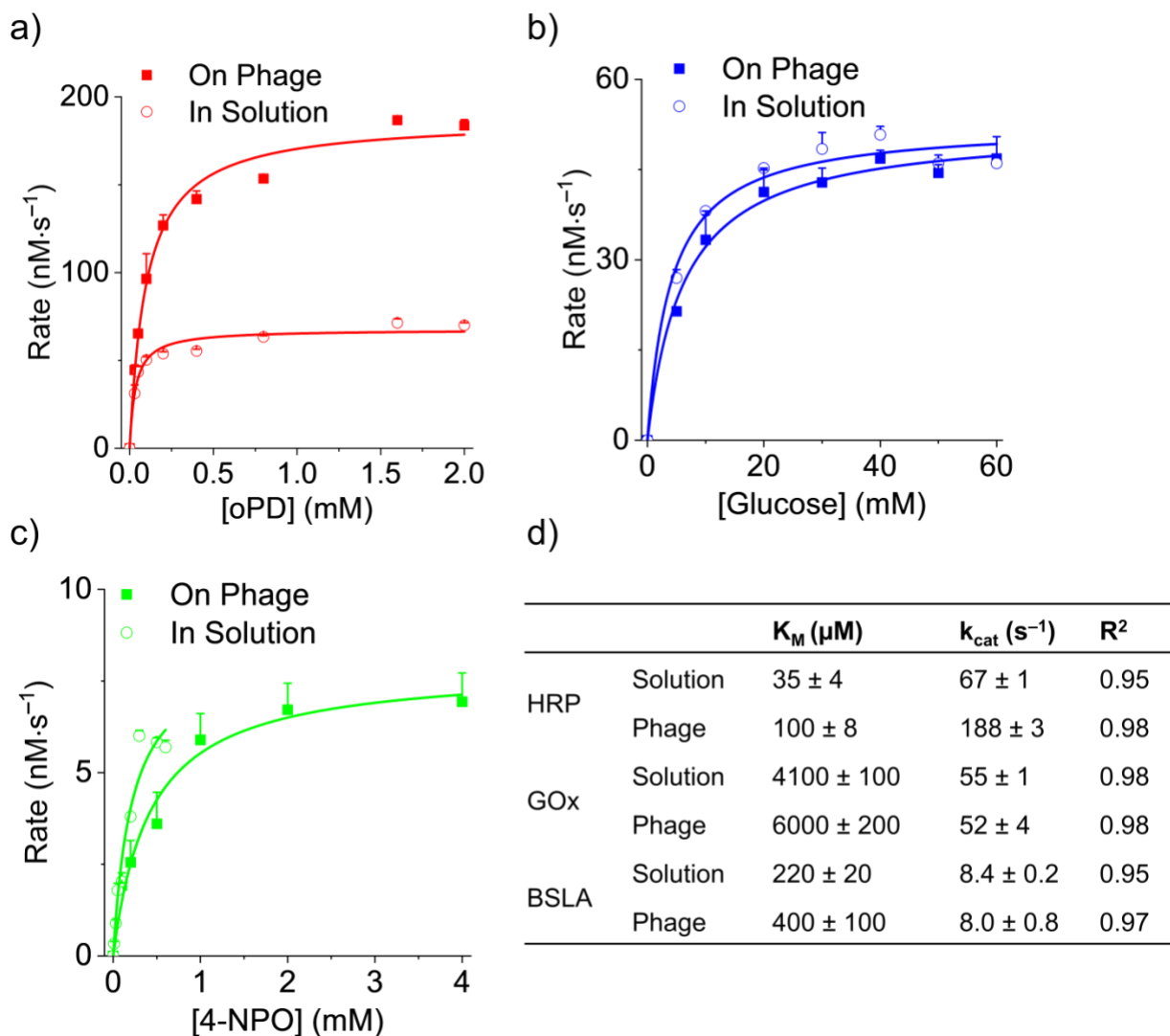


Figure 4.5 Comparison of lipase kinetics analyzed by THz emission technology and ¹H NMR spectroscopy. (a,b) Concentration-dependant reaction rates used to determine enzyme kinetic parameters either using the Hill equation (THz emission) or the Michaelis-Menten equation. The dotted line corresponds to the Michaelis-Menten equation fitted to the THz emission data ($R^2 < 0.92$) to illustrate the poor fit. (c) Fit parameters obtained by non-linear regression of data in (a,b). (d) Comparison of the rate of hydrolysis of four substrates (50 mM) by CALB obtained by ¹H NMR spectroscopy and THz emission technology. The rates measured by THz emission are systematically higher due to adsorption of CALB onto the sensing plate. Data in panes a, b, and d are presented as Mean + SD, n = 3.

Moreover, equivalent curves were obtained by ^1H NMR spectroscopy by converting peak area to units of concentration using a known amount of DMSO as an internal concentration reference (**Figure 4.4**).

Intriguingly, while the data obtained by ^1H NMR spectroscopy fit well with the Michaelis-Menten model, the equivalent was not true for the data obtained by THz emission ($R^2 < 0.92$; dotted lines in **Figures 4.5a,b**). Moreover, the reaction rates measured by THz emission were ~ 1 – 5 times higher than those measured by ^1H NMR spectroscopy. To resolve this difference in kinetics as well as to explore the applicability of THz emission technology for quantitative monitoring of other substrate molecules, the rate of hydrolysis of two additional substrates (50 mM) was measured by both techniques and compared.

As seen in **Figure 4.5d** and **Figure 4.6**, reaction rates measured by both techniques had low standard deviation, though remained systematically ~ 2 – 6 times higher when measured by THz emission. While the reproducibility of the THz data and the high linearity of calibration curves in **Figures 4.3a,b** suggest that THz emission can be used as a quantitative tool, the systematic difference with respect to ^1H NMR spectroscopy warranted some consideration. In this regard, the hyper-activation of lipases has been reported in the literature by others when the latter are adsorbed onto a hydrophobic surface, leading to a ~ 3 -fold increase of activity for certain substrates.^{37,252}

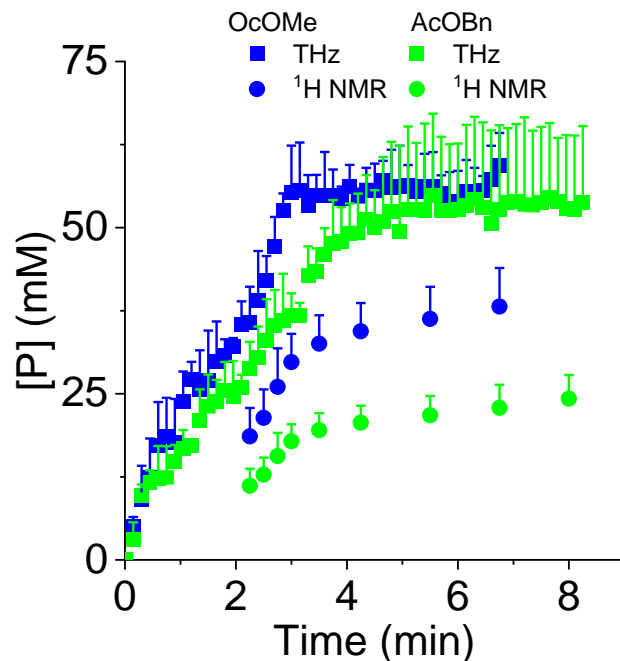


Figure 4.6 Evolution of product concentration upon addition of lipase to the sample solution containing OcOMe or AcOBn, calculated by THz emission technology or ¹H NMR spectroscopy. Time “zero” corresponds to the moment lipase was added. An approximate delay of 2 min was required to lock and shim the sample before ¹H NMR spectra could be recorded. Data presented as Mean + SD, n = 3.

Lipases do indeed have a high affinity for hydrophobic surfaces (such as the sensing plate coated with hydrophobic ester substrate molecules), which places them in a locally hydrophobic environment. This has been suggested to open the lid of the enzyme, thereby facilitating access of substrate to the catalytic site. Analysis of the concentration-dependent reaction rates obtained by THz emission technology in **Figure 4.5** using a Hill model (rather than Michaelis-Menten) produced reliable fits to the data ($R^2 > 0.98$) and indicated the existence of positive cooperativity ($n > 1$; when $n = 1$, the Hill equation reduces to the Michaelis-Menten equation). Positive cooperativity is consistent with a potential alteration of molecular structure of the enzyme upon immobilization onto the sensing plate.³⁹

This would thus explain the higher reaction rates observed by THz emission, without an effect on $K_M/K_{0.5}$ (similar values by both techniques). Note that DMSO, used as an internal integration standard for ^1H NMR spectroscopy, only had a modest effect on activity when measured by THz emission technology (~33% reduction at 1 vol% DMSO; **Figure 4.7**) and is not likely to be dominant cause for the differences observed. Overall, these results confirm that THz emission technology is sensitive to changes that occur in the immediate vicinity of the sensing plate, and likely to adsorbed molecules, and these changes can be used for quantitative monitoring or chemical reactions

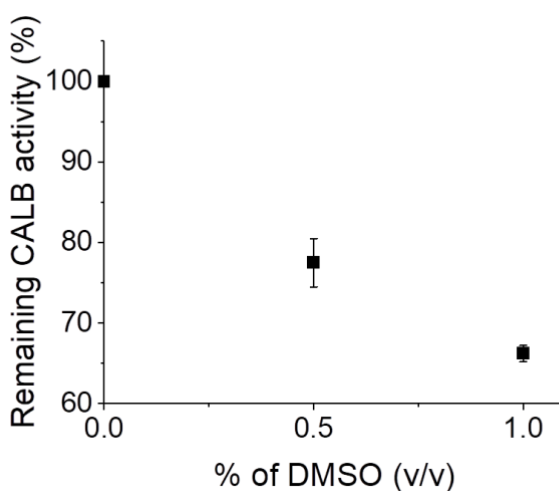


Figure 4.7 Effect of DMSO concentration on the rate of hydrolysis of MeOBu as measured using the THz optical setup. Data presented as Mean \pm SD, n = 3.

To illustrate the potential of the THz emission to qualitatively monitor catalytic processes within complex samples, CALB was added to a sample of whole cow milk. Milk is a quintessential complex substrate consisting of varieties of fats, proteins, sugars, and salts that is difficult to analyze by typical analytical techniques. In the dairy industry, lipases are used to enhance the flavor of cheese products and accelerate cheese ripening and lipolysis of milk/vegetable oil/fat to obtain specific flavours.²⁵³ Lipase catalyzes the

hydrolysis of fat to fatty acids, which are not only aromatic compounds themselves but also precursors of methyl ketones, alcohols, lactones and esters. As illustrated in **Figure 4.8a**, the addition of CALB to whole milk resulted in an increase of THz amplitude over a period of ~12 min due to the hydrolysis of fat molecules. This coincided with a decrease in pH from 6.8 to 5.2 over ~10 min. The 2-min interval during which pH was stable but THz amplitude continued to evolve suggests that minor side-reactions are occurring in the sample that do not produce a change of pH (such as destabilization of casein micelles or other possibilities listed above). Thereafter, a plateau of THz amplitude was observed due to the complete consumption of fat within the sample, and no further evolution of pH was observed. Remarkably, at 40 min, a second increase of THz amplitude was observed due to the early onset of gelation of the milk caused by acid-induced destabilization of casein micelles. Gelation produces a large change in the micro/nano-structure of the solution, thus influencing the chemical interactions with the sensing plate. Thus, in addition to sensing chemical changes within this complex sample, the THz emission amplitude was sensitive to physical changes that may be important for certain industrial processes. Finally, to illustrate that this THz emission technique is applicable to other enzyme systems, the oxidation of oPD by horseradish peroxidase and H₂O₂ was measured, and compared to data obtained by optical absorbance. The activity of this enzyme is commonly used in the biotechnological sector as a quantitative tool in e.g., immunoassays. As illustrated in **Figure 4.8b**, the curves of formation of DAP measured by THz emission technology and optical absorbance were essentially superimposed, indicating a good correlation between both techniques, and the absence of immobilization-induced effects such as those observed for lipase. This data, including the semi-quantitative analysis of the urease-catalyzed hydrolysis of urea into ammonium carbonate by Kiwa et al.,²⁵⁴ provide evidence that THz emission technology can be applied to other enzyme systems.

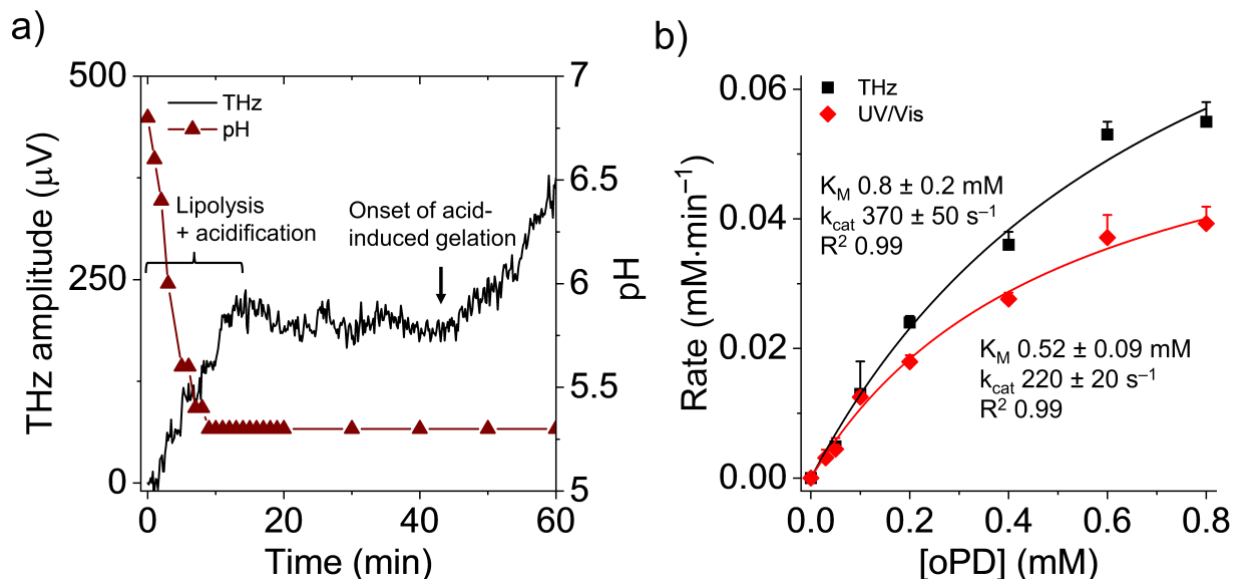


Figure 4.8 Lipase activity in whole milk and activity of horseradish peroxidase by THz emission technology. (a) Changes of pH and THz amplitude of whole cow's milk exposed to CALB ($n = 1$). Time "zero" corresponds to the moment lipase was added. (b) Production of DAP with time upon action of horseradish peroxidase and H_2O_2 on oPD, as measured by THz emission technology and optical absorption. Time "zero" corresponds to the moment horseradish peroxidase was added. Data presented as Mean + SD, $n = 3$.

4.4 Conclusions

THz emission technology was successfully used to quantitatively monitor the kinetics of chemical transformations in a label-free and non-invasive manner, which makes it an ideal tool for screening libraries of substrates (e.g., analysis of enzyme promiscuity). The sensitivity of THz emission to both chemical and physical changes to samples is useful for qualitatively analyzing complex reactions, although future sensing plate designs should aim to increase sensitivity and surface area, and thereby widen the dynamic range of concentrations that can be analyzed quantitatively. Increased sensitivity would also increase sampling rate, which could be useful for monitoring very rapid chemical transformations. Despite the promising nature of the results herein, future research

should establish a better understanding of how molecular structure influences THz emission amplitude (e.g., polarity, aromaticity, charge, hydrophobicity, etc.), address the influence of adsorption to the sensing plate on enzyme kinetics (as seen for lipase herein), and investigate other enzymes and types of chemical reactions, to more firmly conclude on the generality of this technique. Overall, this manuscript sets the stage for investigating THz emission technology as a tool for research and development involving enzymes, and for monitoring industrial processes in the food, cosmetic, detergent, pharmaceutical, and biodiesel sectors.

4.5 Acknowledgments

Takuya Kuwana is gratefully acknowledged for his technical assistance with the THz emission technology. This study was funded by the Natural Sciences and Engineering Council of Canada (NSERC) grants number RGPIN-2015-04254 and STPGP 463418. SN acknowledges a Mitacs-JSPS Internship. AH acknowledges a postdoctoral scholarship from the Fonds de Recherche Québec (FRQ) – Nature et Technologies. MAG is a Research Scholar of the FRQ – Santé.

CHAPTER 5: General Discussion, Conclusion, and Future direction

In this section we tried to answer some questions that provide the most the significant finding, what makes this work different from the work of others, limitations and the future direction of the thesis, and how this thesis will benefit society

1. What is the most significant finding of this thesis?

In the context of this thesis, we:

- i) Provided an outline of the strategies for the enzyme engineering, enzyme immobilization and enzyme's microenvironment engineering for improving of catalytic efficiency of enzymes as well as for the production of robust, stable biocatalyst suitable for application in a broader range of industrial processes. We also discussed about the various scaffold for single or multiple enzymes immobilization, phage display and use of phages as nanoscale scaffold for enzyme immobilization. Overall, these fundamental observations could contribute to the design of innovative single or multienzyme nano-reactors.
- ii) Showcased the expression of BSLA on filamentous phage to explore the effect of this phage template on activity, and the influence of this template on nanoscale distribution in solution. We displayed BSLA on M13 bacteriophage; the most commonly used filamentous phage for phage display technology. Besides, lipases are widely used in industries and the typical lipase reactions occur in organic–aqueous emulsions, therefore, BSLA was an excellent model to investigate the influence of the phage scaffold on enzyme activity in complex colloidal solutions. BSLA display on filamentous phage showed that the stability of BSLA did not seem to be inherently affected by phage display; however the phage itself modified the nanoscale distribution of BSLA within the micellar assay buffer. Therefore, caution should be exerted when selecting enzymes by

- phage display, particularly when the foreseen application involves complex solutions (e.g., colloidal or other). This phenomenon might be true for other proteins.
- iii) Presented a proof-of-concept study of phage-templated three-enzyme cascade model, BSLA→GOx→HRP, this may be promising platforms for one-pot multistep reaction. In this study, first, the effect of this nanoscale template on the cascade reaction was explored. The collective results indicate that BSLA→GOx→HRP cascade can indeed be enhanced compared to the free enzymes in solution by templating on a phage. Second, the effect of nanoscale confinement achieved by various level of Inter-phage crosslinking of enzyme-bearing template was studied. The inter-phage crosslinking appeared to create a favorable microenvironment for individual enzymes as well as the overall cascade reaction.
 - iv) Developed an analytical technique for label-free and quantitative monitoring of enzyme kinetics using Terahertz emission technology. This technique is not only suitable for the label-free analysis of enzyme kinetics of complex and natural substrates, also suitable for the real-time monitoring of any ligand binding applicable to variety of biotechnology and industrial platforms.

2. What are the major limitations of this thesis?

One of the main consideration factors for the industrial application of enzymes is the cost of materials; however, our cascade model was made using the expensive antibodies that is limitation of this work.

The sensitivity of the sensing plate we used was limited; therefore a wide range of concentrations could not be analyzed quantitatively by THz emission. Increased sensitivity would also increase sampling rate, which could be useful for monitoring very rapid chemical transformations.

3. What makes the work different from the work of others?

Phage display of enzyme is not new in biotechnology field, however studying the effect of phage template on the microenvironment of enzyme in a crowded reaction was not studied before (so far in my knowledge). There are only a handful of examples that filamentous bacteriophage were used to assemble enzymes,^{133,134,255,256} however, all most all of them immobilized single enzyme, our work brings a proof of concept for preparing multienzyme cascade model by using filamentous bacteriophage. So far in my knowledge, this is the first work that manifested a new use of protein–bacteriophage conjugation techniques, and provided a convenient system to investigate the clustering effect of enzymes, which nature often harnesses to achieve regulation through enzyme complexation, compartmentalization, and membrane-embedment.

We are the first group that we documented a non-invasive, label-free, and quantitative technology for monitoring of enzyme kinetics using Terahertz emission technology.

4. What is left to be done?

The development of multienzyme cascades capable of complex multistep synthesis or catabolism is considered an important goal of synthetic biology and such transformative systems have yet to be demonstrated. Understanding of the mechanistic processes and many of the functional rules will guide researchers to use natural scaffolding materials (like non-pathogenic viruses) to create multienzyme cascade model for industrial use. The scientific content of this thesis sets the scopes for future researches. By using the phage display technology, it is possible to create engineered phage having diversities of linkers (e.g., streptavidin, etc.) on it that will make the immobilization step easier. Ultimately, this proof-of-concept study suggests that phage-templated enzyme cascade systems may be promising platforms for green manufacturing.

Despite we showed that THz emission technology can be successfully use to quantitatively monitor CALB and HRP kinetics of chemical transformations in a label-free

manner, investigating other enzymes as well as multienzyme cascade, and different types of chemical reactions will make this technique more acceptable to researchers and in industrial sector.

5. How will this work benefit society?

Enzymes are the part of us, it is not only because of our body function is dependent of various types of enzymes; but also they are needed almost in every industrial sector to make our life easy. Therefore, it is a crucial demand of making efficient enzyme system for industrial use. The work of this thesis explores how phage attached enzyme may work differently than the free enzyme due to different nanoscale distribution in a complex or colloidal solution. This phenomenon will help researcher to pay attention when selecting enzymes by phage display. This thesis also explores the strategies and mechanisms to create efficient multienzyme system which can contribute for industrial work. Moreover, real-time monitoring of 'real' samples using THz emission will save time and detection cost that is desired in industrial and healthcare sectors which ultimately contribute to the society.

6. BIBLIOGRAPHY

- 1 Raveendran, S. *et al.* Applications of microbial enzymes in food industry. *Food technology and biotechnology* **56**, 16-30 (2018).
- 2 Madhu, A. & Chakraborty, J. Developments in application of enzymes for textile processing. *Journal of cleaner production* **145**, 114-133 (2017).
- 3 Gébleux, R., Briendl, M., Grawunder, U. & Beerli, R. R. in *Enzyme-Mediated Ligation Methods* 1-13 (Springer, 2019).
- 4 Devine, P. N. *et al.* Extending the application of biocatalysis to meet the challenges of drug development. *Nature Reviews Chemistry* **2**, 409-421 (2018).
- 5 Ray, A. Application of lipase in industry. *Asian Journal of Pharmacy and technology* **2**, 33-37 (2012).
- 6 Souza, P. M. d. Application of microbial α -amylase in industry-A review. *Brazilian journal of microbiology* **41**, 850-861 (2010).
- 7 Padmapriya, B., Rajeswari, T., Nandita, R. & Raj, F. Production and purification of alkaline serine protease from marine *Bacillus* species and its application in detergent industry. *European Journal of Applied Sciences* **4**, 21-26 (2012).
- 8 Jones, G. K., Hoo, Y. & Lee, K. Production technology of lactase and its application in food industry application. *Journal of the Science of Food and Agriculture* **1**, 46 (2017).
- 9 Fazary, A. E. & Ju, Y.-H. The large-scale use of feruloyl esterases in industry. *Biotechnology and Molecular Biology Reviews* **3**, 95-110 (2013).
- 10 Cerminati, S. *et al.* Industrial uses of phospholipases: current state and future applications. *Applied microbiology and biotechnology* **103**, 2571-2582 (2019).
- 11 Tapre, A. & Jain, R. Pectinases: Enzymes for fruit processing industry. *International Food Research Journal* **21** (2014).
- 12 Climent, M. J., Corma, A., Iborra, S. & Sabater, M. J. (ACS Publications, 2014).
- 13 Kung, H. H. & Kung, M. C. Inspiration from nature for heterogeneous catalysis. *Catalysis letters* **144**, 1643-1652 (2014).
- 14 Muschiol, J. *et al.* Cascade catalysis—strategies and challenges en route to preparative synthetic biology. *Chemical Communications* **51**, 5798-5811 (2015).
- 15 Sheldon, R. A. Enzyme immobilization: the quest for optimum performance. *Advanced Synthesis & Catalysis* **349**, 1289-1307 (2007).
- 16 Carr, R. *et al.* Directed evolution of an amine oxidase possessing both broad substrate specificity and high enantioselectivity. *Angewandte Chemie* **115**, 4955-4958 (2003).
- 17 Arnold, F. H. Directed evolution: bringing new chemistry to life. *Angewandte Chemie International Edition* **57**, 4143-4148 (2018).
- 18 Zhou, Y., Pan, S., Wei, X., Wang, L. & Liu, Y. Immobilization of β -glucosidase onto magnetic nanoparticles and evaluation of the enzymatic properties. *BioResources* **8**, 2605-2619 (2013).
- 19 Siegel, J. B. *et al.* Computational protein design enables a novel one-carbon assimilation pathway. *Proceedings of the National Academy of Sciences* **112**, 3704-3709 (2015).
- 20 Cao, L. *Carrier-bound immobilized enzymes: principles, application and design.* (John Wiley & Sons, 2006).
- 21 Cao, L., van Langen, L. & Sheldon, R. A. Immobilised enzymes: carrier-bound or carrier-free? *Current opinion in Biotechnology* **14**, 387-394 (2003).

- 22 Sheldon, R. A. & van Pelt, S. Enzyme immobilisation in biocatalysis: why, what and how. *Chemical Society Reviews* **42**, 6223-6235 (2013).
- 23 Zhang, Y., Ge, J. & Liu, Z. Enhanced activity of immobilized or chemically modified enzymes. *ACS catalysis* **5**, 4503-4513 (2015).
- 24 Zhang, Y. & Hess, H. Microenvironmental engineering: An effective strategy for tailoring enzymatic activities. *Chinese Journal of Chemical Engineering* **28**, 2028-2036 (2020).
- 25 Zhang, Y. & Hess, H. Microenvironmental engineering: An effective strategy for tailoring enzymatic activities. *Chinese Journal of Chemical Engineering* (2020).
- 26 Lancaster, L., Abdallah, W., Banta, S. & Wheeldon, I. Engineering enzyme microenvironments for enhanced biocatalysis. *Chemical Society Reviews* **47**, 5177-5186 (2018).
- 27 Lang, X., Zhu, L., Gao, Y. & Wheeldon, I. Enhancing enzyme activity and immobilization in nanostructured inorganic–enzyme complexes. *Langmuir* **33**, 9073-9080 (2017).
- 28 Dröge, M. J. *et al.* Binding of phage displayed *Bacillus subtilis* lipase A to a phosphonate suicide inhibitor. *Journal of biotechnology* **101**, 19-28 (2003).
- 29 Green, N. Avidin. 1. The use of [¹⁴C] biotin for kinetic studies and for assay. *Biochemical Journal* **89**, 585 (1963).
- 30 Green, N. Thermodynamics of the binding of biotin and some analogues by avidin. *Biochemical Journal* **101**, 774-780 (1966).
- 31 Green, N. M. in *Advances in protein chemistry* Vol. 29 85-133 (Elsevier, 1975).
- 32 Bykhovski, A., Zhang, W., Jensen, J. & Woolard, D. Analysis of electronic structure, binding, and vibrations in biotin–streptavidin complexes based on density functional theory and molecular mechanics. *The Journal of Physical Chemistry B* **117**, 25-37 (2013).
- 33 Aumiller Jr, W. M., Davis, B. W., Hatzakis, E. & Keating, C. D. Interactions of macromolecular crowding agents and cosolutes with small-molecule substrates: effect on horseradish peroxidase activity with two different substrates. *The Journal of Physical Chemistry B* **118**, 10624-10632 (2014).
- 34 Nahar, S., Sokullu, E. & Gauthier, M. A. The phage display of *Bacillus subtilis* Lipase A significantly enhances catalytic activity due to altered nanoscale distribution in colloidal solution. *Biotechnology and bioengineering* **117**, 868-872 (2020).
- 35 Passaretti, P., Sun, Y., Dafforn, T. R. & Oppenheimer, P. G. Determination and characterisation of the surface charge properties of the bacteriophage M13 to assist bio-nanoengineering. *RSC Advances* **10**, 25385-25392 (2020).
- 36 Zhang, Y., Tsitkov, S. & Hess, H. Proximity does not contribute to activity enhancement in the glucose oxidase–horseradish peroxidase cascade. *Nature communications* **7**, 1-9 (2016).
- 37 Facchini, F. D. A. *et al.* Immobilization Effects on the Catalytic Properties of Two *Fusarium Verticillioides* Lipases: Stability, Hydrolysis, Transesterification and Enantioselectivity Improvement. *Catalysts* **8**, 84 (2018).
- 38 Sugiura, M. & Isobe, M. Studies on the Mechanism of Lipase Reaction. III. Adsorption of *Chromobacterium* Lipase on Hydrophobic Glass Beads. *Chem. Pharm. Bull.* **24**, 72-78, doi:10.1248/cpb.24.72 (1976).
- 39 Cardoso, F. P., Aquino Neto, S., Ciancaglini, P. & de Andrade, A. R. The Use of PAMAM Dendrimers as a Platform for Laccase Immobilization: Kinetic Characterization of the Enzyme. *Applied Biochemistry and Biotechnology* **167**, 1854-1864, doi:10.1007/s12010-012-9740-6 (2012).
- 40 Zhao, S. *et al.* Discovery of new enzymes and metabolic pathways by using structure and genome context. *Nature* **502**, 698-702 (2013).
- 41 Siegel, J. B. *et al.* Computational design of an enzyme catalyst for a stereoselective bimolecular Diels-Alder reaction. *Science* **329**, 309-313 (2010).

- 42 Tsitkov, S. & Hess, H. Design principles for a compartmentalized enzyme cascade reaction. *ACS Catalysis* **9**, 2432-2439 (2019).
- 43 Alam, M. T. *et al.* The self-inhibitory nature of metabolic networks and its alleviation through compartmentalization. *Nature communications* **8**, 1-13 (2017).
- 44 Klermund, L., Poschenrieder, S. T. & Castiglione, K. Biocatalysis in polymersomes: improving multienzyme cascades with incompatible reaction steps by compartmentalization. *ACS Catalysis* **7**, 3900-3904 (2017).
- 45 Zhou, Y., Wu, S., Mao, J. & Li, Z. Bioproduction of benzylamine from renewable feedstocks via a nine-step artificial enzyme cascade and engineered metabolic pathways. *ChemSusChem* **11**, 2221-2228 (2018).
- 46 Cedrone, F. *et al.* Directed evolution of the epoxide hydrolase from *Aspergillus niger*. *Biocatalysis and biotransformation* **21**, 357-364 (2003).
- 47 Lingen, B. *et al.* Alteration of the substrate specificity of benzoylformate decarboxylase from *Pseudomonas putida* by directed evolution. *ChemBioChem* **4**, 721-726 (2003).
- 48 Oh, K. H., Nam, S. H. & Kim, H. S. Directed Evolution of N-Carbamyl-d-amino Acid Amidohydrolase for Simultaneous Improvement of Oxidative and Thermal Stability. *Biotechnology progress* **18**, 413-417 (2002).
- 49 Ness, J. E. *et al.* DNA shuffling of subgenomic sequences of subtilisin. *Nature biotechnology* **17**, 893-896 (1999).
- 50 Moore, J. C. & Arnold, F. H. Directed evolution of a para-nitrobenzyl esterase for aqueous-organic solvents. *Nature biotechnology* **14**, 458-467 (1996).
- 51 Rao, A. G. The outlook for protein engineering in crop improvement. *Plant physiology* **147**, 6-12 (2008).
- 52 Bornscheuer, U. T. & Pohl, M. Improved biocatalysts by directed evolution and rational protein design. *Current opinion in chemical biology* **5**, 137-143 (2001).
- 53 Craik, C. S. *et al.* Redesigning trypsin: alteration of substrate specificity. *Science* **228**, 291-297 (1985).
- 54 Carter, P., Nilsson, B., Burnier, J. P., Burdick, D. & Wells, J. A. Engineering subtilisin BPN' for site-specific proteolysis. *Proteins: Structure, Function, and Bioinformatics* **6**, 240-248 (1989).
- 55 Wells, J. A., Powers, D. B., Bott, R. R., Graycar, T. P. & Estell, D. A. Designing substrate specificity by protein engineering of electrostatic interactions. *Proceedings of the National Academy of Sciences* **84**, 1219-1223 (1987).
- 56 McLachlan, M. J., Sullivan, R. P. & Zhao, H. in *Biocatalysis for the Pharmaceutical Industry* (2009).
- 57 Tao, J. A., Lin, G.-Q. & Liese, A. *Biocatalysis for the pharmaceutical industry: discovery, development, and manufacturing*. (John Wiley & Sons, 2009).
- 58 Parikh, M. R. & Matsumura, I. Site-saturation mutagenesis is more efficient than DNA shuffling for the directed evolution of β -fucosidase from β -galactosidase. *Journal of molecular biology* **352**, 621-628 (2005).
- 59 Leemhuis, H., Kelly, R. M. & Dijkhuizen, L. Directed evolution of enzymes: library screening strategies. *IUBMB life* **61**, 222-228 (2009).
- 60 Packer, M. S. & Liu, D. R. Methods for the directed evolution of proteins. *Nature Reviews Genetics* **16**, 379-394 (2015).
- 61 Kelly, R. M., Leemhuis, H., Gätjen, L. & Dijkhuizen, L. Evolution toward small molecule inhibitor resistance affects native enzyme function and stability, generating acarbose-insensitive cyclodextrin glucanotransferase variants. *Journal of Biological Chemistry* **283**, 10727-10734 (2008).

- 62 Kelly, R. M. *et al.* Elimination of competing hydrolysis and coupling side reactions of a
cyclodextrin glucanotransferase by directed evolution. *Biochemical Journal* **413**, 517-525 (2008).
- 63 Aharoni, A. *et al.* High-throughput screening methodology for the directed evolution of
glycosyltransferases. *Nature Methods* **3**, 609-614 (2006).
- 64 Ferrer, M. *et al.* Interplay of metagenomics and in vitro compartmentalization. *Microbial
biotechnology* **2**, 31-39 (2009).
- 65 Zani, M.-L. & Moreau, T. Phage display as a powerful tool to engineer protease inhibitors.
Biochimie **92**, 1689-1704 (2010).
- 66 Hoess, R. H. Protein design and phage display. *Chemical Reviews* **101**, 3205-3218 (2001).
- 67 Pande, J., Szewczyk, M. M. & Grover, A. K. Phage display: concept, innovations, applications and
future. *Biotechnology advances* **28**, 849-858 (2010).
- 68 Chung, W.-J., Lee, D.-Y. & Yoo, S. Y. Chemical modulation of M13 bacteriophage and its
functional opportunities for nanomedicine. *International journal of nanomedicine* **9**, 5825
(2014).
- 69 Russel, M., Lowman, H. B. & Clackson, T. Introduction to phage biology and phage display. *Phage
Display: A practical approach*, 1-26 (2004).
- 70 Gao, C. *et al.* Making artificial antibodies: a format for phage display of combinatorial
heterodimeric arrays. *Proceedings of the National Academy of Sciences* **96**, 6025-6030 (1999).
- 71 Gao, C. *et al.* A method for the generation of combinatorial antibody libraries using pIX phage
display. *Proceedings of the National Academy of Sciences* **99**, 12612-12616 (2002).
- 72 Smith, G. P. Filamentous fusion phage: novel expression vectors that display cloned antigens on
the virion surface. *Science* **228**, 1315-1317 (1985).
- 73 Jaworski, J. W., Raorane, D., Huh, J. H., Majumdar, A. & Lee, S.-W. Evolutionary screening of
biomimetic coatings for selective detection of explosives. *Langmuir* **24**, 4938-4943 (2008).
- 74 Hodyra, K. & Dąbrowska, K. Molecular and chemical engineering of bacteriophages for potential
medical applications. *Archivum immunologiae et therapiae experimentalis* **63**, 117-127 (2015).
- 75 Kehoe, J. W. & Kay, B. K. Filamentous phage display in the new millennium. *Chemical reviews*
105, 4056-4072 (2005).
- 76 Cwirla, S. E., Peters, E. A., Barrett, R. W. & Dower, W. J. Peptides on phage: a vast library of
peptides for identifying ligands. *Proceedings of the National Academy of Sciences* **87**, 6378-6382
(1990).
- 77 Scott, J. K. & Smith, G. P. Searching for peptide ligands with an epitope library. *Science* **249**, 386-
390 (1990).
- 78 Petrenko, V., Smith, G., Gong, X. & Quinn, T. A library of organic landscapes on filamentous
phage. *Protein Engineering, Design and Selection* **9**, 797-801 (1996).
- 79 Smith, G. P. Surface display and peptide libraries. *GENE-AMSTERDAM-* **128**, 1-1 (1993).
- 80 Russel, M. & Model, P. Genetic analysis of the filamentous bacteriophage packaging signal and
of the proteins that interact with it. *Journal of virology* **63**, 3284-3295 (1989).
- 81 Russel, M., Kidd, S. & Kelley, M. R. An improved filamentous helper phage for generating single-
stranded plasmid DNA. *Gene* **45**, 333-338 (1986).
- 82 Vieira, J. & Messing, J. (Academic Press, London, 1987).
- 83 Soltes, G. *et al.* A new helper phage and phagemid vector system improves viral display of
antibody Fab fragments and avoids propagation of insert-less virions. *Journal of immunological
methods* **274**, 233-244 (2003).
- 84 Barbas, C. F., Kang, A. S., Lerner, R. A. & Benkovic, S. J. Assembly of combinatorial antibody
libraries on phage surfaces: the gene III site. *Proceedings of the National Academy of Sciences*
88, 7978-7982 (1991).

- 85 Söderlind, E., Simonsson, A. C. & Borrebaeck, C. A. Phage display technology in antibody engineering: design of phagemid vectors and in vitro maturation systems. *Immunological reviews* **130**, 109-124 (1992).
- 86 Basso, A. & Serban, S. Industrial applications of immobilized enzymes—A review. *Molecular Catalysis* **479**, 110607 (2019).
- 87 Homaei, A. A., Sariri, R., Vianello, F. & Stevanato, R. Enzyme immobilization: an update. *Journal of chemical biology* **6**, 185-205 (2013).
- 88 Wiemann, L. O., Weisshaupt, P., Nieguth, R., Thum, O. & Ansorge-Schumacher, M. B. Enzyme stabilization by deposition of silicone coatings. *Organic Process Research & Development* **13**, 617-620 (2009).
- 89 Petri, A., Marconcini, P. & Salvadori, P. Efficient immobilization of epoxide hydrolase onto silica gel and use in the enantioselective hydrolysis of racemic para-nitrostyrene oxide. *Journal of Molecular Catalysis B: Enzymatic* **32**, 219-224 (2005).
- 90 Diaz, J. F. & Balkus Jr, K. J. Enzyme immobilization in MCM-41 molecular sieve. *Journal of Molecular Catalysis B: Enzymatic* **2**, 115-126 (1996).
- 91 Zhou, Z. & Hartmann, M. Recent progress in biocatalysis with enzymes immobilized on mesoporous hosts. *Topics in Catalysis* **55**, 1081-1100 (2012).
- 92 Kumar, A., Srivastava, A., Galaev, I. Y. & Mattiasson, B. Smart polymers: physical forms and bioengineering applications. *Progress in polymer science* **32**, 1205-1237 (2007).
- 93 Vertegel, A. A., Siegel, R. W. & Dordick, J. S. Silica nanoparticle size influences the structure and enzymatic activity of adsorbed lysozyme. *Langmuir* **20**, 6800-6807 (2004).
- 94 Lan, D., Li, B. & Zhang, Z. Chemiluminescence flow biosensor for glucose based on gold nanoparticle-enhanced activities of glucose oxidase and horseradish peroxidase. *Biosensors and Bioelectronics* **24**, 934-938 (2008).
- 95 Wu, C.-L., Chen, Y.-P., Yang, J.-C., Lo, H.-F. & Lin, L.-L. Characterization of lysine-tagged *Bacillus stearothermophilus* leucine aminopeptidase II immobilized onto carboxylated gold nanoparticles. *Journal of Molecular Catalysis B: Enzymatic* **54**, 83-89 (2008).
- 96 Keighron, J. D. & Keating, C. D. Enzyme: nanoparticle bioconjugates with two sequential enzymes: stoichiometry and activity of malate dehydrogenase and citrate synthase on Au nanoparticles. *Langmuir* **26**, 18992-19000 (2010).
- 97 Cruz, J. C. *et al.* in *Nanoscale biocatalysis* 147-160 (Springer, 2011).
- 98 Kirk, O. & Christensen, M. W. Lipases from *Candida antarctica*: unique biocatalysts from a unique origin. *Organic Process Research & Development* **6**, 446-451 (2002).
- 99 Gupta, M. N., Kaloti, M., Kapoor, M. & Solanki, K. Nanomaterials as matrices for enzyme immobilization. *Artificial Cells, Blood Substitutes, and Biotechnology* **39**, 98-109 (2011).
- 100 Ahmad, R. & Sardar, M. Enzyme immobilization: an overview on nanoparticles as immobilization matrix. *Biochemistry and Analytical Biochemistry* **4**, 1 (2015).
- 101 Rothmund, P. W. Folding DNA to create nanoscale shapes and patterns. *Nature* **440**, 297-302 (2006).
- 102 Ge, Z. *et al.* Constructing submonolayer DNA origami scaffold on gold electrode for wiring of redox enzymatic cascade pathways. *ACS applied materials & interfaces* **11**, 13881-13887 (2018).
- 103 Chidchob, P. & Sleiman, H. F. Recent advances in DNA nanotechnology. *Current opinion in chemical biology* **46**, 63-70 (2018).
- 104 Kang, W. *et al.* Cascade biocatalysis by multienzyme–nanoparticle assemblies. *Bioconjugate chemistry* **25**, 1387-1394 (2014).
- 105 Glover, D. J. & Clark, D. S. Protein calligraphy: a new concept begins to take shape. *ACS central science* **2**, 438-444 (2016).

- 106 Zhang, G., Schmidt-Dannert, S., Quin, M. B. & Schmidt-Dannert, C. in *Methods in enzymology* Vol. 617 323-362 (Elsevier, 2019).
- 107 Culver, J. N. *et al.* Plant virus directed fabrication of nanoscale materials and devices. *Virology* **479**, 200-212 (2015).
- 108 Cardinale, D., Carette, N. & Michon, T. Virus scaffolds as enzyme nano-carriers. *Trends in biotechnology* **30**, 369-376 (2012).
- 109 Poghossian, A. *et al.* Field-effect biosensor using virus particles as scaffolds for enzyme immobilization. *Biosensors and Bioelectronics* **110**, 168-174 (2018).
- 110 Bäcker, M. *et al.* Tobacco mosaic virus as enzyme nanocarrier for electrochemical biosensors. *Sensors and Actuators B: Chemical* **238**, 716-722 (2017).
- 111 Bruckman, M. A. *et al.* Tobacco mosaic virus based thin film sensor for detection of volatile organic compounds. *Journal of Materials Chemistry* **20**, 5715-5719 (2010).
- 112 Zang, F. *et al.* An electrochemical sensor for selective TNT sensing based on Tobacco mosaic virus-like particle binding agents. *Chemical Communications* **50**, 12977-12980 (2014).
- 113 Zang, F., Gerasopoulos, K., Brown, A. D., Culver, J. N. & Ghodssi, R. Capillary microfluidics-assembled virus-like particle bionanoreceptor interfaces for label-free biosensing. *ACS applied materials & interfaces* **9**, 8471-8479 (2017).
- 114 Alarcón-Correa, M. *et al.* Self-assembled phage-based colloids for high localized enzymatic activity. *ACS nano* **13**, 5810-5815 (2019).
- 115 Love, K. R., Swoboda, J. G., Noren, C. J. & Walker, S. Enabling glycosyltransferase evolution: a facile substrate-attachment strategy for phage-display enzyme evolution. *ChemBioChem* **7**, 753-756 (2006).
- 116 Suire, C. N. *et al.* Peptidic inhibitors of insulin-degrading enzyme with potential for dermatological applications discovered via phage display. *PloS one* **13**, e0193101 (2018).
- 117 Cipolatti, E. P., Manoel, E. A., Fernandez-Lafuente, R. & Freire, D. M. G. Support engineering: relation between development of new supports for immobilization of lipases and their applications. *Biotechnology Research and Innovation* **1**, 26-34 (2017).
- 118 Hartmeier, W. *Immobilized biocatalysts: an introduction.* (Springer Science & Business Media, 2012).
- 119 Zaak, H. *et al.* Effect of immobilization rate and enzyme crowding on enzyme stability under different conditions. The case of lipase from *Thermomyces lanuginosus* immobilized on octyl agarose beads. *Process Biochem* **56**, 117-123 (2017).
- 120 Yang, Q. *et al.* The effects of macromolecular crowding and surface charge on the properties of an immobilized enzyme: activity, thermal stability, catalytic efficiency and reusability. *RSC advances* **7**, 38028-38036 (2017).
- 121 Guisan, J. M. Immobilization of enzymes as the 21st century begins. *Immobilization of enzymes and cells*, 1-13 (2006).
- 122 Fernandez-Lopez, L. *et al.* Physical crosslinking of lipase from *Rhizomucor miehei* immobilized on octyl agarose via coating with ionic polymers: Avoiding enzyme release from the support. *Process Biochem* **54**, 81-88 (2017).
- 123 Rehm, F. B., Chen, S. & Rehm, B. H. Enzyme engineering for in situ immobilization. *Molecules* **21**, 1370 (2016).
- 124 Nguyen, H. H. & Kim, M. An overview of techniques in enzyme immobilization. *Applied Science and Convergence Technology* **26**, 157-163 (2017).
- 125 Chapman, J., Ismail, A. E. & Dinu, C. Z. Industrial applications of enzymes: Recent advances, techniques, and outlooks. *Catalysts* **8**, 238 (2018).

- 126 Kommoju, P.-R., Chen, Z.-w., Bruckner, R. C., Mathews, F. S. & Jorns, M. S. Probing oxygen activation sites in two flavoprotein oxidases using chloride as an oxygen surrogate. *Biochemistry* **50**, 5521-5534 (2011).
- 127 Datta, S., Christena, L. R. & Rajaram, Y. R. S. Enzyme immobilization: an overview on techniques and support materials. *3 Biotech* **3**, 1-9 (2013).
- 128 Grosová, Z., Rosenberg, M., Rebroš, M., Šipocz, M. & Sedláčková, B. Entrapment of β -galactosidase in polyvinylalcohol hydrogel. *Biotechnology Letters* **30**, 763-767 (2008).
- 129 Deshpande, A., D'souza, S. & Nadkarni, G. Coimmobilization of D-amino acid oxidase and catalase by entrapment of *Trigonopsis variabilis* in radiation polymerised Polyacrylamide beads. *Journal of biosciences* **11**, 137-144 (1987).
- 130 Sheldon, R. A., Sorgedraeger, M. & Janssen, M. H. Use of cross-linked enzyme aggregates (CLEAs) for performing biotransformations. *Chimica oggi* **25**, 62 (2007).
- 131 Illanes, A., Wilson, L., Caballero, E., Fernández-Lafuente, R. & Guisán, J. M. Crosslinked penicillin acylase aggregates for synthesis of β -lactam antibiotics in organic medium. *Applied Biochemistry and Biotechnology* **133**, 189-202 (2006).
- 132 Kuntz, I., Chen, K., Sharp, K. & Kollman, P. The maximal affinity of ligands. *Proceedings of the National Academy of Sciences* **96**, 9997-10002 (1999).
- 133 Kadiri, V. M. *et al.* Genetically Modified M13 Bacteriophage Nanonets for Enzyme Catalysis and Recovery. *Catalysts* **9**, 723 (2019).
- 134 Patel, A. N. *et al.* Scaffolding of enzymes on virus nanoarrays: effects of confinement and virus organization on biocatalysis. *Small* **13**, 1603163 (2017).
- 135 Weilandt, D. R. & Hatzimanikatis, V. Particle-based simulation reveals macromolecular crowding effects on the Michaelis-Menten mechanism. *Biophysical journal* **117**, 355-368 (2019).
- 136 Balcells, C. *et al.* Macromolecular crowding effect upon in vitro enzyme kinetics: mixed activation–diffusion control of the oxidation of NADH by pyruvate catalyzed by lactate dehydrogenase. *The Journal of Physical Chemistry B* **118**, 4062-4068 (2014).
- 137 Levin, Y., Pecht, M., Goldstein, L. & Katchalski, E. A water-insoluble polyanionic derivative of trypsin. I. Preparation and properties. *Biochemistry* **3**, 1905-1913 (1964).
- 138 Murata, H., Cummings, C. S., Koepsel, R. R. & Russell, A. J. Rational tailoring of substrate and inhibitor affinity via ATRP polymer-based protein engineering. *Biomacromolecules* **15**, 2817-2823 (2014).
- 139 Cebula, M. *et al.* Catalytic conversion of lipophilic substrates by phase constrained enzymes in the aqueous or in the membrane phase. *Scientific reports* **6**, 1-8 (2016).
- 140 Gao, Y. *et al.* Tuning enzyme kinetics through designed intermolecular interactions far from the active site. *Acs Catalysis* **5**, 2149-2153 (2015).
- 141 Azuma, Y., Bader, D. L. & Hilvert, D. Substrate sorting by a supercharged nanoreactor. *Journal of the American Chemical Society* **140**, 860-863 (2018).
- 142 Getzoff, E. D. *et al.* Electrostatic recognition between superoxide and copper, zinc superoxide dismutase. *Nature* **306**, 287-290 (1983).
- 143 Gao, Y., Or, S., Toop, A. & Wheeldon, I. DNA nanostructure sequence-dependent binding of organophosphates. *Langmuir* **33**, 2033-2040 (2017).
- 144 Goldstein, L., Levin, Y. & Katchalski, E. A water-insoluble polyanionic derivative of trypsin. II. Effect of the polyelectrolyte carrier on the kinetic behavior of the bound trypsin. *Biochemistry* **3**, 1913-1919 (1964).
- 145 Harada, A. & Kataoka, K. Pronounced activity of enzymes through the incorporation into the core of polyion complex micelles made from charged block copolymers. *Journal of controlled release* **72**, 85-91 (2001).

- 146 Kurinomaru, T., Tomita, S., Hagihara, Y. & Shiraki, K. Enzyme hyperactivation system based on a
complementary charged pair of polyelectrolytes and substrates. *Langmuir* **30**, 3826-3831 (2014).
- 147 Lin, J.-L. & Wheeldon, I. Kinetic enhancements in DNA–enzyme nanostructures mimic the
sabatier principle. *ACS Catalysis* **3**, 560-564 (2013).
- 148 Harada, A. & Kataoka, K. Novel polyion complex micelles entrapping enzyme molecules in the
core: preparation of narrowly-distributed micelles from lysozyme and poly (ethylene glycol)–
poly (aspartic acid) block copolymer in aqueous medium. *Macromolecules* **31**, 288-294 (1998).
- 149 Caruso, F., Trau, D., Möhwald, H. & Renneberg, R. Enzyme encapsulation in layer-by-layer
engineered polymer multilayer capsules. *Langmuir* **16**, 1485-1488 (2000).
- 150 Comellas-Aragonès, M. *et al.* A virus-based single-enzyme nanoreactor. *Nature nanotechnology*
2, 635-639 (2007).
- 151 Walde, P. Enzymatic reactions in liposomes. *Current Opinion in Colloid & Interface Science* **1**,
638-644 (1996).
- 152 Nallani, M. *et al.* Polymersome nanoreactors for enzymatic ring-opening polymerization.
Biomacromolecules **8**, 3723-3728 (2007).
- 153 Einfalt, T. *et al.* Biomimetic artificial organelles with in vitro and in vivo activity triggered by
reduction in microenvironment. *Nature communications* **9**, 1-12 (2018).
- 154 Liu, Y. *et al.* Substrate channeling in an artificial metabolon: a molecular dynamics blueprint for
an experimental peptide bridge. *Acs Catalysis* **7**, 2486-2493 (2017).
- 155 Liu, Y. *et al.* Cascade kinetics of an artificial metabolon by molecular dynamics and kinetic Monte
Carlo. *ACS Catalysis* **8**, 7719-7726 (2018).
- 156 Leskovac, V. The pH dependence of enzyme catalysis. *Comprehensive enzyme kinetics*, 283-315
(2003).
- 157 Goldstein, L. Microenvironmental effects on enzyme catalysis. Kinetic study of polyanionic and
polycationic derivatives of chymotrypsin. *Biochemistry* **11**, 4072-4084 (1972).
- 158 Zhang, Y., Wang, Q. & Hess, H. Increasing enzyme cascade throughput by pH-engineering the
microenvironment of individual enzymes. *ACS Catalysis* **7**, 2047-2051 (2017).
- 159 Edgcomb, S. P. & Murphy, K. P. Variability in the pKa of histidine side-chains correlates with
burial within proteins. *Proteins: Structure, Function, and Bioinformatics* **49**, 1-6 (2002).
- 160 Goldstein, L. & Katchalski, E. Use of water-insoluble enzyme derivatives in biochemical analysis
and separation. *Fresenius' Zeitschrift für analytische Chemie* **243**, 375-396 (1968).
- 161 Yang, D. *et al.* Immobilization adjusted clock reaction in the urea–urease–H⁺ reaction system.
RSC advances **9**, 3514-3519 (2019).
- 162 Wilner, O. I. *et al.* Enzyme cascades activated on topologically programmed DNA scaffolds.
Nature nanotechnology **4**, 249-254 (2009).
- 163 Fu, J., Liu, M., Liu, Y., Woodbury, N. W. & Yan, H. Interenzyme substrate diffusion for an enzyme
cascade organized on spatially addressable DNA nanostructures. *Journal of the American
Chemical Society* **134**, 5516-5519 (2012).
- 164 Xin, L., Zhou, C., Yang, Z. & Liu, D. Regulation of an enzyme cascade reaction by a DNA machine.
Small **9**, 3088-3091 (2013).
- 165 You, C., Myung, S. & Zhang, Y. H. P. Facilitated substrate channeling in a self-assembled
trifunctional enzyme complex. *Angewandte Chemie International Edition* **51**, 8787-8790 (2012).
- 166 You, C. & Zhang, Y.-H. P. Self-assembly of synthetic metabolons through synthetic protein
scaffolds: one-step purification, co-immobilization, and substrate channeling. *ACS synthetic
biology* **2**, 102-110 (2013).
- 167 Daniel, R. M. & Danson, M. J. Temperature and the catalytic activity of enzymes: A fresh
understanding. *FEBS letters* **587**, 2738-2743 (2013).

- 168 Blankschien, M. D. *et al.* Light-triggered biocatalysis using thermophilic enzyme–gold nanoparticle complexes. *Acs Nano* **7**, 654-663 (2013).
- 169 Wang, C. *et al.* Dynamic Modulation of Enzyme Activity by Near-Infrared Light. *Angewandte Chemie* **129**, 6871-6876 (2017).
- 170 Zhang, S., Wang, C., Chang, H., Zhang, Q. & Cheng, Y. Off-on switching of enzyme activity by near-infrared light-induced photothermal phase transition of nanohybrids. *Science advances* **5**, eaaw4252 (2019).
- 171 Fothergill-Gilmore, L. A. & Michels, P. A. Evolution of glycolysis. *Progress in biophysics and molecular biology* **59**, 105-235 (1993).
- 172 Ryan, D. G., Frezza, C. & O’Neill, L. A. TCA cycle signalling and the evolution of eukaryotes. *Current opinion in biotechnology* **68**, 72-88 (2021).
- 173 Broadwater, S. J., Roth, S. L., Price, K. E., Kobašlija, M. & McQuade, D. T. One-pot multi-step synthesis: a challenge spawning innovation. *Organic & biomolecular chemistry* **3**, 2899-2906 (2005).
- 174 Schrittwieser, J. H., Velikogne, S., Hall, M. I. & Kroutil, W. Artificial biocatalytic linear cascades for preparation of organic molecules. *Chemical reviews* **118**, 270-348 (2017).
- 175 Clomburg, J. M., Crumbley, A. M. & Gonzalez, R. Industrial biomanufacturing: the future of chemical production. *Science* **355**, aag0804 (2017).
- 176 Lin, J.-L., Palomec, L. & Wheeldon, I. Design and analysis of enhanced catalysis in scaffolded multienzyme cascade reactions. *Acs Catalysis* **4**, 505-511 (2014).
- 177 Yamada, Y. *et al.* Nanocrystal bilayer for tandem catalysis. *Nature chemistry* **3**, 372-376 (2011).
- 178 Wang, Y., Ren, H. & Zhao, H. Expanding the boundary of biocatalysis: design and optimization of in vitro tandem catalytic reactions for biochemical production. *Critical reviews in biochemistry and molecular biology* **53**, 115-129 (2018).
- 179 Morello, G., Megarity, C. F. & Armstrong, F. A. The power of electrified nanoconfinement for energising, controlling and observing long enzyme cascades. *Nature communications* **12**, 1-9 (2021).
- 180 KÜchler, A., Yoshimoto, M., Luginbühl, S., Mavelli, F. & Walde, P. Enzymatic reactions in confined environments. *Nature Nanotechnology* **11**, 409 (2016).
- 181 Giannakopoulou, A., Gkantzou, E., Polydera, A. & Stamatis, H. Multienzymatic nanoassemblies: recent progress and applications. *Trends in biotechnology* **38**, 202-216 (2020).
- 182 Hwang, E. T. & Lee, S. Multienzymatic cascade reactions via enzyme complex by immobilization. *ACS Catalysis* **9**, 4402-4425 (2019).
- 183 Meyer, A., Pellaux, R. & Panke, S. Bioengineering novel in vitro metabolic pathways using synthetic biology. *Current opinion in microbiology* **10**, 246-253 (2007).
- 184 Shaeri, J., Wright, I., Rathbone, E. B., Wohlgemuth, R. & Woodley, J. M. Characterization of enzymatic D-xylulose 5-phosphate synthesis. *Biotechnology and bioengineering* **101**, 761-767 (2008).
- 185 Chi, Y., Scroggins, S. T. & Fréchet, J. M. One-pot multi-component asymmetric cascade reactions catalyzed by soluble star polymers with highly branched non-interpenetrating catalytic cores. *Journal of the American Chemical Society* **130**, 6322-6323 (2008).
- 186 Kragl, U. & Aivasidis, A. *Technology transfer in biotechnology: from lab to industry to production*. Vol. 92 (Springer Science & Business Media, 2005).
- 187 Zhang, Y. H. P. & Lynd, L. R. Toward an aggregated understanding of enzymatic hydrolysis of cellulose: noncomplexed cellulase systems. *Biotechnology and bioengineering* **88**, 797-824 (2004).

- 188 Shearer, G., Lee, J. C., Koo, J. a. & Kohl, D. H. Quantitative estimation of channeling from early glycolytic intermediates to CO₂ in intact *Escherichia coli*. *The FEBS journal* **272**, 3260-3269 (2005).
- 189 Srivastava, D. & Bernhard, S. A. Metabolite transfer via enzyme-enzyme complexes. *Science* **234**, 1081-1086 (1986).
- 190 Díaz, S. A. *et al.* Gold Nanoparticle Templating Increases the Catalytic Rate of an Amylase, Maltase, and Glucokinase Multienzyme Cascade through Substrate Channeling Independent of Surface Curvature. *ACS Catalysis* **11**, 627-638 (2020).
- 191 Peters, R. J. *et al.* Cascade reactions in multicompartmentalized polymersomes. *Angewandte chemie* **126**, 150-154 (2014).
- 192 Li, F. & Wang, Q. Fabrication of nanoarchitectures templated by virus-based nanoparticles: strategies and applications. *Small* **10**, 230-245 (2014).
- 193 Linda G. Otten 1, W. J. Q. Directed evolution: selecting today's biocatalysts
. *Biomolecular Engineering*, 1-9, doi:10.1016/j.bioeng.2005.02.002 (2004).
- 194 Frenzel, A., Schirrmann, T. & Hust, M. in *MAbs*. 1177-1194 (Taylor & Francis).
- 195 Bornscheuer, U. T., Hauer, B., Jaeger, K. E. & Schwaneberg, U. Directed Evolution Empowered Redesign of Natural Proteins for the Sustainable Production of Chemicals and Pharmaceuticals. *Angewandte Chemie International Edition* **58**, 36-40 (2019).
- 196 Sidhu, S. S., Fairbrother, W. J. & Deshayes, K. Exploring protein-protein interactions with phage display. *Chembiochem* **4**, 14-25 (2003).
- 197 Beckmann, C., Waggoner, J. D., Harris, T. O., Tamura, G. S. & Rubens, C. E. Identification of novel adhesins from group B streptococci by use of phage display reveals that C5a peptidase mediates fibronectin binding. *Infection and immunity* **70**, 2869-2876 (2002).
- 198 Wagner, S. *et al.* Vaccination with a human high molecular weight melanoma-associated antigen mimotope induces a humoral response inhibiting melanoma cell growth in vitro. *The Journal of Immunology* **174**, 976-982 (2005).
- 199 Buchwald, U. K., Lees, A., Steinitz, M. & Pirofski, L.-a. A peptide mimotope of type 8 pneumococcal capsular polysaccharide induces a protective immune response in mice. *Infection and immunity* **73**, 325-333 (2005).
- 200 Cohen, C. J. *et al.* Direct phenotypic analysis of human MHC class I antigen presentation: visualization, quantitation, and in situ detection of human viral epitopes using peptide-specific, MHC-restricted human recombinant antibodies. *The Journal of Immunology* **170**, 4349-4361 (2003).
- 201 Riemer, A. B. *et al.* Generation of peptide mimics of the epitope recognized by trastuzumab on the oncogenic protein Her-2/neu. *The Journal of Immunology* **173**, 394-401 (2004).
- 202 Woiwode, T. F. *et al.* Synthetic compound libraries displayed on the surface of encoded bacteriophage. *Chemistry & biology* **10**, 847-858 (2003).
- 203 Yin, J., Liu, F., Schinke, M., Daly, C. & Walsh, C. T. Phagemid encoded small molecules for high throughput screening of chemical libraries. *Journal of the American Chemical Society* **126**, 13570-13571 (2004).
- 204 Anees, P. *et al.* Evidence, Manipulation, and Termination of pH 'Nanobuffering' for Quantitative Homogenous Scavenging of Monoclonal Antibodies. *ACS Nano* **13**, 1019-1028, doi:10.1021/acsnano.8b07202 (2019).
- 205 Belien, T. *et al.* Functional display of family 11 endoxylanases on the surface of phage M13. *Journal of biotechnology* **115**, 249-260 (2005).
- 206 VERHAERT, R. M. & Jan, V. Processing and functional display of the 86 kDa heterodimeric penicillin G acylase on the surface of phage fd. *Biochemical Journal* **342**, 415-422 (1999).

- 207 Soumilion, P. *et al.* Selection of β -lactamase on filamentous bacteriophage by catalytic activity. *Journal of molecular biology* **237**, 415-422 (1994).
- 208 Maenaka, K. *et al.* A Stable Phage-Display System Using a Phagemid Vector: Phage Display of Hen Egg-White Lysozyme (HEL), Escherichia coli Alkaline Phosphatase, and Anti-HEL Monoclonal Antibody, HyHEL10. *Biochemical and biophysical research communications* **218**, 682-687 (1996).
- 209 Dröge, M. J. *et al.* Binding of phage displayed Bacillus subtilis lipase A to a phosphonate suicide inhibitor. *Journal of biotechnology* **101**, 19-28 (2003).
- 210 Liu, S.-Q., Holland, R. & Crow, V. Esters and their biosynthesis in fermented dairy products: a review. *International Dairy Journal* **14**, 923-945 (2004).
- 211 Tripathi, R., Singh, J., Kumar Bharti, R. & Thakur, I. S. Isolation, purification and characterization of lipase from Microbacterium sp. and its application in biodiesel production. *Energy Procedia* **54**, 518-529 (2014).
- 212 Smith, G. Phage-Display Vectors and Libraries Based on Filamentous Phage Strain fd-tet. *Science* **228**, 1315 (1985).
- 213 Zhou, J. C. *et al.* Biotemplating rod-like viruses for the synthesis of copper nanorods and nanowires. *Journal of nanobiotechnology* **10**, 18 (2012).
- 214 LESUISSE, E., SCHANCK, K. & COLSON, C. Purification and preliminary characterization of the extracellular lipase of Bacillus subtilis 168, an extremely basic pH-tolerant enzyme. *European Journal of Biochemistry* **216**, 155-160 (1993).
- 215 Kumar, S., Kikon, K., Upadhyay, A., Kanwar, S. S. & Gupta, R. Production, purification, and characterization of lipase from thermophilic and alkaliphilic Bacillus coagulans BTS-3. *Protein Expression and Purification* **41**, 38-44 (2005).
- 216 Ma, J. *et al.* Overexpression and characterization of a lipase from Bacillus subtilis. *Protein expression and purification* **45**, 22-29 (2006).
- 217 Lianghua, T. & Liming, X. Purification and partial characterization of a lipase from Bacillus coagulans ZJU318. *Applied biochemistry and biotechnology* **125**, 139-146 (2005).
- 218 Nawani, N., Khurana, J. & Kaur, J. A thermostable lipolytic enzyme from a thermophilic Bacillus sp.: purification and characterization. *Molecular and cellular biochemistry* **290**, 17-22 (2006).
- 219 Hoarau, M., Badieyan, S. & Marsh, E. N. G. Immobilized enzymes: understanding enzyme-surface interactions at the molecular level. *Organic & biomolecular chemistry* **15**, 9539-9551 (2017).
- 220 Barbosa, O. *et al.* Strategies for the one-step immobilization-purification of enzymes as industrial biocatalysts. *Biotechnology Advances* **33**, 435-456 (2015).
- 221 Mao, C. *et al.* Virus-based toolkit for the directed synthesis of magnetic and semiconducting nanowires. *Science* **303**, 213-217 (2004).
- 222 Douglas, T. & Young, M. Host-guest encapsulation of materials by assembled virus protein cages. *Nature* **393**, 152-155 (1998).
- 223 Minten, I. J., Hendriks, L. J., Nolte, R. J. & Cornelissen, J. J. Controlled encapsulation of multiple proteins in virus capsids. *Journal of the American Chemical Society* **131**, 17771-17773 (2009).
- 224 Carette, N. *et al.* A virus-based biocatalyst. *Nature nanotechnology* **2**, 226-229 (2007).
- 225 Regulski, K., Champion-Arnaud, P. & Gabard, J. Bacteriophage manufacturing: From early twentieth-century processes to current GMP. *Bacteriophages; Harper, D., Ed.; Springer: Cham, Switzerland* (2018).
- 226 Vranish, J. N., Ancona, M. G., Oh, E., Susumu, K. & Medintz, I. L. Enhancing coupled enzymatic activity by conjugating one enzyme to a nanoparticle. *Nanoscale* **9**, 5172-5187 (2017).
- 227 Nahar, S., Sokullu, E. & Gauthier, M. A. The phage display of Bacillus subtilis Lipase A significantly enhances catalytic activity due to altered nanoscale distribution in colloidal solution. *Biotechnology and bioengineering* (2019).

- 228 Tan, Y. H. *et al.* A nanoengineering approach for investigation and regulation of protein immobilization. *ACS nano* **2**, 2374-2384 (2008).
- 229 Mizutani, N., Korposh, S., Selyanchyn, R., Wakamatsu, S. & Lee, S.-W. Application of a quartz crystal microbalance (QCM) twin sensor for selective label-free immunoassay to simultaneous antigen-antibody reactions. *Sensors & Transducers* **137**, 1 (2012).
- 230 Xu, G., Xu, Y., Li, A., Chen, T. & Liu, J. Enzymatic bioactivity investigation of glucose oxidase modified with hydrophilic or hydrophobic polymers via in situ RAFT polymerization. *Journal of Polymer Science Part A: Polymer Chemistry* **55**, 1289-1293 (2017).
- 231 Ritter, D. W., Newton, J. M., Roberts, J. R. & McShane, M. J. Albuminated Glycoenzymes: Enzyme Stabilization through Orthogonal Attachment of a Single-Layered Protein Shell around a Central Glycoenzyme Core. *Bioconjugate chemistry* **27**, 1285-1292 (2016).
- 232 Tan, S., Gu, D., Liu, H. & Liu, Q. Detection of a single enzyme molecule based on a solid-state nanopore sensor. *Nanotechnology* **27**, 155502 (2016).
- 233 Kuzuya, A., Numajiri, K., Kimura, M. & Komiyama, M. in *Nucleic Acids Symposium Series*. 681-682 (Oxford University Press).
- 234 Yang, Y. R., Liu, Y. & Yan, H. DNA nanostructures as programmable biomolecular scaffolds. *Bioconjugate chemistry* **26**, 1381-1395 (2015).
- 235 Fu, J. *et al.* Multi-enzyme complexes on DNA scaffolds capable of substrate channelling with an artificial swinging arm. *Nature nanotechnology* **9**, 531 (2014).
- 236 Wheeldon, I. *et al.* Substrate channelling as an approach to cascade reactions. *Nature chemistry* **8**, 299 (2016).
- 237 Kitov, P. I. *et al.* A quantitative, high-throughput method identifies protein–glycan interactions via mass spectrometry. *Communications biology* **2**, 1-7 (2019).
- 238 Qian, J. *et al.* Study the effect of trypsin enzyme activity on the screening of applying frontal affinity chromatography. *International journal of biological macromolecules* **139**, 740-751 (2019).
- 239 Kawahara-Nakagawa, Y. *et al.* New assay method based on Raman spectroscopy for enzymes reacting with gaseous substrates. *Protein Science* **28**, 663-670 (2019).
- 240 Her, C., Alonzo, A. P., Vang, J. Y., Torres, E. & Krishnan, V. V. Real-time enzyme kinetics by quantitative NMR spectroscopy and determination of the Michaelis–Menten constant using the Lambert-W function. *Journal of Chemical Education* **92**, 1943-1948 (2015).
- 241 Kiwa, T. *et al.* Chemical sensing plate with a laser-terahertz monitoring system. *Applied optics* **47**, 3324-3327 (2008).
- 242 Kiwa, T., Tenma, A., Takahashi, S., Sakai, K. & Tsukada, K. Label free immune assay using terahertz chemical microscope. *Sensors and Actuators B: Chemical* **187**, 8-11 (2013).
- 243 Kiwa, T. *et al.* Terahertz chemical microscope for label-free detection of protein complex. *Applied Physics Letters* **96**, 211114 (2010).
- 244 Kiwa, T., Kamiya, T., Morimoto, T., Sakai, K. & Tsukada, K. pH measurements in 16-nL-volume solutions using terahertz chemical microscopy. *Optics express* **26**, 8232-8238 (2018).
- 245 Minami, Y., Kiwa, T., Kawayama, I., Tonouchi, M. & Tsukada, K. in *2009 34th International Conference on Infrared, Millimeter, and Terahertz Waves*. 1-3 (IEEE).
- 246 Hassan, E. M. *et al.* High-sensitivity detection of metastatic breast cancer cells via terahertz chemical microscopy using aptamers. *Sensors and Actuators B: Chemical* **287**, 595-601 (2019).
- 247 Kuwana, T., Ogawa, M., Sakai, K., Kiwa, T. & Tsukada, K. Label-free detection of low-molecular-weight samples using a terahertz chemical microscope. *Applied Physics Express* **9**, 042401 (2016).

- 248 Rickert, J., Brecht, A. & Göpel, W. Quartz crystal microbalances for quantitative biosensing and characterizing protein multilayers. *Biosensors and Bioelectronics* **12**, 567-575, doi:[https://doi.org/10.1016/S0956-5663\(96\)00077-2](https://doi.org/10.1016/S0956-5663(96)00077-2) (1997).
- 249 Brígida, A. I., Pinheiro, Á. D., Ferreira, A. L. & Gonçalves, L. R. in *Biotechnology for Fuels and Chemicals* 293-307 (Springer, 2007).
- 250 Houde, A., Kademi, A. & Leblanc, D. Lipases and their industrial applications. *Applied Biochemistry and Biotechnology* **118**, 155-170, doi:10.1385/ABAB:118:1-3:155 (2004).
- 251 Stauch, B., Fisher, S. J. & Cianci, M. Open and closed states of *Candida antarctica* lipase B: protonation and the mechanism of interfacial activation. *Journal of lipid research* **56**, 2348-2358, doi:10.1194/jlr.M063388 (2015).
- 252 Sugiura, M. & Isobe, M. Studies on the Mechanism of Lipase Reaction. III. Adsorption of *Chromobacterium* Lipase on Hydrophobic Glass Beads. *CHEMICAL & PHARMACEUTICAL BULLETIN* **24**, 72-78, doi:10.1248/cpb.24.72 (1976).
- 253 Jooyandeh, H., Amarjeet, K. & Minhas, K. Lipases in dairy industry: a review. *Journal of Food Science and Technology (Mysore)* **46**, 181-189 (2009).
- 254 Kiwa, T., Jyunichi, K., Iwo, K., Tonouchi, M. & Tsukada, K. in *2008 33rd International Conference on Infrared, Millimeter and Terahertz Waves*. 1-2.
- 255 Torbensen, K. *et al.* Immuno-Based Molecular Scaffolding of Glucose Dehydrogenase and Ferrocene Mediator on fd Viral Particles Yields Enhanced Bioelectrocatalysis. *ACS Catalysis* (2019).
- 256 Alarcón-Correa, M. *et al.* Self-Assembled Phage-Based Colloids for High Localized Enzymatic Activity. *ACS nano* **13**, 5810-5815 (2019).

7. APPENDIX

7.1 Letters of copyright permission

Copyright for Figure 1.1

This Agreement between INRS-EMT -- Sharifun Nahar ("You") and Oxford University Press ("Oxford University Press") consists of your license details and the terms and conditions provided by Oxford University Press and Copyright Clearance Center.

License Number	5083310837353
License date	Jun 06, 2021
Licensed content publisher	Oxford University Press
Licensed content publication	CONFIDENTIAL - Plant Physiology
Licensed content title	The Outlook for Protein Engineering in Crop Improvement
Licensed content author	Rao, A. Gururaj
Licensed content date	May 7, 2008
Type of Use	Thesis/Dissertation
Institution name	
Title of your work	Graduate student
Publisher of your work	Institut national de la recherche scientifique
Expected publication date	Jul 2021
Permissions cost	0.00 CAD
Value added tax	0.00 CAD
Total	0.00 CAD
Title	Graduate student
Institution name	Institut national de la recherche scientifique
Expected presentation date	Jul 2021
Portions	Figure 1 on page 7

Copyright for Figure 1.4



Filamentous Phage Display in the New Millennium

Author: John W. Kehoe, Brian K. Kay

Publication: Chemical Reviews

Publisher: American Chemical Society

Date: Nov 1, 2005

Copyright © 2005, American Chemical Society

PERMISSION/LICENSE IS GRANTED FOR YOUR ORDER AT NO CHARGE

This type of permission/license, instead of the standard Terms and Conditions, is sent to you because no fee is being charged for your order. Please note the following:

- Permission is granted for your request in both print and electronic formats, and translations.
- If figures and/or tables were requested, they may be adapted or used in part.
- Please print this page for your records and send a copy of it to your publisher/graduate school.
- Appropriate credit for the requested material should be given as follows: "Reprinted (adapted) with permission from {COMPLETE REFERENCE CITATION}. Copyright {YEAR} American Chemical Society." Insert appropriate information in place of the capitalized words.
- One-time permission is granted only for the use specified in your RightsLink request. No additional uses are granted (such as derivative works or other editions). For any uses, please submit a new request.

A 1111111111

Copyright for Figure 1.6

This Agreement between INRS-EMT -- Sharifun Nahar ("You") and Springer Nature ("Springer Nature") consists of your license details and the terms and conditions provided by Springer Nature and Copyright Clearance Center.

License Number	5083310007540
License date	Jun 06, 2021
Licensed Content Publisher	Springer Nature
Licensed Content Publication	Nature
Licensed Content Title	Folding DNA to create nanoscale shapes and patterns
Licensed Content Author	Paul W. K. Rothemund
Licensed Content Date	Mar 16, 2006
Type of Use	Thesis/Dissertation
Requestor type	academic/university or research institute
Format	print and electronic
Portion	figures/tables/illustrations
Number of figures/tables/illustrations	1
High-res required	no
Will you be translating?	no
Circulation/distribution	1 - 29
Author of this Springer Nature content	no
Title	Graduate student
Institution name	Institut national de la recherche scientifique
Expected presentation date	Jul 2021
Portions	Figure 2 on page 299

Copyright for Figure 1.9a



Tuning Enzyme Kinetics through Designed Intermolecular Interactions Far from the Active Site

Author: Yingning Gao, Christopher C. Roberts, Jie Zhu, et al

Publication: ACS Catalysis

Publisher: American Chemical Society

Date: Apr 1, 2015

Copyright © 2015, American Chemical Society

PERMISSION/LICENSE IS GRANTED FOR YOUR ORDER AT NO CHARGE

This type of permission/license, instead of the standard Terms and Conditions, is sent to you because no fee is being charged for your order. Please note the following:

- Permission is granted for your request in both print and electronic formats, and translations.
- If figures and/or tables were requested, they may be adapted or used in part.
- Please print this page for your records and send a copy of it to your publisher/graduate school.
- Appropriate credit for the requested material should be given as follows: "Reprinted (adapted) with permission from (COMPLETE REFERENCE CITATION). Copyright (YEAR) American Chemical Society." Insert appropriate information in place of the capitalized words.
- One-time permission is granted only for the use specified in your RightsLink request. No additional uses are granted (such as derivative works or other editions). For any uses, please submit a new request.

Copyright for Figure 1.9b



Dear Sharifun Nahar,

Your permission requested is granted and there is no fee for this reuse. In your planned reuse, you must cite the ACS article as the source, add this direct link <https://pubs.acs.org/doi/abs/10.1021/jacs.7b11210> and include a notice to readers that further permissions related to the material excerpted should be directed to the ACS.

If you need further assistance, please let me know.

Sincerely,
Simran Mehra
ACS Publications Support
Customer Services & Information
Website: <https://help.acs.org/>

Incident Information:

Incident #: 4400658

Date Created: 2021-06-07T04:12:20

Copyright for Figure 1.10a

This Agreement between INRS-EMT -- Sharifun Nahar ("You") and Elsevier ("Elsevier") consists of your license details and the terms and conditions provided by Elsevier and Copyright Clearance Center.

License Number	5098330474809
License date	Jun 29, 2021
Licensed Content Publisher	Elsevier
Licensed Content Publication	Chinese Journal of Chemical Engineering
Licensed Content Title	Microenvironmental engineering: An effective strategy for tailoring enzymatic activities
Licensed Content Author	Yifei Zhang, Henry Hess
Licensed Content Date	Aug 1, 2020
Licensed Content Volume	28
Licensed Content Issue	8
Licensed Content Pages	9
Start Page	2028
End Page	2036
Type of Use	reuse in a thesis/dissertation
Portion	figures/tables/illustrations
Number of figures/tables/illustrations	1
Format	both print and electronic
Are you the author of this Elsevier article?	No
Will you be translating?	No
Title	Graduate student
Institution name	Institut national de la recherche scientifique
Expected presentation date	Jul 2021
Portions	Figure 2 on page 9

Copyright for Figure 1.10b

Increasing Enzyme Cascade Throughput by pH-Engineering the Microenvironment of Individual Enzymes



Author: Yifei Zhang, Qin Wang, Henry Hess

Publication: ACS Catalysis

Publisher: American Chemical Society

Date: Mar 1, 2017

Copyright © 2017, American Chemical Society

PERMISSION/LICENSE IS GRANTED FOR YOUR ORDER AT NO CHARGE

This type of permission/license, instead of the standard Terms and Conditions, is sent to you because no fee is being charged for your order. Please note the following:

- Permission is granted for your request in both print and electronic formats, and translations.
- If figures and/or tables were requested, they may be adapted or used in part.
- Please print this page for your records and send a copy of it to your publisher/graduate school.
- Appropriate credit for the requested material should be given as follows: "Reprinted (adapted) with permission from {COMPLETE REFERENCE CITATION}. Copyright {YEAR} American Chemical Society." Insert appropriate information in place of the capitalized words.
- One-time permission is granted only for the use specified in your RightsLink request. No additional uses are granted (such as derivative works or other editions). For any uses, please submit a new request.

Copyright for Figure 1.11a

Light-Triggered Biocatalysis Using Thermophilic Enzyme–Gold Nanoparticle Complexes



Author: Matthew D. Blankschien, Lori A. Pretzer, Ryan Huschka, et al

Publication: ACS Nano

Publisher: American Chemical Society

Date: Jan 1, 2013

Copyright © 2013, American Chemical Society

PERMISSION/LICENSE IS GRANTED FOR YOUR ORDER AT NO CHARGE

This type of permission/license, instead of the standard Terms and Conditions, is sent to you because no fee is being charged for your order. Please note the following:

- Permission is granted for your request in both print and electronic formats, and translations.
- If figures and/or tables were requested, they may be adapted or used in part.
- Please print this page for your records and send a copy of it to your publisher/graduate school.
- Appropriate credit for the requested material should be given as follows: "Reprinted (adapted) with permission from {COMPLETE REFERENCE CITATION}. Copyright {YEAR} American Chemical Society." Insert appropriate information in place of the capitalized words.
- One-time permission is granted only for the use specified in your RightsLink request. No additional uses are granted (such as derivative works or other editions). For any uses, please submit a new request.

Copyright for Figure 1.11b

This Agreement between INRS-EMT -- Sharifun Nahar ("You") and John Wiley and Sons ("John Wiley and Sons") consists of your license details and the terms and conditions provided by John Wiley and Sons and Copyright Clearance Center.

License Number	5083110712382
License date	Jun 06, 2021
Licensed Content Publisher	John Wiley and Sons
Licensed Content Publication	Angewandte Chemie
Licensed Content Title	Dynamic Modulation of Enzyme Activity by Near-Infrared Light
Licensed Content Author	Yiyun Cheng, Ruijuan Qi, Jianhua Xu, et al
Licensed Content Date	May 8, 2017
Licensed Content Volume	129
Licensed Content Issue	24
Licensed Content Pages	6
Type of use	Dissertation/Thesis
Requestor type	University/Academic
Format	Print and electronic
Portion	Figure/table
Number of figures/tables	1
Will you be translating?	No
Title	Graduate student
Institution name	Institut national de la recherche scientifique
Expected presentation date	Jul 2021
Portions	Figure 1 on page 1

Copyright for Figure 1.12

This Agreement between INRS-EMT -- Sharifun Nahar ("You") and Elsevier ("Elsevier") consists of your license details and the terms and conditions provided by Elsevier and Copyright Clearance Center.

License Number	5087010464625
License date	Jun 13, 2021
Licensed Content Publisher	Elsevier
Licensed Content Publication	Trends in Biotechnology
Licensed Content Title	Multienzymatic Nano assemblies: Recent Progress and Applications
Licensed Content Author	Archontoula Giannakopoulou, Elena Gkantzou, Angeliki Polydera, Haralambos Stamatis
Licensed Content Date	Feb 1, 2020
Licensed Content Volume	38
Licensed Content Issue	2
Licensed Content Pages	15
Start Page	202
End Page	216
Type of Use	reuse in a thesis/dissertation

Portion	figures/tables/illustrations
Number of figures/tables/illustrations	1
Format	both print and electronic
Are you the author of this Elsevier article?	No
Will you be translating?	No
Title	Graduate student
Institution name	Institut national de la recherche scientifique
Expected presentation date	Jul 2021
Portions	Figure 1 on page 3

Copyright for Figure 1.13



Multienzymatic Cascade Reactions via Enzyme Complex by Immobilization

Author: Ee Taek Hwang, Seonbyul Lee

Publication: ACS Catalysis

Publisher: American Chemical Society

Date: May 1, 2019

Copyright © 2019, American Chemical Society

PERMISSION/LICENSE IS GRANTED FOR YOUR ORDER AT NO CHARGE

This type of permission/license, instead of the standard Terms and Conditions, is sent to you because no fee is being charged for your order. Please note the following:

- Permission is granted for your request in both print and electronic formats, and translations.
- If figures and/or tables were requested, they may be adapted or used in part.
- Please print this page for your records and send a copy of it to your publisher/graduate school.
- Appropriate credit for the requested material should be given as follows: "Reprinted (adapted) with permission from {COMPLETE REFERENCE CITATION}. Copyright {YEAR} American Chemical Society." Insert appropriate information in place of the capitalized words.
- One-time permission is granted only for the use specified in your RightsLink request. No additional uses are granted (such as derivative works or other editions). For any uses, please submit a new request.